Development of the integration of microwave technology with microfluidic systems for sensing and heating

by

Weijia Cui

A thesis

presented to the University of Waterloo

in fulfillment of the

thesis requirement for the degree of

Doctor of Philosophy

in

Mechanical and Mechatronics Engineering

Waterloo, Ontario, Canada, 2021

Examining Committee Membership

The following served on the Examining Committee for this thesis. The decision of the Examining Committee is by majority vote.

External Examiner	Dr. Siyuan He Professor Department of Mechanical and Industrial Engineering Ryerson University, Ontario, Canada
Supervisor	Dr. Carolyn L. Ren Professor Department of Mechanical and Mechatronics Engineering University of Waterloo, Ontario, Canada
Internal Member	Dr. Dongqing Li Professor Department of Mechanical and Mechatronics Engineering University of Waterloo, Ontario, Canada
Internal Member	Dr. Fue-Sang Lien Professor Department of Mechanical and Mechatronics Engineering University of Waterloo, Ontario, Canada
Internal Member	Dr. Slim Boumaiza Professor Department of Electrical and Computer Engineering University of Waterloo, Ontario, Canada

Author's Declaration

I hereby declare that I am the sole author of this thesis. This is a true copy of the thesis, including any required final revisions, as accepted by my examiners.

I understand that my thesis may be made electronically available to the public.

Abstract

Microfluidics-based Lab-on-a-Chip platforms have drawn ever-increasing attention from both academy and industry due to their advantages for dealing with small volume of fluids and for integrating multiple processes into one platform [1, 2]. These advantages are the direct benefits of miniaturization which also brings challenges, especially in sensing and heating [3, 4]. The challenges are augmented in the context of droplet microfluidics because of their fast motion, curved interface and reduced volume (i.e. pico- to nano-liter). Droplet microfluidics utilizes water-in-oil or oil-in-water droplets that can be generated in microchannel networks at kHz rates as mobilized test tubes [5]. It presents tremendous potential to serve as a tool for high throughput analysis that are in high demand in many areas such as material synthesis, life science research, pharmaceutical industry and environmental monitoring [6-8]. Many applications require temperature control and both fundamental and applied research need droplet sensing to assist in understanding droplet motion and developing techniques for manipulating droplets [9].

Microwave sensing offers unique advantages by differentiating materials based on their electrical properties at high speeds [4, 10]. Moreover, it enables simultaneous heating of individual droplets [11]. Previous studies demonstrated the potential of microwave resonator for point of care (POC) applications and for simultaneous sensing and heating [10, 11]. However, neither of them has yet be fully realized. In addition to the technical challenges such as the use of bulky and expensive vector network analyzer (VNA) for sensing that limits the potential for POC applications, fundamental understanding of microwave heating and its coupling with droplet microfluidics is lacking. This thesis is designed to fill the gap with the ultimate goal of enhancing droplet

microfluidics as an enabling tool for a wide range of applications by realizing the full potential of microwave sensing and heating.

With the goal of maximizing the capacity of droplet microfluidics serving as an enabling tool for many applications, this thesis focuses on exploring microwave sensing and heating for droplet microfluidics. The thesis started with the investigation of the coupling between microwave heating and droplet motion to shine light on the mechanism of microwave heating induced droplet mixing. Followed the improved understanding of microwave heating, on-demand droplet generation via microwave heating was explored and demonstrated. To realize simultaneous sensing and heating which is powerful for droplet microfluidics, two resonators need to be considered and the primary concern for two resonators in a single microfluidic chip is the crosstalk between the two resonators. The third chapter was designed to investigate the fundamental challenges of integrating two resonators within a typical microfluidic device footprint. Finally, a POC application of microwave sensing is demonstrated for real time detecting lead in drinking water system which has been one of the crisis raised recently.

Acknowledgements

First, I would like to sincerely thank my supervisor Dr. Carolyn L. Ren for guiding and supporting me during my PhD period. Her passion for research has always inspired me and I am grateful for her encouragement to help me grow into a professional researcher.

Next, I would like to thank my committee members Dr. Siyuan He from Ryerson University, Dr. Slim Boumaiza, Dr. Dongqing Li, and Dr. Fue-Sang Lien from University of Waterloo for their perceptive suggestions and comments.

I would like to appreciate all my group members who always provide insightful advice and support to me and work together with me as a great cooperative team.

I would also like to express my deep gratitude to my family who always support and encourage me. Thank you for your absolute love and support to make me have motivation and strength to continue my research study.

Finally, I acknowledge the financial support from the Natural Science and Engineering Research Council of Canada (NSERC) and University of Waterloo.

Table of Contents

List of Figures

List of Tables

Chapter 1 : Introduction

1.1. Introduction

In today's world, miniaturization has become a trend of advanced techniques to allow faster and higher efficiency of processes and contributed to the introduction of the concept of Lab on a Chip (LOC) [2] by leveraging the continuous flow nature of microfluidics. LOC concept refers to the integration and automation of multiple techniques in a small device with the size ranging from millimeter to centimeter, which are normally carried out in bulk laboratories [12, 13]. Microfluidics, an interchangeable terminology of LOC, enables the use of small amount of fluids to operate regular reactions and applications in small devices [2, 13]. Microfluidics featured by the length scale on the order of micrometer possesses significant advantages over traditional fluid systems such as lower consumption of reagents, shortened analysis time, and portability for POC applications [14, 15]. The reduction in scale also brings in confinement to the sample, which would result in higher resolution and sensitivity in analysis [1, 16]. The development of microfluidics has been stimulated by the demand from chemical and biochemical researchers and industries for tools that can exceed the performance of current macro-sized assays [17-19]. In the meantime, this miniaturization of dealing with small samples using microfluidics enables the great advances for various types of applications including drug delivery, materials synthesis, cell sorting, and materials sensing [8, 20-22].

As the development of microfluidics at the early stages, it appears to show some disadvantages. The chemical and physical influence such as materials interaction and capillary forces tend to be more noticeable when the scale goes down to micro or millimeter sizes. Fluid mixing is however

challenging in microfluidics systems due to the laminar flow nature in microfluidics devices and is usually dominated by diffusion resulting in a very slow process [23, 24]. The materials interaction may also lead to the cross contamination resulting in the imprecise results. And these disadvantages make microfluidics-based devices not perform as efficient as traditional lab equipment which could be one of the reasons contributing to the fact that the industrial scale has not matched with the numerous microfluidics innovations reported.

One of the emerged solutions to tackle these disadvantages is droplet microfluidics. Droplet microfluidics is also termed as two phases flow which employs two immiscible fluid to generate droplets in microchannel by injecting one into another fluid [5]. The droplets can serve as mobilized reaction tubes allowing for big reductions in reagent volume (i.e. μl to nl or even pl) and reaction time [25]. A dominated advantage of using droplets as reactors for various assays is that its contact with solid walls is eliminated by a thin film of the carrier fluid, which minimizes the problems caused by adsorption of the dissolved components on the channel walls, and increases the efficiency of chemical reactions [26]. Since droplets are isolated and protected by the immiscible phase, droplets can serve as encapsulated cargos for cells, particles, or biomolecules (DNA, proteins, metabolites); can be a microreactor for chemical or biological synthesis; and can be used for biosensing and a broad range of applications [5, 27-29]. Nowadays, using droplet microfluidics can address the aforementioned fundamental problems encountered in conventional microfluidics [30].

For most applications, reliable droplet generation marks the initial and important step, which is expected to have stable and predictable outcomes [31, 32]. A well-controlled droplet generation process is required for various applications [31]. Rapid droplet mixing with accurate control is of

vital importance for initializing reactions and increasing reaction rate in various applications [23]. Two main methods, passive and active methods, have been developed for droplet generation and mixing [31, 33]. Passive methods generally utilize the change in the applied pressures or geometries of the microchannel to manipulate droplets with the constant pressure actuation to the fluids, while active methods often employ external sources such as electric and magnetic forces or acoustic wave to disturb droplet motion at a certain frequency (non-constant actuation) [34, 35].

Passive and active methods own their advantages and disadvantages. Passive methods can manipulate a huge number of droplets offering high throughput with the cost of low robustness in general because of the coupling physics between the applied pressures and droplet motion through the carrier fluids [25]. However precise control of individual droplets becomes challenging because any design flaws, fabrication defects and pressure fluctuations would affect the designed functionality [35]. Active methods however can work with individual droplets offering additional control over each function with the cost of complicating the hardware system [35]. In droplet microfluidics, each droplet can serve as a single unit for reacting and storage purposes, therefore the control over individual droplets can benefit the precision of the process and improve system efficiency. Active methods hence are good candidates to well manipulate droplets and droplet motions [35, 36]. Furthermore, a series of active methods can be integrated and connected together to realize an automatic microfluidic systems. As more versatile and complex applications including polymerase chain reaction (PCR), molecule synthesis, enzyme kinetic, and cell cultures have been purposed and developed, precise and automatic controls for droplet microfluidics are needed to fit the new challenges and requirements from these applications [21, 37]. Therefore, it is important to develop proper active methods for droplet manipulation. And fundamental study of the active

methods can benefit to understand the working mechanism in order to provide strategies to better design and control the process.

Besides droplet manipulations, there are other functions which are required for applications based on LOC applications. Heating is a general requirement for various application including PCR and materials synthesis to provide energy to meet the reaction conditions [38]. Also heating methods can serve as active methods motioned above for droplet generation and mixing [39]. Many LOC devices have been employed for POC use to provide quick and precise diagnose which requires sensing function for LOC systems [40]. Sensing in the system can acquire materials information including materials temperature, concentration, droplet size and rate, and reaction information [41-43]. Conventional materials detection methods such as mass spectroscopy, atomic adsorption spectroscopy, or high performance liquid chromatography suffer from the shortcoming including high cost, bulk size, tedious sample preparation and requirement for professional personnel, which limit the use of these methods for real-time and in-situ detection [44]. The realization of microfluidics system with sensing performance can offer a low cost and portable way for real-time and in-situ detection applications [44].

With more tasks assigned to microfluidics systems, they are required to carry out multiple tasks at the same time. When applying sensing and other functions in a microfluidics device, selective process can be realized which is indeed desired for some applications. Microwave is an electromagnetic wave and the frequency ranges from 0.3 to 300 GHz, corresponding to wavelength from 1 mm to 1 m [45]. The miniaturization of microwave devices enables the combination of itself and microfluidics systems. Microwave can realize heating function in microfluidics systems if applying proper conditions such as certain microwave frequency, which can be characterized by

microwave sensing [11]. Microwave heating can serve as an active method to induce droplet manipulations [46]. Microwave heating has great advantages over traditional thermal methods and it can selectively heat droplets leaving the surrounding carrier fluid unheated according to different dielectric properties [45]. Moreover, microwave heating exhibits strong localization and features fast heating and cooling [11, 47], which enables pulse heating because heating stops once the power is off. Microwave can also be used for sensing purposes and a well-designed microwave sensor is able to detect materials based on their electoral properties including permittivity and conductivity for sensing purposes [48].

In this thesis, the target lies on the development of microwave technology with microfluidic platforms for sensing and heating. At the beginning, the fundamental study is carried out to investigate microwave heating induced droplet mixing, which is a multi-physics phenomena involving the coupling of electromagnetic field, fluid flow and heat transfer within moving droplets. The understanding of droplet mixing induced by microwave heating inspires us to carry out the on demand droplet generation realized by microwave heating. The active microwave method enables the on demand droplet generation process by using microwave heating to induce Laplace pressure change at the interface. And in order to realize the multiple functions in a single microfluidic chips, two resonators are put together in a single chip. The challenges of integrating two or more microwave resonators within a typical microfluidic device footprint (i.e. 1”x3”) are investigated. Finally a sensing application is then performed to realize real-time detection of heavy metals based on a microfluidic platform. Gold nanoparticles have been used to modify the surface of microwave sensor to enhance sensing performance. And a portable VNA is used to justify that this method can serve as real time sensing platform. The accomplishment of this thesis fundamentally and practically contributes to the field of microfluidics with the cooperation of

microwave technology by 1) developing and understanding the microwave heating as an active methods to induce droplet mixing and generation; 2) investigating the conditions for a microfluidic system to realize multiple microwave functions i.e. heating and sensing, simultaneously; 3) discovering the potential to use microwave as a sensing method to monitor the environments pollution levels in real time.

1.2. Thesis outline

Chapter 2 exhibits the literature review regarding to microfluidics and microwave including the fundamental studies and practical applications. At the beginning, it gives an overall introduction about microfluidics followed by droplet microfluidics. The physical view of droplet microfluidics is presented to show the fundamental of droplet microfluidics. Active and passive methods for droplet motion including droplet generation and mixing are then discussed which are important for many related applications. Sensing and heating are required for microfluidics as more and more applications have been developed. The following session introduces the sensing and heating methods especially the microwave technology which can be used for droplet sensing and heating.

Chapter 3 introduces the experimental and numerical methodology used in this thesis. Experimental methods include microfluidic chips fabrication, microwave resonator fabrication and materials and equipments. Numerical part presents the governor equation, boundary and initial conditions using Ansys Fluent and HFSS.

Chapter 4 exhibits the work related to numerically investigation of the effects of temperature-dependent fluid properties including viscosity, density, diffusivity, and interfacial tension, on heating induced mixing. A model including a spiral resonator integrated with a microchannel with

aqueous droplets moving with a carrier oil is considered. The electromagnetic field is calculated in Ansys HFSS and calculated energy field is imported to Ansys Fluent where flow and tracer concentration field is calculated. In this work, the dominated role of interfacial tension in microwave induced droplet mixing is demonstrated.

Chapter 5 follows the work in last session to present a work using microwave to induce droplet generation. This work focuses on developing the on-demand droplet generation mediated by microwave heating which generates disturbance to the interface by reducing the interfacial tension. The microwave heater is capable of confining power into a small region realizing localized heating which is advantageous for controlling droplet generation on-demand because the temperature of the fluid can be increased or decreased quickly. The relationship between generation time and droplet volume is discussed in this session.

Chapter 6 demonstrates the strategies to construct a double microwave resonators system based on microfluidic system. To fully realize the potential of simultaneous droplet sensing and heating, at least two resonators with one sensing the droplet and the other heating it are needed. But the crosstalk between resonators limit the number of resonators. In order to prevent crosstalk, numerical simulation and experimental studies are carried out to investigate the limitation of the distance between two adjacent resonators as well as the resonator design. An optimized distance between two resonators is suggested.

Chapter 7 introduces an application related to lead detection based on a microfluidic platform with microwave sensing. As it becomes serious for heavy metals pollution, it is necessary and impactful to construct early monitor and warning for lead standard in water to prevent any damage to human health. The sensor is based on a microfluidic platform with microwave sensor integrated and

nanomaterials are used to modify the sensor for an enhanced performance. Tap water is used in the experiment to show that this method is eligible to detect lead amount in real samples. The utilization of a portable NanoVNA is used to carry out detection and demonstrates the portability of this method to be widely used for real time sensing.

Chapter 8 summarizes the work in this thesis and lists the contribution of this thesis to the fundamental and practical research. It also discusses the future development of microfluidics with microwave technology as well as the potential to use for biochemical applications.

Chapter 2 : Literature Review

In this chapter, a comprehensive literature review used to accomplish this thesis is presented. At the beginning, this chapter exhibits an introduction about microfluidics in terms of physical understanding, droplet manipulation, and relative applications. Followed by this, heating and sensing functions in microfluidics have been introduced. In particular, the utilization of microwave heating and sensing with microfluidics are introduced.

2.1. Microfluidics introduction

Microfluidic system is regarded as a promising interdisciplinary platform and has been developed well for several decades [9]. The development of microfluidic system is driven by the demand to scale down volumes and channel sizes from chemical and biochemical researchers. They prefer to realize reactions and analysis with minimized amounts of reactants to save processing time or to perform special experiments such as studying the kinetics of particular chemical reactions, fabricating special materials, and screening biological properties [7, 49-52]. Lab on a Chip (LOC) is a related concept referring to a microfluidic platform for research work and practical application with a controlled condition and a series of fluid operation [50]. In such a system, microfluidics is capable to operate conventional laboratory tasks with big reduction of reaction time and sample use in microliters and milliliters scales.

Among microfluidics classifications, two-phase microfluidics, otherwise known as droplet microfluidics has gained more attention for fundamental study and practical application [5]. The use of droplets in the microfluidic system allows reductions in the sample volume and procedure time. And one of the key changes of droplet microfluidics over the single phase flow is the thin

film formed by the carrier fluid between the channel wall and the droplets when a good wetting condition is applied [53]. In this way, cross contamination could be avoided and the fluid motion inside the droplet is enhanced, which could increase the reaction rate [54]. The laminar flow in microfluidic devices makes it difficult to achieve the efficient mixing in microfluidic devices. In a single phase flow device as shown in Figure 2.1(a), mixing is slow with two streams being injected into a channel flow side-by-side by diffusion. Also, the dispersion of solutes along the channel is large. However, as shown in Figure 2.1(b), by employing the droplet microfluidic systems, both problems above could be overcome. In droplet microfluidics system, due to high surface to volume ration, mass and heat transfer happens in a short time and distance resulting in a higher reaction efficiency [55]. Another advantage of the two phase system is the good manipulation of the droplets [56]. Because the droplets are isolated by the immiscible carrier phase, each droplets can serve as a single microreactor for different purposes [57]. And individual control or manipulation over droplets including merging, splitting, and mixing can be realized by passive methods or active methods [5].

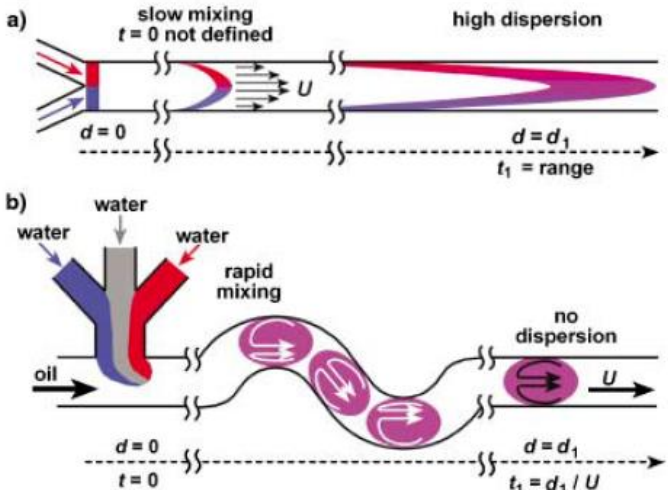

Figure 2.1. Comparison of a typical A + B reaction (a) single Phase flow case (b) Two phase flow case [52]

2.2. Physical view of droplet microfluidics

Dimensionless Number

Two-phase microfluidic flows are generated when two immiscible fluids or partially miscible fluids are injected to microfluidic devices [9]. The carrier fluid is named as continuous phase flow and the droplet fluid is called the disperse phase. At the beginning of the introduction for the two-phase flow, it is appropriate to clearly explain the physical ingredients for the two-phase flow. A balance exists in two-phase flow among four primary forces; interfacial tension, viscous shear, inertia and buoyancy. The effect of these forces is qualified by the combination of dimensionless numbers [58]. The group of those dimensionless numbers describes the relative importance of different forces between the two fluids. The definition, equation, and scaling of size of the Grashof number, Bond number, Reynolds number, Weber number, and Capillary number are summarized in the following

Table 2.1 [16, 59]. In the equations, L [m] stands for characteristic length-scale; ρ [kg/m3] is the fluid density; β [1/K] is the coefficient of thermal expansion; ΔT [K] is the temperature difference; $\Delta\rho$ [kg/m3] is the density difference; g [m/s^2] refers to the gravitational acceleration; U [m/s] is the fluid velocity; μ [Pa·s] is the fluid viscosity; and γ [N/m] is the interfacial tension. The droplet based microfluidic system features by the high surface to volume ration and low flow velocities, and the role of inertia and gravity is not significant compared with the viscous force and interfacial tension. To study the manipulation and control of two-phase flow, more focus will be on the Capillary number other than the Grashof, Bond, Reynold and Weber numbers. The Capillary number is the competition between the viscous force and interfacial tension. The viscous force tends to elongate the interface, while the surface tension is working to minimize the surface area.

Droplet formation is often categorized into different regimes based on the Capillary number. Some other dimensionless number such as viscosities ratio, and flow rate ratio also influence the droplet motions.

Table 2.1. Summary of the dimensionless number

Dimensionless	Definition	Equation	Scaling
Grashof	Buoyancy/viscous	$\frac{L^3\rho^2\beta\Delta T}{\mu^2}$	3
Bond	Graitational/Interfacial	$\frac{L^2\Delta\rho g}{\gamma}$	2
Reynolds	Inertia/Viscous	$\frac{\rho UL}{\mu}$	1
Weber	Inertia/Interfacial	$\frac{\rho U^2 L}{\gamma}$	1
Capillary	Viscous/Interfacial	$\frac{\mu U}{\gamma}$	0

Two-phase droplet based microfluidic system shows great difference in macro and micro scales. In micro scale, the close proximity of the walls strongly influences the fluid dynamics. Droplets confinement suppresses hydrodynamic instabilities from forming, and also influences on the global pressures and flow fields. To realize the analytical approximation, the scaling arguments are performed based on a balance of drag, and viscous force, as well as lubricant theory for fluid flow [60, 61].

Interfacial tension wetting surfactant

As discussed above, Capillary number is significant in micro scale two-phase flow system. Interfacial tension becomes a dominant property when the length scale is reduced to the micro scale. When two immiscible fluid flows are generated in the microchannel, two interfaces between fluid-fluid and fluid-wall arise. The origin of the stability and definition of the droplets lies in the interfacial tension. And this is one of the improvement for two-phase flow system over the single-phase flow [61, 62]. Interfacial tension arises because of an imbalance of forces on fluid molecules near the interface when two immiscible phases come in contact. Interior molecules are completely surrounded by molecules of the same type. However, at the interface the molecules are exposed to both phases and the attractive force of its own molecules creates a net force that draws the molecules inwards. This force is in turn balanced by the fluids resistance to compression. As a consequence of the force balance, the interface attempts to minimize its surface energy by reducing interfacial area and ends up taking on a spherical shape. And this spherical shape results in a pressure difference across the interface which is the Young Laplace pressure. It can be written as $\Delta P = \gamma * (\frac{1}{R_1} + \frac{1}{R_2})$. ΔP [Pa] is the pressure difference across the fluid interface. The γ [N/m] is defined as interfacial tension. R_1 [m] and R_2 [m] are the radius of curvature [63].

Wettability should be put in considerations because a good wetting condition is important for the droplet motion. There are normally two wetting conditions. One condition refers to one liquid perfectly wets the wall and separates the other liquid from the wall. The other one is both liquids partly wetting the wall with an equilibrium angle. The contact angle between the fluids with the substrate represents its wettability. Figure 2.2 [64] illustrates the contact angle

between three phases, which are solid, liquid and vapor. Young's equation is used to show the nature of their relationship. Because of the close proximity of the walls to the liquid, the wetting condition plays an important role in the droplet formation and manipulation. With a low wetting condition, droplets can get stuck as the two phases flip between the wetting walls and device operation is completely irreproducible. With a good condition, where the continue phase perfectly wets the channel wall, there is a thin film between the wall and disperse phase, which helps to lubricate the motion and prevent the cross contamination. PDMS is widely used for microfluidic chip and hydrophobic naturally. It turns to hydrophilic after the plasma treatment for bonding which is unideal for the droplet formation. Several methods including the thermal method, chemical method can be applied to turn it back to hydrophobic [46, 65, 66].

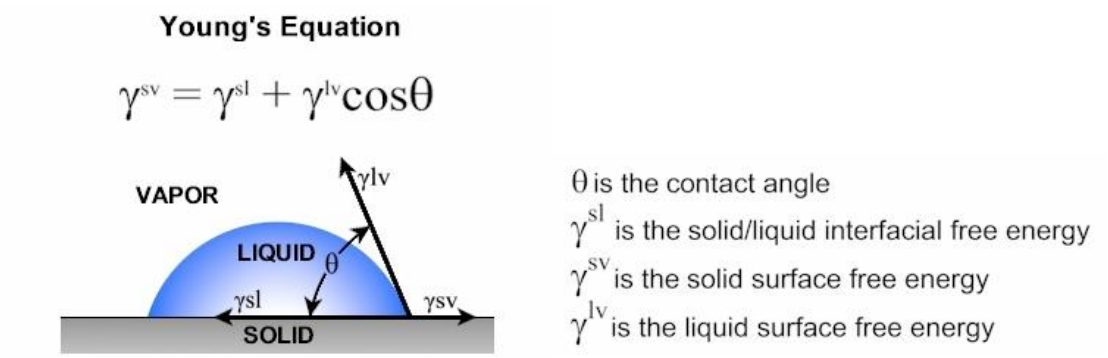

Figure 2.2. Young's Equation [64]

Surfactant

In droplet based microfluidic system, surfactants are added to system to generate stable droplet and stabilize droplets against coalescence [67]. With the surfactant added in the microfluidic device, interfacial tension can be greatly lowered. The critical micelle concentration (CMC) is an

important term for surfactant above which micelles form and additional surfactants added to the system become micelles. To have a stable interface and avoid the surface tension gradients at the interface, the surfactant concentrate should be above the CMC.

2.3. Droplet manipulation

2.3.1. Droplet generation

The starting point for droplet based microfluidic system is the droplet generation. When the continuous phase fluid and disperse phase fluid are injected into the microchannel, droplet can be generated when applying the suitable experimental condition. Based on the mechanism of generation method, it can be categorized into passive methods and active methods [31]. Among those methods, passive methods always make the use of the change of the pressure or the structure of the microchannel to manipulate the droplets. Besides, active methods employ the external source to influence the droplet motion [35].

Passive method

Among the passive methods, there are typically three different channel structures used in microfluidics which are T-junction, flow-focusing and co-flowing [27], shown in Figure 2.3.

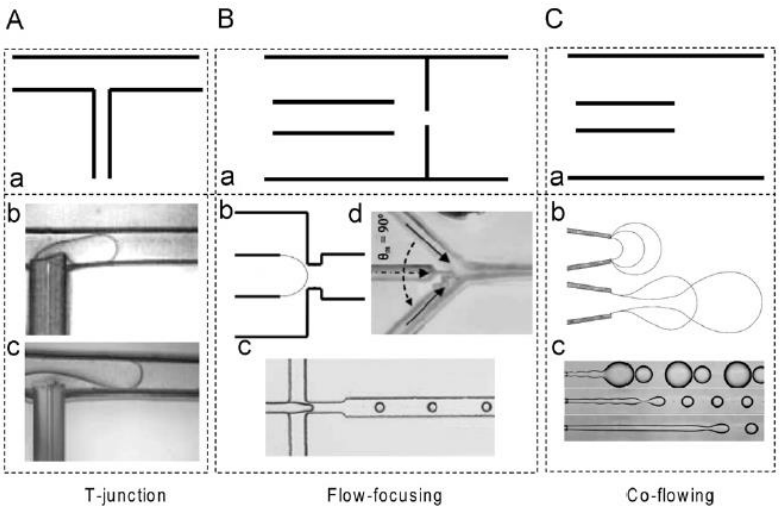

Figure 2.3. Three structures of generators A: T-junction B: Flow-focusing C: Co-flowing. Lowercase a is the sketch of each structure. Lowercase b and c show the different design or regime of these generators [27].

T-junction structure for droplet generation has been widely used since 2001 [26, 66]. The continuous phase and disperse phase are injected from two different channel which are perpendicular to each other. Droplets are generated at the two phase interface as a result of the shear force and interfacial tension. The generation process including the droplet size and frequency is determined by the flow rate ratio, viscosity ratio, and channel size [26]. The geometry of T-junction is shown in Figure 2.3-A.

The flow focusing structure in Figure 2.3-B has always been used to generate the spherical monodisperse droplets [68, 69]. Different from the T-junction, there are three main channels involved in the generation process. The disperse phase is injected in the middle channel and the continuous phase is injected from two vertical channel to squeeze the disperse phase. The disperse phase then becomes narrow and forms droplets because of the shear stress at the orifice. In compaction with the T-junction, droplets are usually generated in the flow focusing structure instead of the plugs due to the confinement of disperse phase in the main channel [26]. The

generation process including the droplet size and frequency is also determined by the flow rates ratio, viscosity ration, and channel size.

Co-flowing design in Figure 2.3-C is another method to generate the monodisperse droplets for two-phase flow. Droplets are generated as the disperse phase injected from a needle or a capillary in to the co-flowing continuous phase [70, 71]. Droplets in the co-flowing device can be generated at the beginning of the capillary or far from the tubing.

Active method

The passive methods generating droplets are mostly based on the competition between interfacial tension and viscous stresses. Besides of passive methods, active methods can also be used for droplet generation. Compared with the passive method, active methods tend to provide more control over the droplet generation by applying external energy to facilitate interfacial instabilities for droplet generation [31]. There are more flexibility to adjust droplet size and production rate and there are chances for some cases to realize on demand droplet generation. Active methods usually are employed to induce droplet generation either by apply external force or by using external source to change intrinsic force [31]. External force can be added to the microfluidic system by using external elements to produce electric and magnetic field [72-75]. Tan et.al have utilized electrodes with high frequency AC control to realize droplet generation and enabled the droplet to be generated at milliseconds [76]. The thermal control technique is straightforward to change fluid properties including interfacial tension or viscosity and achieved using the integrated microheater to induce temperature change [39, 77]. Optical methods can also provide methods to disturb the interface by induce fluid pressure change or change interfacial tension [78, 79]. Park et.al. used the laser to induce rapid cavitation bubble to change fluid pressure and thus generate

high throughput droplets and in this process droplet size and generation rate can be tuned by adjusting laser position and power [78]. Cordero et al. have reported the use of a laser beam to generate different optical patterns that were able to localize heating at the desired locations for generating and directing droplets [79].

2.3.2. Droplet mixing

Droplets are not only used as a carrier for material but also served as a reactor [80, 81]. Rapid mixing inside the droplets is crucial for many microfluidic applications including chemical reaction and biochemical synthesis [82, 83] with the help of accelerating the reaction rate and increasing the reaction efficiency. As discussed before, single phase flow is limited by the low efficient mixing, and mixing is a big challenge in microchannel to overcome the interfacial forces. It has been reported that the rapid mixing is based on chaotic flow [2] and turbulent flow [84]. However, in droplet based microfluidic devices, the flow is always characterized by a low Reynolds (Re) number due to the dominance of viscous forces and laminar flow [2, 83, 84]. Molecular diffusion usually dominates mixing in microfluidics, which is a slow and inefficient process [2].

Passive method

Benefit from two-phase flow, droplets in the microchannel can achieve the equal recirculation vortices and mixing happens in each half inside the droplets. However, each half in the droplet remain unmixed. To achieve the internal mixing in droplets, the passive methods tend to generate the chaotic flow by varying microchannel structures. Passive methods provide a simple way to achieve the mixing inside the droplet by making the channel geometry complex, for example the

Zig-zag structure [85], serpentine design [19], or with grooves [86] or blocks [87] on the bottom wall. The chaotic advection is achieved due to the different circulation in different half of the droplets. For the half close to the inner arc of the serpentine channel, the circulation is smaller compared with the other half. And many simulation work related to the passive methods for mixing are presented, for example Muradoglu et al. studied the mixing process in the microchannel with a sinusoidal mixer and analyzed the influence of Capillary number (Ca), viscosity ratio, droplet size and Re number on mixing [83]. Wang et al. focused on analyzing the detailed mixing mechanism of droplets in the serpentine structure [88]. They demonstrated that the asymmetrical circulations led to the occurrence of fluid reorientation and the best mixing performance happened when droplet size was comparable with the microchannel geometry.

Active method

Active methods cause the droplet mixing based on the same principle as passive methods - inducing the chaotic flow. In our group, microwave induced thermal-capillary mixing has been achieved. This microwave heating induces non-uniform Marangoni stresses on the interface, which results in three-dimensional motion inside the droplet and thus fast mixing. Here is another promising method for mixing, which is alternating, preferably periodical switching of the flow from a high to a low flow rate [89]. By using this method, the mixing is achieved by a pulsation of the whole stream. The acoustic method has also been employed for promoting the mixing in microfluidic system. The air bubble in the liquid medium could serve as the actuator, and when acoustically driven, the membranes (liquid/air interfaces) of these trapped bubbles started to oscillate [82, 90]. The strong pressure and fluctuations of velocity are induced by the bubble oscillation, which results in the fast mixing of the flowing fluids. The electrowetting is also

developed for mixing inside the droplets. The multiple electrode arrays are used to improve the effective for merging droplets to lead a fast mixing [91].

2.4. Applications

Droplet microfluidics has grown to be a hot topic in the past decades and there is a growing number of published papers regarding to droplet microfluidics [9]. In droplet microfluidics systems, they hold the promise to provide a platform to carry out the conventional chemical or biochemical processes in individual droplets. A big mass and thermal transfer rate due to high surface to volume ratio allows a high reaction efficiency and the small scale footprint enables the portability of the entire systems and the reduction of sample use. These offer droplet microfluidics much potential to be used for chemical and biochemical applications.

One of the wide-use applications for microfluidics is the polymerase chain reaction (PCR). A PCR process is an enabling technology for biological applications to amplify DNA with high efficiency at certain temperature. Conventional PCR process is carried out in a bulk device which is limited by spatial constraints and a slow thermal ramp rate. It also suffers from the disadvantages about sample preparations, which needs to isolate purified nucleic acid templates from a population of cells [37]. This process increases the risk for sample loss and contaminations. Droplet microfluidics have dominated advantages to be used as platform for PCR, which even better than other microfluidic system like single phase microfluidics. Droplet microfluidic is able to use less sample volume and shorter reaction time to carry out PCR due to the reduction in thermal mass [37]. Each individual droplets isolated by carrier fluid can avoid the cross contamination. Droplet microfluidics can also offer efficient mixing and rapid heating methods to benefit the PCR process and integrated sensors in droplet microfluidics can be used for diagnose purposes. Hindson et al.

have present a high-throughput droplet digital PCR (ddPCR) system, which is able to process about 2 million PCR reactions using TaqMan assays and a 96-well plate workflow [92]. Schuler et al. demonstrated an integrated system which is compatible to mass fabrication and combines emulsification, PCR and fluorescence readout in a single chamber [38].

Droplet microfluidics can also be employed to carry out tasks for life science research. Each droplet is separated and protected by carrier oil and is the functional equivalent of an independent culture for cells [93]. Droplet microfluidics used for cell culture can compete with tradition 96 or 24-well plates due to low risk for contamination and sample use. In each droplets, encapsulated cells can stay viable for design periods and additional cell-based assays can be carried out on chip [8]. Yu et al. have developed a droplet microfluidics system which can be used to form alginate beads with entrapped breast tumor cells [94]. Zhao et.al exhibited a work to realize droplet based 3D cell culture method with droplet array attached on the sidewall of a PDMS piece. The realization of this 3D cell culture avoid cells from adhering on the chip surface and also allow many operation to be performed on chip [95]. Schlicht et al. have utilized droplet microfluidics systems to produce artificial lipid bilayers. This platform allow the controlled positioning and storage of droplets and is able carry out on chip droplet-interface-bilayer assays to mimic cell membrane processes [96].

Droplet microfluidics can also take the tasks to carry out materials detection with low sample amount use, small devices and precise liquid handling [97]. Droplet microfluidics can offer a compact and miniaturized system to detect droplet contents with integrated sensors or detection devices such as mass spectrometry, fluorescence spectrometry, and Raman spectrometry [98-100]. Kim et al. have developed 4-cyno-4-pentylbiphenyl droplets used for glucose detection. The

functionalized droplets can detect glucose at concentrations as low as 0.3 mM in about 3 min and show a good selectivity towards galactose [101]. Hsieh et al. have reported a DNA detection methods based on droplet microfluidics. This work is able to capture the mutants and dynamic hybridization process of DNA relying on a fluorescence resonance energy transfer biomarker, Molecular beacon (MB). The detection is based on analyzing the change of the FRET signal of MB-DNA duplex. The presence of target DNA can be detected within seconds using this methods.

There are other applications based on droplet microfluidics including imaging, drug deliver, enzyme kinetic analyzing [7, 102-104]. Droplet microfluidics tend to play more and more important roles in many areas of science research and practical applications. Therefore more advanced functions and technology are required to be developed for droplet microfluidics to meet the new requirements and challenges.

2.5. Heating in microfluidics

The development of microfluidics system aims to construct it a platform for many chemical and biochemical applications. As we have discussed in last part, sensing in microfluidics plays an important role for researchers to acquire materials information including speed, concentration, pressure or temperature to better control the entire process in microfluidics. Besides sensing of microfluidics, heating is another key function which is required for many applications. The utilization of PCR can duplicate DNA with high efficiency and is a crucial method for biochemical detection. The realization of PCR requires at least three temperature points, e.g. 95^{o}C, 65^{o}C, 73^{o}C, to precisely product duplicated DNA materials. As we have mentioned above, some active methods are employed to realize droplet microfluidics manipulation including generation, mixing or merging. Among those methods, thermal methods are used to induce materials change such as

interfacial tension, viscosity to realize droplet manipulation. There are some other applications in microfluidics systems which also requires a heating process to initiate or accelerate including thermal induced nanomaterials synthesis, temperature gradient induced electrophoresis. Traditional methods for droplet heating in microfluidic system always combine with the bulk external heating source including the laser technique [105], joule heating [106, 107], and macroscopic peltier elements [108] and endothermal chemical reactions [109].

2.6. Microwave Heating

Besides these methods for heating, the microwave method for droplet heating is a fundamentally different approach because of its preferential heating capability and non-contact delivery energy. Microwave is an electromagnetic wave and the frequency ranges from 0.3 to 300 GHz, corresponding to wavelength from 1 mm to 1 m [45]. Materials with different dielectric properties can be heated using microwave by converting electromagnetic energy to heat. Microwave heating for materials is based on the mechanism that molecules tend to align themselves with the applied electric field and thus cause the dipolar loss [110]. Microwave heating is volumetric and can selectively heating materials based on their dielectric properties, which means that microwave power is directly delivered to the fluid in the microfluidics device with little adsorption from the substrate material. Another unique advantages needs to mention is the faster heating rate and cooling rate. These allow microwave heating to serve as pulse heating, because heating stops once the power is off. Benefiting from the nature of inertialess, enhanced thermos-cycling rates and reduced reaction time are realized compared with traditional heating methods. Microwave heating has been used for PCR [111] and also employed by the measurement of enzymatic activity [21], investigation of the thermophoresis [5], chemical separation [11]. The integration of microwave

technology with microfluidics allows a fast and efficient heating method for small amount of volume fluids [112]. Shah et al. have utilized a thin film microwave transmission line in a coplanar waveguide configuration to be integrated in a PDMS based microfluidic device for heating purpose. The fluid passing through the selected microchannel region can be heated at a rate of 95°C mW−1 at 15 GHz frequency [113]. Issadore et al. have demonstrated a work to use microwave to heat individual droplets based on the unique character of microwave, which can selectively heat materials [45]. The key parts for their system include a flow-focusing microchannel structure for generation, and metal electrodes which receives microwave power from a commercially available source and amplifier. A temperature rise of 30°C can be achieved within 15 ms by using this demonstrated method. To fully realize the potential of microwave heating in microfluidic systems, Shaw et al. have presented a work to carry out PCR relying on microwave heating in microfluidic systems [114]. In the heating system with air impingement for cooling, it can realize a heating and cooling rate up to 65°C/s. And as PCR requires very precise temperature control, in this work the temperature can be accurately maintained within 0.1°C when reaching target temperature. This microfluidic with microwave heating system allows 28 cycles PCR in 42 minutes. Koziej et al. have demonstrated a microwave heating method in microfluidic system to heat non-aqueous droplets at frequency 700-900 MHz [115]. A highest temperature of 50°C can be achieved in 15 ms. In this work, an infrared camera is used to record the microwave heating process and shows the dielectric heating process. This work lights up the way for synthesis of metal oxides in microfluidic systems by heating of benzyl alcohol droplets. The authors demonstrated the utilization of this microwave heating methods for metal oxide nanoparticles synthesis, achieving crystallization of tungsten oxide nanoparticles and remarkable microstructure, with a reaction time of 64 ms.

2.7. Sensing in microfluidics

Sensing in the droplet based microfluidic system is an important part which helps to identify the droplets and acquire droplet information such as concentration or temperature. In the previous section, the methods and mechanism for the droplet manipulation and motions are introduced. As the development of microfluidics, to fit the requirements for multiple applications related to the biochemical engineering and chemical engineering using microfluidics, there are needs for people to develop sensing methods to detect materials contents in microfluidics systems. So far, a lot of methods have been listed as electrical and optical methods [116].

Among those methods, optical methods are widely used for sensing microfluidics. Optical methods tend to rely on the materials with specific optical properties and track optical signal change including fluorescence intensity, UV intensity, refractive index, light adsorption, color change, and ramen intensity. For fluorescence methods, the fluorescence dye with a fluorescence microscopy is employed as marked and visualized tool for optical methods. The detection is based on the interaction of fluorophore and analyte, which leads to a change in the physicochemical properties of fluorophore including fluorescence intensity, lifetime and anisotropy. Alizadeh et.al have purposed a method for fluorescent sensing of dopamine (DA) with high selectivity and sensitivity by using self-synthetized polymer dots (Pdots) [117]. The synthesized Pdots shows a strong fluorescence intensity, and the addition of DA can trigger a remarkable fluorescence quenching based on inner filter effect and static quenching effect. They finally realize a detection range for DA from 0.001 μM - 900 μM. For further application, this detection method can be used for inaging DA in single living PC_{12} cells based on droplet microfluidics systems. Rane et al. have utilized a peptide nucleic acid fluorescence resonance energy transfer (FRET) probe to detect the

existence of 16s rRNA in pathogenic cells [118]. The detection is based on a droplet microfluidic chip to realize the amplification-free detection of single pathogenic cells. The realization of their work with pathogen samples with intact pathogenic cells shows the promise for clinic diagnostic with this platform. Streptavidin-biotin has a strong binding performance and it is always important to understand the kinetics of this reaction. Srisa-art et.al present a study to investigate the streptavidin−biotin binding kinetics in a droplet microfluidic platform [119]. In the experiments, Alex Fluor 488 is conjugated with streptavidin to serve as energy donor and the acceptor is Alexa Fluor 647 with biotin. The binding kinetics between streptavidin and biotin are observed and investigated through FRET. Surface enhanced Raman scattering (SERS) is a surface-sensitive technique. Raman scattering can be strengthened by either materials with nanostructures or molecules adsorbing on rough metal surfaces [120]. The combination of SERS and microfluidics system can not only improve the SERS performance because previous SERS process are performed on a large scale in the laboratory with human error, now can be applied in microfluidics with automatic and reproducible manner, but also offer a sensitive optical sensing methods for small amounts of materials. Gold nanoparticles and Mercury ions have a strong binding performance which can contribute to SERS sensing. Wang et al. have demonstrated that using this method to detect Hg^{2+} in a droplet based microfluidic system [120]. The detection of Rhodamine B (RB) SERS signal is carried out under the presence and absence of Hg^{2+}. When RB molecules are adsorbed on gold nanoparticles, there is an enhancement in the SERS signal. But as the involvement of Hg^{2+}, some of the RB molecules are released from Au-NPs resulting in a decreasing in SERS signal, and this is related to Hg^{2+} concentration. Raman spectrum is sharp and easy to resolve, which makes it really convenient to analyze sample content and realize a limit of detection (LOD) 500 ppt by using this approach.

Electrical methods are another common methods being used in microfluidic systems, which deal with the electric signal instead of optical signal. In the past decades, tons of literature which are related to heavy metals detection using electrochemical methods in microfluidics devices have been published [44, 121]. The mechanism is based on the movement of electrons on the electrodes surface. Electrical signal is detected to distinguish heavy metals ions based on their different redox potential using electrochemical methods [122-124]. Subramanian et al. have demonstrated to use a microfluidic device with radial structure allowing electro kinetic preconcentration by ion concentration polarization (ICP) and coupled with an electroactive surface for Arsenic sensing [125]. There are two steps for arsenic sensing here starting from giving a stipulated external DC voltage to the platinum wire put in the micropipette tip with sample to induce ICP. Linear sweep voltammetry for electrochemical sensing is operated after the ICP procedures in order to reduce the noise effect from ICP procedure on the working electrode for electrochemical sensing process. Finally 1 ppb LOD is achieved using this method for Arsenic detection. Elbuken et al. have purposed a method to detect the presence of droplet, droplet size and speed using capacitive sensors based on microfluidics devices [41]. Coplanar electrodes are employed to integrate with microfluidic channel and to form a capacitance. When a droplet passes through the sensor areas, the resulted change in the capacitance is monitored and used to determine the droplet size and speed. The single pair electrodes and interdigital finger design are used for the detection of the presence of droplets, and size and speed of droplets respectively. In this designed system, cross-contamination between droplets is avoided by applying a passivation layer between the sensor electrodes and microchannel. Yoon et al. have reported a capacitance based sensing method in microfluidics platforms which can be used for multimodal sensing performances [126]. The sensors are designed to detect localized pressure and ambient temperature changes. Ionic liquids

are employed to fabricate microfluidic capacitive sensors as electrodes and a carbon nanotube and PDMS composite is served as a dielectric layer. The sensors with microfluidic platform are then applied to a bottle and human skin to monitor the variation of pressure and temperature. This whole system offer a promise and strategy for future related applications such as wearable monitor devices and soft robotics.

2.8. Microwave sensing

Besides the methods mentioned above, microwave technology for sensing draws a lot of attention which can be combined with microfluidic systems for sensing purposes. As showed in the last sessions, optical and electrical sensing methods have been utilized to integrate with microfluidics for many applications. However there are still spaces for improvement which can be addressed by microwave sensing. For optical methods, they require bulk and expensive devices which rise the challenges for in-situ and real time detection. Also some methods need to optical markers to observe optical signal changes but it will bring some uncertainties especially in harsh environments.

Microwave can provide a way to sense materials with advantages over other methods. Microwave sensing requires no physical contact with the target materials for sensing which can reduce the risk for cross contamination in microfluidic systems [11]. Also, microwave sensing can realize label free detection, meaning chemical modification with materials like biomarkers are not necessary [127]. And it also features by the low power requirement, portability and compatibility with microfluidics [128, 129]. Many microwave device structures have been employed for sensing job including the transmission lines [45], planar structures [130, 131], and split ring resonators [47]. An eighth-mode substrate integrated waveguide antenna with microfluidic channel is presented by

Seo et al. [132]. The demonstrated sensor can be used to detect ethanol with concentration from 0% to 100% corresponding the resonance frequency from 4.2- 4.6 GHz. The relationship of resonance frequency and ethanol concentration is achieved for tracking ethanol concentration. Krivosudský et al. have demonstrated the use of microwave sensing in biochemical fields [43]. The self-assembly process of nano materials is of prime importance for biochemical research. By utilizing microwave sensor integrated in a microfluidics device, the tubulin self-assembly process at the molecular level can be label-free monitored. And this microwave-microfluidic system uses coplanar waveguide transmission line structure and allow a sample use less than 30 nL. Liu et al. have utilized a microwave hairpin resonator to detect biological cells fabricated and integrated with microfluidics [133]. The detection is performed by using a hairpin resonator to get the relationship between S-parameters and the number of cells. And a model in terms pf capacitances is set up to analyze the effects of culture medium and cells. This work shows the opportunities for microwave methods to detect cells numbers. Split ring resonators (SRR) have shown a strong localization and enhancement of fields so that they can be used to actually improve the sensor selectivity to enable detection of extremely small amounts of samples. Abduljabar et al. has developed the microwave microfluidic sensor for detecting the dielectric properties of the common liquids [134]. The resonator contains two gaps and are both compact and planar. They also used the microwave sensors to measure the length, volume, speed and dielectric properties of different liquids in a segmented flow. The detection is based on the changes of the resonant frequency and quality factor when a segment enters the sensing region. In this work, the numerical simulation using COMSOL software was also exhibited and the sensing results met with the experimental data [135]. Rowe et al. has provided a modification of making SSRs for microfluidic sensing using silver-coated copper wire [48]. The square cross-section wire they use could offer great electric

field confinement in the capacitive region, thus improve the performance of the SSRs. Zhang et al. has demonstrated the potential of microwave frequencies for biological analysis and cell discrimination [136]. They present the work using microwave resonators as biosensors to measure individual cell dielectric permittivity and get characteristic signature as a function of cell type. Torun et al. has developed an antenna-coupled split-ring resonator used as microwave sensor for bio-sensing application [137]. The sensor consists a metallic ring with a slit and integrated monopole antenna on top of a dielectric substrate. Sharafadinzadeh et al. have compared the performance in terms of sensitivity for three different split ring resonators [138]. The three regular sensors including implemented in complementary split ring resonator, extended gap split ring resonator, and conventional circular split ring resonator are discussed with resonance frequency at 1.7, 1.9, and 3.6 GHz, respectively. The results show that the circular resonator has the good sensitivity in terms of sample volume and is able to improve 50% sensitivity for permittivity range from 1 to 30. Lee et al. proposed a split-ring resonator at microwave regime for DNA sensing [139, 140]. In this study, double SSR is used and one at close proximity to the microstrip line offering excitation with magnetic field. The second split ring is placed inside the outer ring to increase the capacitance in the small gap. Microwave sensing methods have been applied as diagnostic tool and offered quantitative detection results. Zhou et al. have come up with the design of low cost membrane compatible split ring resonators to integrate with microchannel in flexible strips [141]. The microwave sensor is based on an immunochromatographic strip and microwave sensing with the existence of target molecules can cause a microwave resonance frequency shift. The detection target is Staphylococcus aureus and the detection limit can be reached as 0.784 ng/mL, which is great improvement compared with color based strip method.

In recent years, more and more applications rely on the sensing to perform more operation for droplet microfluidics. As a promising sensing method, microwave technology provides novel opportunities for a lot of on-chip research. However, they also face a lot of challenges. For example, the fluctuation phenomena will result in the noise appearing in the signal output which finally influence the sensor performance. More fundamental mechanism is needed to decrease the influence of the noise. In addition, the sensitivity and accuracy of the microwave sensors needs to be improved which require more advanced fabrication methods. Besides these, the combination of the sensing technology with other functions also draws people's attention. The sensing technology could serve as the tool to realize the intelligent feedback control of other microfluidic functions. The integration of this multiplex system need to be solved.

Chapter 3 : Methodology

In this section, the experimental methodology is presented including the fabrication and observation protocol. The experimental devices and samples used in the experiments are also introduced. For numerical simulation, the methodology for the simulation work is also exhibited in this section.

3.1. Microfluidic chip fabrication

The fabrication of microfluidic chip is based on the soft-lithography technology. The soft-lithography was firstly developed by Xia et.al in 1998, which provided an inexpensive and simply way to fabricate microfluidics devices [142]. The polydimethylsiloxane (PDMS) material possesses a good thermal stability and is optically transparent which is really suitable to work with microscope to observe the microfluidic process. In addition, the surface properties of PDMS can easily be tuned either to hydrophilic or hydrophobic which makes it universal for multiple applications.

The first step for microfluidic chip fabrication is carried out in AutoCAD software by designing the microchannel structure. The designs are then printed in Mylar film for next step use to pattern with the silicon wafers. The silicon wafers are coated with negative photoresist by using spin coater. The first step is to coat a thin layer onto the silicon wafer using Su-2005 to create a photoresist substrate. Then different kinds of photoresist are used for different height of channel, for example, Su-2025 is spin coated at a rate of 1350 rpm to create a channel height of 40 μm. After the spin coating, the silicon wafer is baked in two hot plates at 65^{o}C and 95^{o}C respectively to solidify the layer. The baking time varies from desired microchannel height. Next, the baked wafer is put into

the UV machine for exposure with the designed pattern film on top of it. Then it is required experience the baking process again and followed by the washing process by photoresist developer. The completed mask needs to be stored in a dark and dry place to maintain its quality.

To fabricate microfluidic chips, PDMS is mixed with the curing agent at 10:1 ratio. After degassing in the vacuum oven, it is molded against the master and cured for at least one hour. The mold is then peeled off from the master, and the fluidic pass-through hole is punched using 1.5 mm biopsy punch. The PDMS mold and the glass slide integrated with the resonator are treated with a plasma machine at 29.7 W, 500mTorr for 2 min. Immediately remove from the plasma machine, the mold and the glass slide are bonded together to localize the resonator in the microchannel. The Aquapel (PPG Industries) is then injected to the microchannel to change the surface property to hydrophobic. It is a crucial part to make sure the channel wall is perfectly wetted by the oil. An SMA connector is then soldered to the resonator to connect to the external microwave signal generator or vector network analysis. The fabrication schematic is shown in Figure 3.1.

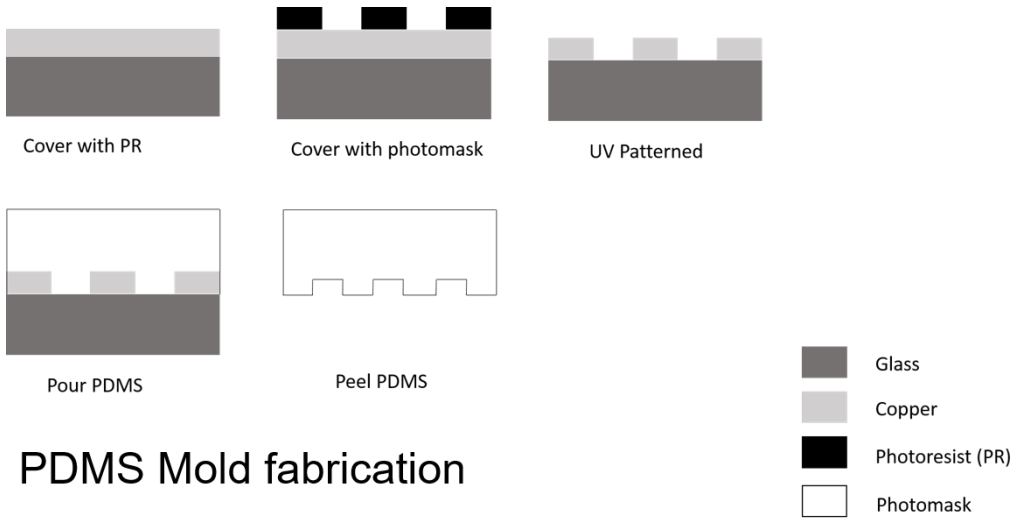

Figure 3.1. Schematic of PDMS mold fabrication

3.2. Resonator fabrication

To fabricate the microwave resonator, it is a combination of the photolithography technique and electroplating. The positive photoresist S1813 is spin-coated onto the cooper coated glass (EMF Corporation) slide at 2000 rpm for 60 s following the baking in hot plate for 120 s. The resonator design then patterns in the slide with the UV exposure. After developed in the negative photoresist developer MF-319, the glass slide is immersed in the electroplating solution (0.2 M $CuSO_4$, 0.1 M H_3BO_3, and 0.1 M H_2SO_4) and electroplated at 2 mA for 5 min, 4 mA for 5 min and 7mA for 10min. After the electroplating, photoresist is removed by acetone and $FeCl_3$ is used to remove the copper base. The resonator structure is then checked under the microscope to ensure that all the residues have been washed away. The fabrication schematic is shown in Figure 3.2. For storage, S1813 photoresist is coated at the resonator at 2000 rpm for 60 s to prevent oxidization. To prevent the potential for contamination and short circuit of microwave resonator, a thin PDMS layer is coated on top of the microwave components to serve as a passivation layer before bonded with PDMS chip.

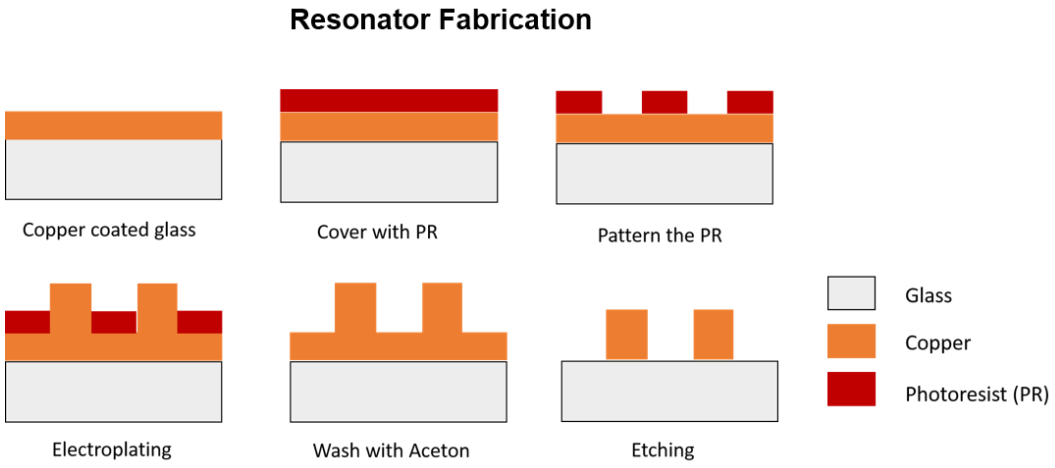

Figure 3.2. Schematic of microwave resonator fabrication

3.3. Experimental setup

The microfluidic pressure control system (Fluigent MFCS-8C) is used to control the fluid. Fluids were connected to the device by ETFE tubing (Tefzel, Upchurch Scientific). Fluids are connected to the device by ETFE (ethyltrifluoroethylene) tubing (Tefzel, Upchurch Scientific). Droplets are observed by using an inverted epifluorescence microscope system (Eclipse Ti, Nikon) equipped with a CCD camera (Qimaging). The video result is analyzed by the ImageJ (National Institute of Health, MD, USA) and PhotoShop (Adobe, USA). The Labview software (National Instruments) will be served as the control system and create computer interface. For the sensing and heating part, vector network analyzer (VNA) (MS2028C, Anritsu) is used to detect sensing and signal and a microwave signal generator (HMC-T2100, Hittite) is used to provide power for microwave heating. A portable NanoVNA is employed for microwave sensing experiments. The picture of the experimental setup is shown in Figure 3.3.

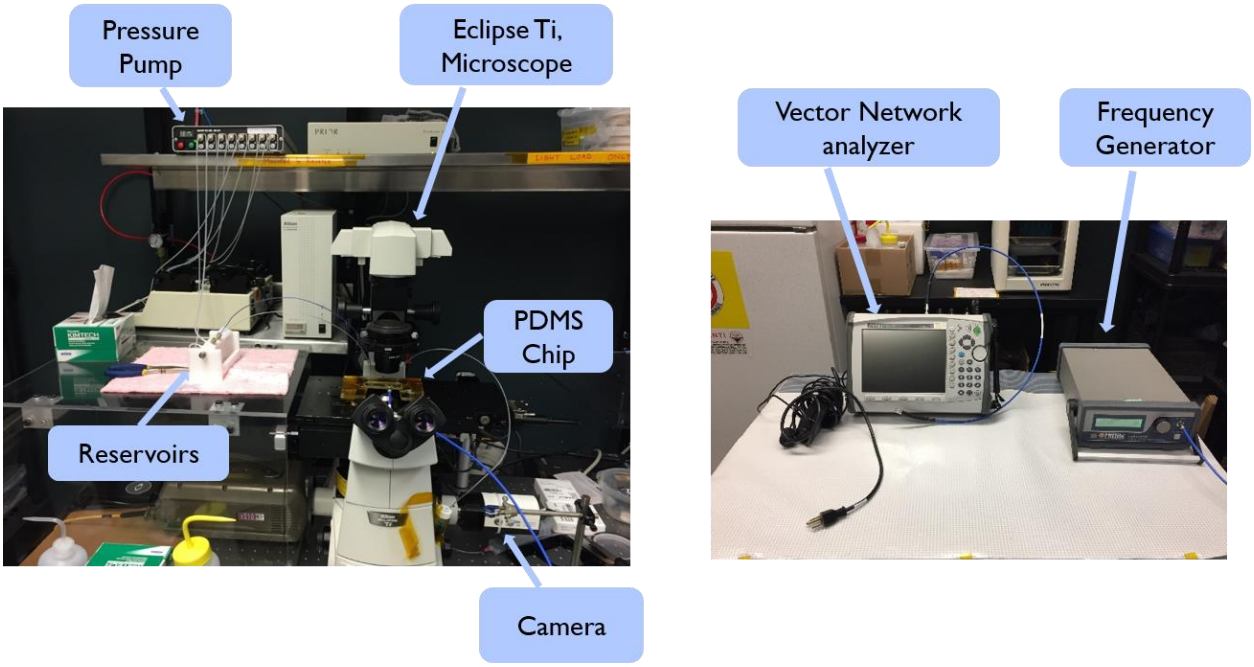

Figure 3.3 Experimental Setup

3.4. Numerical methods in Ansys Fluent

Geometric conditions and fluid properties

For Chapter 4, the channel width and height are 200 [μm] and 50 [μm] respectively and the largest diameter of the spiral microwave resonator is 200 [μm] with the gap and metal trace width both being 20 [μm]. The drop fluid is Deionized (DI) water and the carrier fluid is a fluorocarbon oil (FC40), a fluorinated oil. A fluorescent dye of 100 [μM] was doped with half of the droplet to visualize the mixing between the two halves of the droplet in the previous experimental study [46]. As the dye concentration is sufficiently low, its effects on the fluid properties are ignored. In the current numerical model, a user defined scalar is then used to describe the mixing process and can be regarded as a tracer concentration [84, 88]. The tracer is provided with the same diffusion coefficient as the fluorescent dye used in the experiments. Half of the droplet is filled with DI water while the other half is filled with tracer doped DI water. In reality, most fluid properties such as viscosity and interfacial tension are temperature dependent, and thus spatially and temporally vary within the droplet when temperature gradients are present. Their temperature dependences all contribute to the mixing through their influences on convection and diffusion, which have proven to be difficult to decouple experimentally. This numerical study, however, is able to evaluate the effect of each individual temperature dependent property on mixing performance while maintaining the rest of the fluid properties independent of temperature.

Governing Equations

The volume of fluid method (VOF) is used to simulate the flow field inside droplets. The VOF method belongs to the category of Eulerian methods that could effectively track and locate the

sharp liquid and liquid interface which is important for droplet microfluidics. The continuum surface model is a common method to carry out interfacial tension and is added to the momentum equation for the interfacial tension force [143]. Based on this model, the interfacial tension is treated as a body force and serves as the source term in the momentum equation. Phase change, viscous dissipation, and phase diffusion are not taken into consideration due to little effect on mixing between the two phases considered here, DI water and FC40 oil [88]. The four basic governing equations are:

Continuity Equation:

$$\frac{\partial \rho}{\partial t} + \nabla \cdot (\rho \vec{v}) = 0 \tag{3-1}$$

Momentum Equation:

$$\frac{\partial (\rho \vec{v})}{\partial t} + (\rho \vec{v} \cdot \nabla)\vec{v} = -\nabla p + \nabla \cdot \left\{ \mu \left[(\nabla \vec{v} + \nabla \vec{v}^{T}) - \frac{2}{3} \nabla \cdot \vec{v} I \right] \right\} + \vec{F} \tag{3-2}$$

Energy Equation:

$$\frac{\partial (\rho E)}{\partial t} + \nabla \cdot (\vec{v} \rho E) = \nabla \cdot (k \nabla T) + S_h \tag{3-3}$$

Convection and diffusion Equation:

$$\frac{\partial (\rho f)}{\partial t} + \nabla \cdot (\rho f \vec{v}) = \nabla \cdot (\rho D \nabla f) \tag{3-4}$$

where ρ [kg/m^3], $\vec{v}$[m/s], μ [$kg/(m \cdot s)$], $\vec{F}$[N], T [K], k [$W/(m \cdot K)$], E [J/kg], S_h [W/m^3], D [m^2/s] and f are the density, velocity, viscosity, body force, temperature, thermal conductivity, energy density, volumetric heat sources, diffusion coefficient and mixture fraction of the fluid,

respectively. For each cell in the mesh, the fluid properties such as density are calculated by a volume fraction average of all the fluids in the cell [144]. The force term in Eqn. (3-2) represents the interfacial tension force.

The density, viscosity, specific heat capacity and thermal conductivity of the dispersed phase at room temperature are $998\,[\mathrm{kg/m^3}]$, $0.00103\,[\mathrm{kg/(m\cdot s)}]$, $4178\,[\mathrm{J/(K\cdot kg)}]$ and $0.6[\mathrm{W/(m\cdot K)}]$, respectively. The diffusion coefficient of the user define scalar is $4.18*10^{-10}\,[\mathrm{m^2/s}]$. The density, viscosity, specific heat capacity and thermal conductivity of the continuous phase at room temperature are $1855\,[\mathrm{kg/m^3}]$ $0.0041\,[\mathrm{kg/(m\cdot s)}]$, $1100\,[\mathrm{J/(K\cdot kg)}]$ and $0.065\,[\mathrm{W/(m\cdot K)}]$, respectively. The specific heat capacity is used to calculate the specific energy via $\mathrm{E}=\mathrm{C}\Delta\mathrm{T}$. The interfacial tension is set as $0.052\,[\mathrm{N/m}]$ and the contact angle is $5\pi/6$ [46].

The Force Term in the Momentum Balance

The body force in the momentum balance $\vec{\mathrm{F}}$, represents the interfacial tension force, where the interfacial tension is carried out using the continuous surface model. The equations for calculating the force term are shown below, where σ is the surface tension coefficient, α is the volume fraction, i.e. α =1 or 0 for cell filled with oil or water respectively, ρ is the volume average density and κ is the free surface curvature with expression shown below and n is the normal vector to the interface between the two phases, ρ_c and ρ_d are the density of continuous and dispersed phase, respectively.

$$\vec{\mathrm{F}}=\frac{\sigma\rho\kappa\nabla\alpha}{0.5*(\rho_c+\rho_d)} \tag{3-5}$$

$$\vec{n} = \nabla\alpha \tag{3-6}$$

$$\hat{n} = \frac{\vec{n}}{|\vec{n}|} \tag{3-7}$$

$$\kappa = \nabla \cdot \hat{n} \tag{3-8}$$

$$\frac{\partial(\rho_c \alpha)}{\partial t} + \nabla \cdot (\alpha \rho_c \vec{v}) = 0 \tag{3-9}$$

Boundary and Initial Conditions for the flow field and concentration field

The schematic of the microchannel filled with aqueous droplets and its carrier fluid (i.e. oil) and the resonator is shown in Figure 3.4.

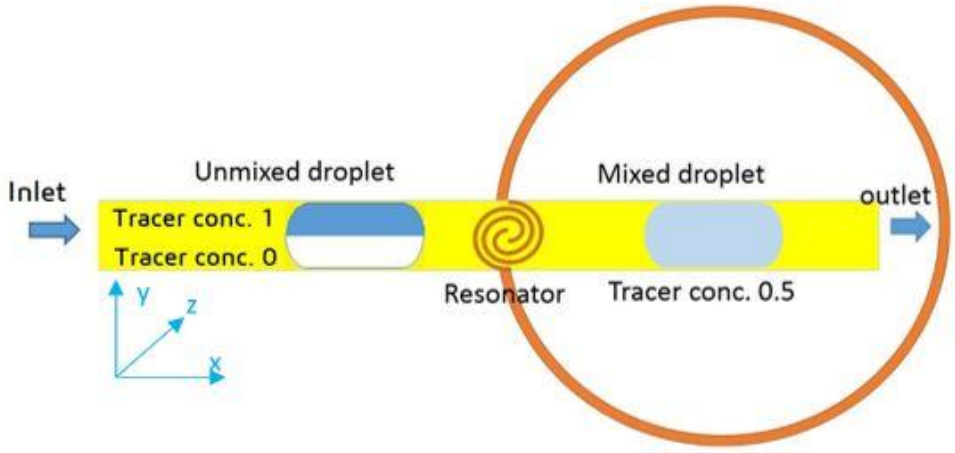

Figure 3.4. The schematic of droplet mixing model

Boundary conditions

The boundary conditions are set as follows. At the inlet, the velocity includes an average velocity of 4 [mm/s] in x-direction recommended by the previous experiments [46] and zero velocity in y- and z-direction; the temperature is room temperature set as 293.15 [K], and the tracer concentration

is zero because the inlet is only filled with the continuous phase and the tracer (i.e. the fluorescent dye used in the previous experiments [46]) is only present in the dispersed droplets. At the wall, the velocity is zero with no-slip boundary condition applied for impermeable walls; no flux condition is applied to the tracer concentration and no heat flux condition is considered for the energy equation considering the polymeric chip materials serving as an insulator for the channel.

At the outlet, a zero gauge pressure is applied because the outlet is normally a reservoir open to the air in the previous experiments and the zero flux condition is applied to the velocity, temperature and concentration.

Initial Conditions

The initial conditions are shown in Figure 3.5. In Figure 3.5 (a), it presents the phase distribution with red and blue representing the droplet and carrier fluid phases respectively. In Figure 3.5 (b), it exhibits the concentration distribution of the tracer with red representing the highest tracer concentration of 1 and blue the lowest concentration of 0. At the beginning, the top half of the droplet is filled tracer (red). The velocity components are $v_x = 4$ [mm/s], $v_y = 0$ [mm/s] and $v_z = 0$[mm/s]. The gauge pressure is 0 [Pa]. The temperature is set as room temperature 293.15 [K] for the entire model. All the variables are consistent in the Z-direction.

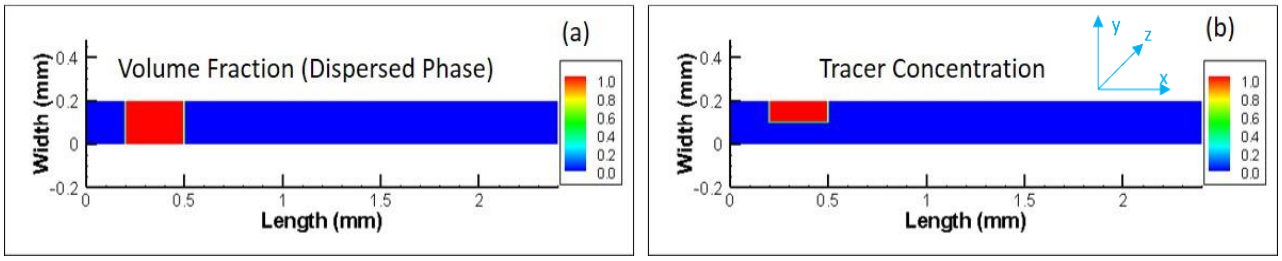

Figure 3.5. Initial conditions: (a) Phase distribution and (b) Concentration field.

Numerical details

For the VOF method, the coupled pressure-based algorithm is chosen because it allows more accurate results to be obtained than the segregate algorithm [144]. The second order upwind method is employed to calculate the momentum and energy equations. The second order implicit time-stepping formulation is used to deal with the transient formulation. The compressive interface capturing scheme is a high-resolution differencing scheme used to get accurate interface calculation results [145]. The mesh is generated by Ansys Gambit and contains 210 [K] cubic cells in our model with a cell size of 5 [μm]. Mesh grid independence analysis is carried out to reduce the effect of grid size on numerical simulation results and optimize computation time [10]. The residual criterion is 10^{-12} for the Energy equation, and 10^{-4} for other equations. The time step in the simulation is 0.1 [ms]. In the heating process, the temperature can rise from room temperature to 90°C. It takes about 100 [ms] to equilibrate after heating.

Flow and Energy Field Coupling

The flow field is obtained using Ansys Fluent. When a droplet covers the resonator region, it triggers the microwave heater to work and then starts to receive the energy induced by the microwave resonator characterized by the increased temperature within the droplet. The electrical field is numerically obtained using Ansys HFSS and then the deposited power within the droplet is calculated by

$$S_h = \frac{1}{2}\omega\varepsilon_0\varepsilon''|E|^2 \quad (3\text{-}10)$$

where $\omega[\mathrm{rad/s}]$ is the angular frequency, $\varepsilon_0[\mathrm{C/(Vm)}]$ is the permittivity of vacuum, ε'' is the imaginary part of the relative permittivity, and $E[\mathrm{V/m}]$ is the electric field. The deposited power

distribution in the droplet is imported as a source term in Eqn. (3-3), which is used to obtain the temperature field. The flow field and the tracer concentration distribution with temperature-dependent parameter are then obtained using Ansys Fluent, the latter of which is used to evaluate the mixing performance. The User Define Function (UDF) is integrated with the software to import the heat source to the droplet. The UDF also guarantees that the heating only works on the individual droplet and the surrounding fluid and chip material is unaffected.

Quantitative evaluation of mixing process

To quantitatively analyze the degree of mixing process and the influences of different physical parameters on microwave induced droplet mixing, mixing index (MI) is used in our work based on the following equations [82]:

$$\mathrm{MI} = 1 - \frac{\sqrt{\frac{1}{n}\Sigma(c_{av}-c)^2}}{c_{av}} \tag{3-11}$$

where n is the number of the calculated cells, c_{av} is the average concentration of the tracer, and c is the tracer concentration of each cell.

3.5. Numerical methods in Ansys HFSS

Model Schematic

Figure 3.6 (a) shows a schematic of the proposed microwave-microfluidic device, including a sensing resonator (resonator 1), and a heating resonator (resonator 2), fabricated on a glass substrate. The form of the experimental microfluidic system and the shape of droplets are also shown in Figure 3.6 (a). The designed microchannel is responsible for carrying the droplets and

the details of the microfluidic chip is shown in Figure 3.6 (b). The side view of our model exhibited the complex layers of the devices including the glass substrate, two resonators, a passivation layer separating the resonators from the microchannel molded in PDMS and the dashed lines sketching the electrical field line.

The key objective of this work is to numerically and experimentally investigate the impact of different design factors on the crosstalk between the two-resonators integrated in a microfluidic system. The influence of the distance between the two resonators (refer to as gap distance, d, in Figure 3.7), microwave power, and resonator design on crosstalk are investigated. To focus on the crosstalk, the design of the two resonators are considered to be the same. Numerical simulation in this work is served as a main tool to construct the chip model and investigate the crosstalk between the two resonators.

The numerical model is constructed in HFSS with two resonators illustrated in Figure 3.7. A microfluidic system with two identical resonators is designed and simulated, and the dimensions of the design are also included in Figure 3.7. The microwave signal is fed through the outer loop microstrip line, the ports connected to SMA connectors and coaxial cables. The inner loop is the SRR with a small gap, which is the hotspot of the resonator for sensing application. It is designed in a spiral shape to confine microwave energy and maximize its interaction with the microchannel aligned with the gap area.

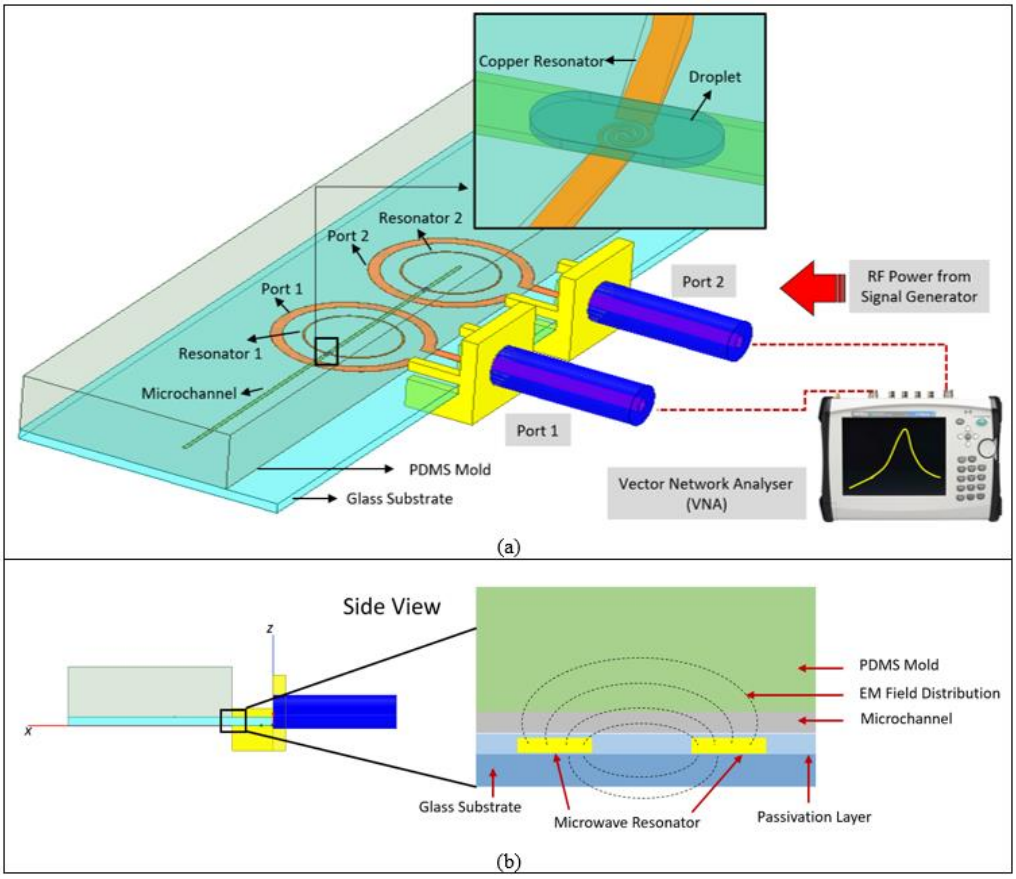

Figure 3.6. Schematic of simulation model and side view of the microfluidic chip of model.

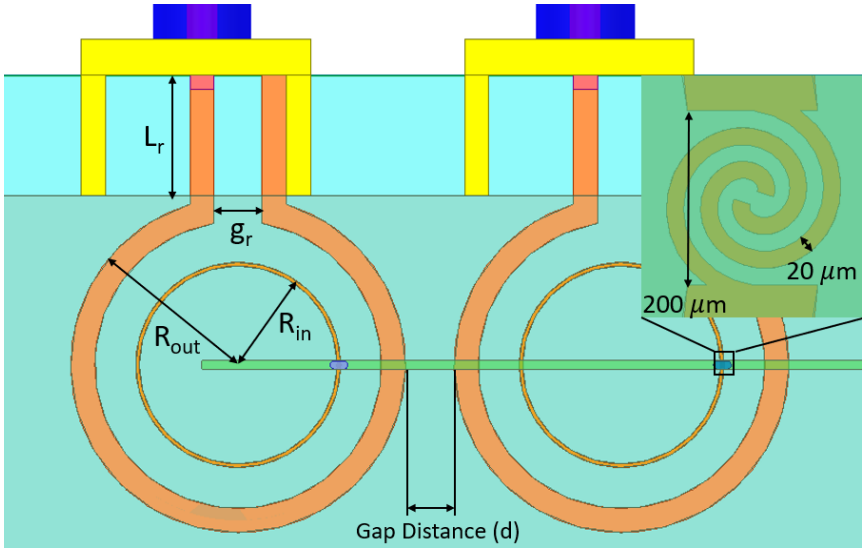

Figure 3.7. An illustration of studied parameters in this work.

Governing equation

Ansys HFSS will be used for the electromagnetic analysis. HFSS delivers 3-D full-wave accuracy for components to enable RF and high-speed design. The governing equations-Maxcell equations are listed below:

Gauss's law:

$$\nabla \cdot \vec{D} = \rho_e \tag{3-12}$$

Gauss's law for magnetism:

$$\nabla \cdot \vec{B} = 0 \tag{3-13}$$

Maxwell-Faraday equation:

$$\nabla \times \vec{E} = -\frac{\partial \vec{B}}{\partial t} \tag{3-14}$$

Ampere's circuital law:

$$\nabla \times \vec{H} = -\frac{\partial \vec{D}}{\partial t} + J \tag{3-15}$$

$\vec{D}$ [C/m2], $\vec{E}$ [V/m], ρ_e [C/m3], $\vec{B}$ [T], J[A/m2], $\vec{H}$ [A/m] are the electric displacement field, electric field, free electric charge density, magnetic flux density, free current density and magnetic field strength respectively.

Boundary conditions and numerical simulation setup

Boundary conditions setup is of great importance in simulating and understanding the numerical problems in HFSS. Boundary conditions give the definition of field behavior in the discontinuous boundaries. Applying the boundary conditions in HFSS helps control the characteristics of planes' faces or interface between objects and reduce the complexity of the model. The boundary conditions in this work are presented in Figure 3.8. The Perfect E boundary conditions are used here to show a perfect conducting surface, which is the coaxial cables in this case. The surface with this condition has the electric field perpendicular to the surface. Radiation boundary condition is applied to simulate a boundary which will not reflect wave and let it radiate far into space. A common way to define the size of the boundary is to set it as quarter of the largest wavelength in this work. Excitations are served as the sources of electromagnetic fields to allow microwave signal to flow into the components in the model. The wave port structure is used in this work and the cross section surface of the coaxial cable is assigned as the wave port excitation. The maximum passes is 21 and the maximum delta S is 0.001.The sweep frequencies range from 2 [GHz] to 2.4 [GHz] in this work with the step size of 0.25 [MHz].

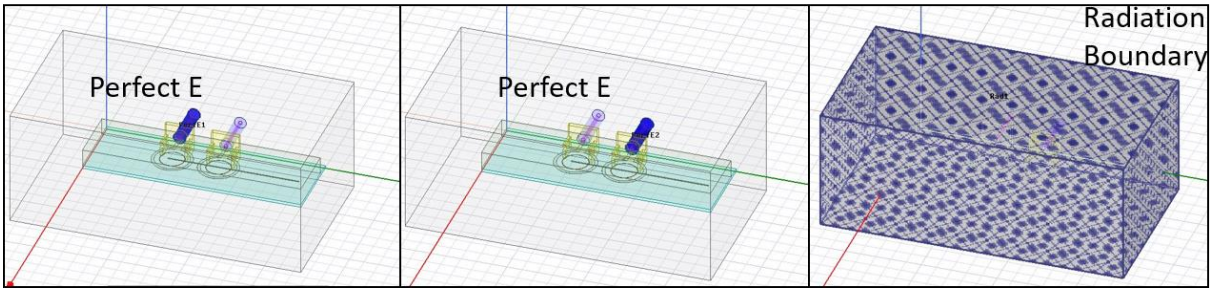

Figure 3.8. Boundary conditions in the simulation work

Chapter 4 : Numerical Analysis on Droplet Mixing Induced by Microwave Heating: Decoupling of Influencing Physical Properties

4.1. Overview

This chapter has been published: Cui, Weijia, Gurkan Yesiloz, and Carolyn L. Ren. "Numerical Analysis on Droplet Mixing Induced by Microwave Heating: Decoupling of Influencing Physical Properties." Chemical Engineering Science (2020): 115791.

Microwave resonator offers simultaneous sensing and heating of individual droplets in microchannels presenting unique advantages for applications requiring well-controlled reaction time. This study numerically investigates the effects of the temperature-dependent fluid properties including viscosity, density, diffusivity, and interfacial tension, on heating induced mixing. A system consisting of a spiral resonator integrated with a microchannel with aqueous droplets moving with a carrier oil is considered. The electromagnetic field which provides heating to the droplets, and the flow and tracer concentration fields inside the droplet are obtained using commercial software, Ansys HFSS and Fluent, respectively. It is found that the mixing index can be increased from 0.4 to 0.84 within 320 ms with microwave heating and it would be slightly increased to 0.47 when only the interfacial tension was made independent on temperature, which suggests that the temperature-dependent interfacial tension is the dominant factor for microwave heating induced mixing.

4.2. Introduction

Droplet microfluidics has gained ever-increasing attention in the past two decades due to its capability to perform high throughput analysis using pico- to nano-liter sized drops as reaction

vesicles, a function highly demanded in the areas spanning from life science research to material synthesis to drug screening [10, 27, 46, 67, 146, 147]. In most applications, rapid, homogenous mixing is critical to the overall quality of the resulted products as it directly affects the efficiency to increase reaction rate [82, 83, 148-150]. In addition, many reactions start within seconds, which requires precise control of reaction time [151, 152] and thus demands rapid and homogeneous mixing as well. Mixing is normally influenced by convection and diffusion, the relative importance of them is evaluated by Peclet number, $\mathrm{Pe} = \mathrm{UL/D}$, where $\mathrm{U}\ [\mathrm{m/s}]$ is the flow speed, $\mathrm{L}\ [\mathrm{m}]$ is the characteristic length, and $\mathrm{D}\ [\mathrm{m^2/s}]$ is the diffusion coefficient of the species of interest. In most microfluidic applications, Peclet number ranges from 10 to 10^5 indicating that convection is dominant over diffusion in enhancing mixing [24, 153]. Microchannel flow is generally laminar, characterized by low Reynolds number ($\mathrm{Re} = \mathrm{UL}/\nu$), where $\nu\ [\mathrm{m^2/s}]$ is the kinematic viscosity of the fluid, due to the dominance of viscous force over inertial force [2, 83, 84]. Flow cross the streams is very limited and therefore cross-stream mixing is mainly dominated by molecular diffusion, which is slow and inefficient [2]. Droplet microfluidics offers almost instantaneous mixing due to the three-dimensional (3D) motion present in droplets , which however only occurs within each half of the droplet when being pumped through straight channels resulting in diffusion dominated mixing between the two halves [154].

4.2.1. Passive and active methods

To achieve mixing in the entire droplet, both passive and active methods have been developed. Passive methods often involve the use of long serpentine channels [34, 52, 155] and induce flow disturbance to droplets [156], which in general requires higher pressure drops for pumping the fluids and is challenging to precisely control the reaction start time when the reaction occurs faster

than the time required to achieve homogeneous mixing. In addition, the robustness of passive methods is challenged by any uncertainties such as fabrication defects and pressure fluctuations. Active methods, on the other hand, employ external forces such as electric [157-160], magnetic [161-163], optical [164, 165], acoustic [166-169] and thermocapillary [46, 170, 171] forces to bring flow disturbance and thus enhance mixing. These methods can work with simple microchannel structures but with the cost of adding external components.

4.2.2. Microwave heating induced droplet mixing

Yesiloz et al. recently reported an active mixing method, which utilized a microwave resonator as a heater to achieve rapid mixing over the entire droplet [46]. Microwave heating was chosen to realize selective and localized heating of individual nanoliter-sized droplets. This is enabled by the ability of microwave to deliver volumetric heating to a localized region with a self-switch, which is droplet entering and exiting the heater region. When a droplet enters the heater region, the resonance frequency is shifted from what it was for the carrier oil to respond to the droplet material. The energy is only supplied at this shifted frequency, as a result, droplet entering the heater region switches on the heater and droplet existing switches off the heater. The heating induced mixing is almost initiated simultaneously. Other common heating methods such as resistive [172], joule [173] or Peltier [174] modules however rely on heat conduction to deliver energy to the material, which is challenging to achieve selective and localized heating. Laser-based [175] techniques can achieve selective and localized heating with a cost of exhausting the system for alignment and synchronization.

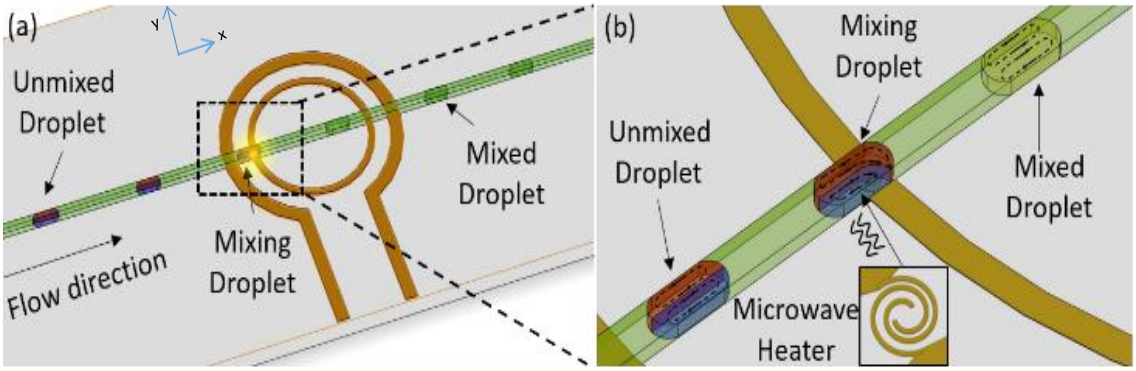

Figure 4.1. (a) The schematic of the entire model illustrating unmixed droplets become homogeneously mixed after passing through the resonator; and (b) A blow-up of the spiral resonator.

Figure 4.1 illustrates the microfluidic chip integrated with the microwave resonator used in their study, which is also considered in this study for modelling. This mixing method not only provides more flexibility and controllability for the mixing process by simply switching the microwave resonator on and off, but also has the potential to be integrated with microwave sensing for selective heating of individual droplets offering unique control of reaction.

In their study, a qualitative analysis was performed to evaluate the relative importance of the competing factors on mixing using the Buckingham π theorem [46]. It was hypothesized that Marangoni flow induced by the non-uniform temperature distribution at the interface that is resulted from the non-uniform electromagnetic fields played the key role. Verifying this hypothesis is critical to guide the design and operation of the microwave resonator as well as the microfluidic chip for selective sensing and heating of individual droplets, which finds many applications in single particle and single cell analysis. This study aims to numerically investigate the effects of influencing parameters on microwave heating induced mixing.

4.2.3. Parameters influencing microwave heating induced droplet mixing

Many parameters influence microwave heating induced mixing in a coupling manner. Considering a simple scenario where the geometric conditions for both the chip and microwave resonator are fixed, the operating conditions such as droplet size, content and speed (not the internal flow field) are fixed, and the microwave resonating frequency and chip material, which affect the microwave energy deposition within droplets, are also fixed, the mixing performance is still influenced by microwave power and several temperature-dependent fluid properties including the interfacial tension between the droplet fluid (dispersed phase) and carrier fluid (continuous phase), γ $[N/m]$; the diffusion coefficient of the species of interest (i.e. the fluorescent dye doped in the droplet for demonstrating the mixing phenomena), D $[m^2/s]$; and the viscosity and density of the droplet fluid, μ $[kg/(m \cdot s)]$ and ρ $[kg/m^3]$, respectively.

These parameters affect the competition between convection and diffusion and thus the mixing. It is very challenging to design experiments that allow the effects of these parameters to be decoupled to reveal the mixing mechanism. Therefore, numerical simulation is employed and the numerical results are compared with the experimental observations. Considering the focus of this study is to develop a better understanding about the mixing mechanism, the above-mentioned scenario is considered.

4.2.4. Numerical methods

Many numerical methods have been utilized to study the internal droplet flow field and mixing mechanism. Malsch et al. have numerically studied the flow field inside droplets and revealed its symmetric pattern, which suggests that diffusion dominates the mixing between the two halves of

the droplets [54]. Chandorkar et al. [84] simulated the mixing process in the serpentine structure using Volume of Fluid (VOF) method while Jeon et al. investigated the mixing performance of passive planar mixers with different geometric variables based on numerical simulations and experiments [176]. Muradoglu et al. numerically studied the mixing process in a serpentine microchannel and analyzed the influence of Capillary number (Ca) which compares viscous and interfacial tension forces, viscosity ratio between the drop and carrier fluids, droplet size and Re number on mixing [83]. Fu et al. investigated the mixing in multiphase flow by using a Lattice Boltzmann method with the effect of initial distribution of species [177, 178]. Wang et al. focused on analyzing the detailed mixing mechanism of droplets in the serpentine microchannel [88]. Nevertheless, the microwave heating induced mixing within droplets is more complicated than that induced by passive methods because of the coupling between electromagnetic energy deposition within the droplet and the flow field and mass transport within the droplet.

4.2.5. Work Overview

In this study, we employ the VOF method through Ansys Fluent to numerically obtain the 3D flow field and concentration distribution of a tracer used to evaluate the mixing inside droplets. VOF is chosen because it is capable of simulating two or more immiscible fluids in microchannels with one set of momentum equations [144, 179, 180], which is the situation considered in this study. The electromagnetic energy field is obtained numerically using Ansys HFSS and then imported to Ansys Fluent to couple with the flow field inside droplets. Parametric studies of the effects of several fluid properties on heating and thus fluid flow and mixing within the droplets are carried out. The numerically predicted flow field and concentration distribution are used to evaluate the

effects of the influencing parameters on the mixing performance which is then compared with the experimental observations presented previously by Yesiloz et.al [46].

4.3. Methodology

4.3.1. Problem Definition and assumption

The coupling between the electromagnetic field and the flow field in a microchannel with moving aqueous droplets in oil streams is very complicated, which tends to make it prohibitively expensive to computationally consider this coupling without making any assumptions. Therefore, the following assumptions are made in numerical simulation to concentrate computation power on investigating the mixing mechanism. It is worth noting that some of the assumptions do not seem realistic, but they will not affect the investigation of the mixing mechanism, which is mainly associated with the interaction between the electromagnetic field and the flow and mass transport within the droplets via temperature-dependent fluid properties.

The major assumptions include: i) flow is incompressible which is typical for microfluidics; ii) no gravity is considered; iii) no droplet generation dynamics is considered, instead, a straight channel with well-developed moving droplets is considered; iv) the electromagnetic field is coupled with the flow field only when the droplet completely covers the sensor region meaning that if the sensor is partially covered by the carrier oil, the electromagnetic field is not coupled with the flow field and thus no microwave energy is deposited in droplets. This assumption allows one single simulation case to be completed within a reasonable computation time (i.e. days instead of weeks or months) while capturing the effects of temperature distribution on the mixing performance; and v) a user defined scalar (0-1) is introduced to demonstrate the mixing performance. Its distribution

(called tracer concentration) is mimicking the concentration of the dye that was doped in droplets in experiments for the same purpose.

One of the appealing features of microwave heating is that no external trigger is needed to turn on/off the microwave heater because the droplet is the trigger. When a droplet covers more than half of the resonator, it causes the shift of the resonating frequency due to its different permittivity from the carrier fluid (i.e. oil). Energy is only provided at this shifted frequency and thus the droplet starts to receive the electromagnetic energy converting to thermal energy via dielectric heating. The electromagnetic energy is numerically obtained using Ansys HFSS, which is then imported to the Ansys Fluent to simulate the heating process occurring in the droplet. The details about HFSS simulation are provided in the supplementary information (SI) [181]. It should be noted that the droplet fluid properties such as temperature-dependent dielectric constant also affect the electromagnetic field. This effect is not considered in this study because of the following reasons. First, the complete dynamic coupling between the electromagnetic field and the flow and concentration fields is prohibitively expensive in computational modeling. It takes months to complete one case. Second, considering the focus of the study is to understand the relative importance of the temperature-dependent droplet properties on mixing that are accounted for in the momentum and convection-diffusion equations (i.e. interfacial tension, density, viscosity and diffusivity), it is reasonable to neglect the influence of droplet fluid properties on the electromagnetic field which ultimately affects the temperature field within the droplet. Please also note that the relative distance between the droplet and the resonator also affects the electromagnetic field which is neglected as well. Experimental studies show that the resonator is not triggered on until the droplet covers the majority of the resonator [46]. In the simulation, the energy deposition in the droplet is considered when the droplet completely covers the resonator (absorbing its energy

fully). Therefore, we did not consider the effect of the relative droplet position to the resonator on the electromagnetic field.

4.3.2. Geometric conditions and fluid properties

In order to verify the hypothesis made in the previous study [46], the geometric and fluid properties in this study are kept the same. Briefly, the channel width and height are $200\ [\mu m]$ and $50\ [\mu m]$ respectively and the largest diameter of the spiral microwave resonator is $200\ [\mu m]$ with the gap and metal trace width both being $20\ [\mu m]$. The drop fluid is Deionized (DI) water and the carrier fluid is a fluorocarbon oil (FC40), a fluorinated oil. A fluorescent dye of $100\ [\mu M]$ was doped with half of the droplet to visualize the mixing between the two halves of the droplet in the previous experimental study [46]. As the dye concentration is sufficiently low, its effects on the fluid properties are ignored. In the current numerical model, a user defined scalar is then used to describe the mixing process and can be regarded as a tracer concentration [84, 88]. The tracer is provided with the same diffusion coefficient as the fluorescent dye used in the experiments. Half of the droplet is filled with DI water while the other half is filled with tracer doped DI water. In reality, most fluid properties such as viscosity and interfacial tension are temperature dependent, and thus spatially and temporally vary within the droplet when temperature gradients are present. Their temperature dependences all contribute to the mixing through their influences on convection and diffusion, which have proven to be difficult to decouple experimentally. This numerical study, however, is able to evaluate the effect of each individual temperature dependent property on mixing performance while maintaining the rest of the fluid properties independent of temperature.

4.3.3. Governing Equations

In this work, the VOF method is used to simulate the flow field inside droplets. The VOF method belongs to the category of Eulerian methods that could effectively track and locate the sharp liquid and liquid interface which is important for droplet microfluidics. The continuum surface model is a common method to carry out interfacial tension and is added to the momentum equation for the interfacial tension force [143]. Based on this model, the interfacial tension is treated as a body force and serves as the source term in the momentum equation. Phase change, viscous dissipation, and phase diffusion are not taken into consideration due to little effect on mixing between the two phases considered here, DI water and FC40 oil [88]. The four basic governing equations are:

Continuity Equation:

$$\frac{\partial \rho}{\partial t} + \nabla \cdot (\rho \vec{v}) = 0 \tag{4-1}$$

Momentum Equation:

$$\frac{\partial (\rho \vec{v})}{\partial t} + (\rho \vec{v} \cdot \nabla)\vec{v} = -\nabla p + \nabla \cdot \left\{ \mu \left[(\nabla \vec{v} + \nabla \vec{v}^T) - \frac{2}{3} \nabla \cdot \vec{v} I \right] \right\} + \vec{F} \tag{4-2}$$

Energy Equation:

$$\frac{\partial (\rho E)}{\partial t} + \nabla \cdot (\vec{v} \rho E) = \nabla \cdot (k \nabla T) + S_h \tag{4-3}$$

Convection and diffusion Equation:

$$\frac{\partial (\rho f)}{\partial t} + \nabla \cdot (\rho f \vec{v}) = \nabla \cdot (\rho D \nabla f) \tag{4-4}$$

where $\rho\ [kg/m^3]$, $\vec{v}[m/s]$, $\mu\ [kg/(m \cdot s)]$, $\vec{F}\ [N]$, $T\ [K]$, $k\ [W/(m \cdot K)]$, $E\ [J/kg]$, $S_h\ [W/m^3]$, $D\ [m^2/s]$ and f are the density, velocity, viscosity, body force, temperature, thermal conductivity, energy density, volumetric heat sources, diffusion coefficient and mixture fraction of the fluid, respectively. For each cell in the mesh, the fluid properties such as density are calculated by a volume fraction average of all the fluids in the cell [144]. The force term in Eqn. (4-2) represents the interfacial tension force. The detailed calculation of this force term is provided in the SI [181].

The boundary and initial conditions are provided in detail in the supplementary information [181]. The physical properties of the fluids at room temperature are as follows and are also summarized in a table provided in the SI [181] together with their temperature dependences. The density, viscosity, specific heat capacity and thermal conductivity of the dispersed phase at room temperature are $998\ [kg/m^3]$, $0.00103\ [kg/(m \cdot s)]$, $4178\ [J/(K \cdot kg)]$ *and 0.6* $[W/(m \cdot K)]$, respectively. The diffusion coefficient of the user define scalar is $4.18 * 10^{-10}$ [m^2/s] [182]. The density, viscosity, specific heat capacity and thermal conductivity of the continuous phase at room temperature are $1855\ [kg/m^3]$, $0.0041\ [kg/(m \cdot s)]$, $1100\ [J/(K \cdot kg)]$ and $0.065\ [W/(m \cdot K)]$, respectively. The specific heat capacity is used to calculate the specific energy via $E = C\Delta T$. The interfacial tension is set as $0.052\ [N/m]$ and the contact angle is $5\pi/6$ [46]. The temperature dependence of the physical properties is provided in the supplementary information [181].

4.3.4. Numerical details

For the VOF method, the coupled pressure-based algorithm is chosen because it allows more accurate results to be obtained than the segregate algorithm [144]. The second order upwind

method is employed to calculate the momentum and energy equations. The second order implicit time-stepping formulation is used to deal with the transient formulation. The compressive interface capturing scheme is a high-resolution differencing scheme used to get accurate interface calculation results [145]. The mesh is generated by Ansys Gambit and contains 210 [K] cubic cells in our model with a cell size of 5 [μm]. Mesh grid independence analysis is carried out to reduce the effect of grid size on numerical simulation results and optimize computation time [10]. The residual criterion is 10^{-12} for the Energy equation, and 10^{-4} for other equations. The time step in the simulation is 0.1 [ms]. In the heating process, the temperature can rise from room temperature to 90 ºC. It takes about 100 [ms] to equilibrate after heating.

4.3.5. Flow and Energy Field Coupling

The flow field is obtained using Ansys Fluent. When a droplet covers the resonator region, it triggers the microwave heater to work and then starts to receive the energy induced by the microwave resonator characterized by the increased temperature within the droplet. The electrical field is numerically obtained using Ansys HFSS and then the deposited power within the droplet is calculated by

$$S_h = \frac{1}{2}\omega\varepsilon_0\varepsilon^{"}|E|^2 \tag{4-5}$$

where ω [$rad/$s] is the angular frequency, ε_0 [$C/(Vm)$] is the permittivity of vacuum, $\varepsilon^{"}$ is the imaginary part of the relative permittivity, and E [$V/$m] is the electric field. The deposited power distribution in the droplet is imported as a source term in Eqn. (4-3), which is used to obtain the temperature field. The flow field and the tracer concentration distribution with temperature-dependent parameter are then obtained using Ansys Fluent, the latter of which is used to evaluate

the mixing performance. The User Define Function (UDF) is integrated with the software to import the heat source to the droplet. The UDF also guarantees that the heating only works on the individual droplet and the surrounding fluid and chip material is unaffected.

4.3.6. Quantitative evaluation of mixing process

To quantitatively analyze the degree of mixing process and the influences of different physical parameters on microwave induced droplet mixing, mixing index (MI) is used in our work based on the following equations [82]:

$$\mathrm{MI} = 1 - \frac{\sqrt{\frac{1}{n}\Sigma(c_{av}-c)^2}}{c_{av}} \tag{4-6}$$

where n is the number of the calculated cells, c_{av} is the average concentration of the tracer, and c is the tracer concentration of each cell.

4.4. Results and Discussion

4.4.1. Droplets Considered

In the previous experiments [46], droplets were generated within the squeezing regime, which produces highly monodispersed droplets in general suitable for most applications for quantitative analysis [65]. The droplets generated in this regime are generally characterized by the fact that the droplets are almost in direct contact with the channel walls with a thin film of the carrier fluid in between and have curved head and tail due to the interfacial tension. The thin film is around a few micrometers and causes slight velocity differences between the droplet and the carrier oil (i.e. ~ 6% in this study [183, 184]). To consider this thin film in the simulation is very expensive

computationally with limited benefits to the understanding of the mixing mechanism induced by microwave heating. Therefore it is neglected. This study considers this type of droplets as shown in Figure 4.2 for comparison with the experimental observations.

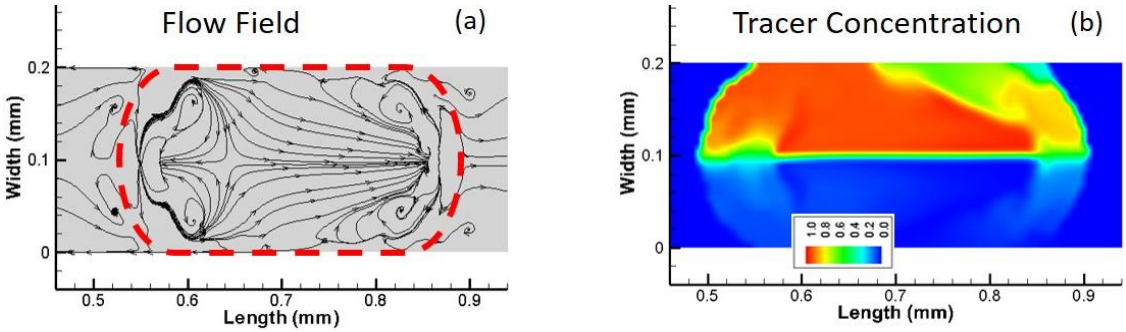

Figure 4.2. Droplets without heating: (a) streamline function at the x-y plane, and (b) concentration distribution of the tracer.

4.4.2. Flow and concentration field without heating

The microwave resonator is placed in the middle of the straight microchannel in the length direction. The flow field should be symmetric about the horizontal centerline of the droplet without heating and mixing between the two halves of the droplet is minimal, merely through diffusion. Figure 4.2 (a) confirms the symmetric flow field [54] inside a droplet by showing the streamlines of the x-y plane at the center of the height direction (z-direction). Figure 4.2 (b) shows the tracer concentration field, where only slight mixing occurs at the head and tail of the droplet induced by small vortices present in that region.

4.4.3. Energy deposition within the droplet

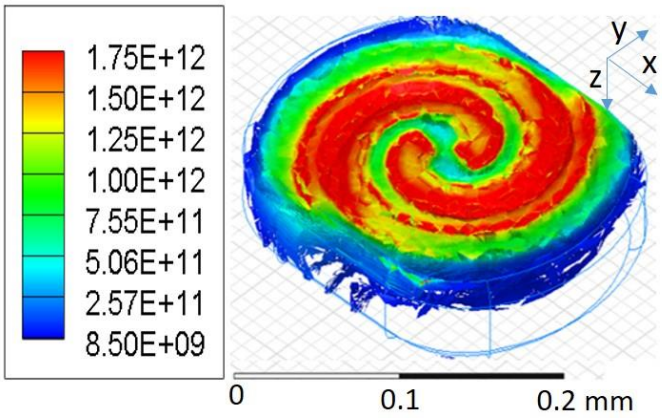

Figure 4.3. An example of the volume loss density inside a droplet.

When a droplet is passing through the microwave heater, it receives energy via dielectric heating, which is expressed by the volume loss density numerically obtained using Ansys HFSS (Figure 4.3) and is incorporated into the flow field as the heat source. A slice-by-slice presentation of the energy deposition inside the droplet is presented in the SI [185]. The 3D non-uniform volume loss density results in a 3D non-uniform temperature distribution, which leads to 3D non-uniform gradients in the fluid properties, such as interfacial tension, viscosity, diffusion coefficient and density. The effect of each individual parameter on mixing will be discussed later to investigate the mixing mechanism of microwave heating. A brief validation of microwave heating induced mixing is presented.

4.4.4. Flow and concentration field with heating

The nonuniform interfacial tension distribution resulted from the nonuniform temperature distribution would induce Marangoni flow at the droplet interface distorting the symmetric flow field inside the droplet, which can be seen from the streamlines shown in Figure 4.4 (a). Mixing

between the two halves of the droplet is then expected to be enhanced by the lateral flow (streamlines across the horizontal centerline of the droplet) as reported by Muradoglu et.al [83], which is also confirmed by the tracer concentration at different time (Figure 4.4 (b)-(d)). The concentration distribution remains almost the same before the droplet arrives at the microwave heater and then is being distorted when it starts to pass the microwave heater (Figure 4.4 (b) and (c)). Almost homogenous mixing is achieved within 320 $[ms]$ as shown in Figure 4.4 (d).

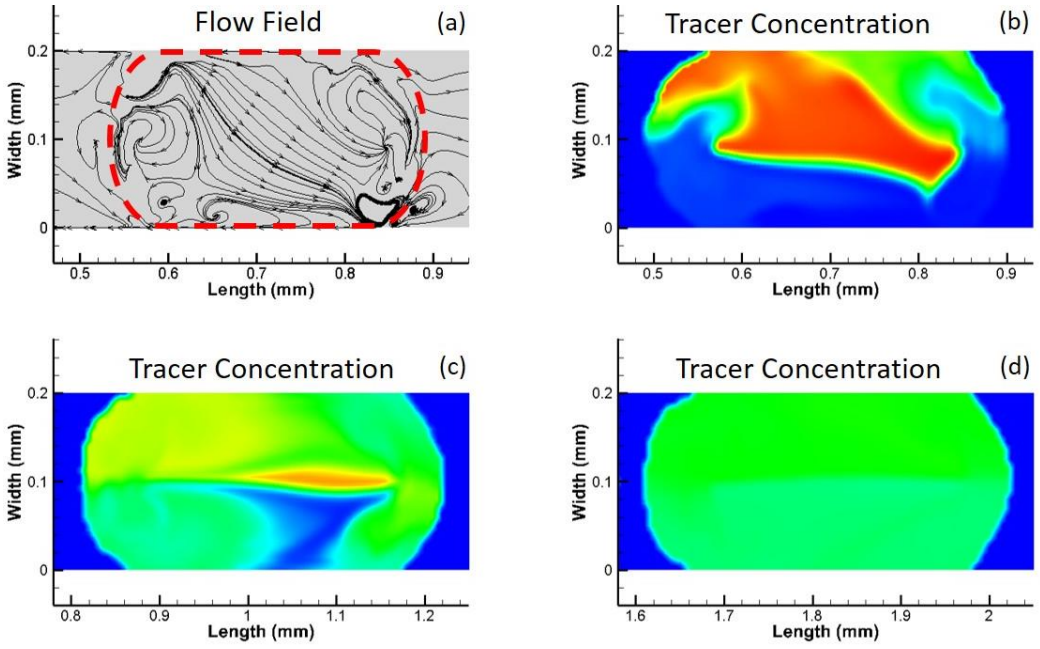

Figure 4.4. Streamlines (a) and tracer concentrations inside the droplet with microwave heating at (b)40 $[ms]$; (c) 120 $[ms]$ and (d) 320 $[ms]$.

The mixing process is also tracked using the mixing index, MI, and a comparison of the mixing performance with and without microwave heating is presented in Figure 4.5. The results show that a droplet without heating has a slow mixing process while the droplet with microwave heating achieved a much faster mixing. For example, a mixing index of 0.41 is reached at 320 $[ms]$ for the droplet without heating while the mixing index of the droplet with microwave heating increased rapidly from the time that the microwave heating is on (0 $[ms]$) and reached 0.6 at

around 140 $[ms]$. The mixing index reached around 0.84 at 320 $[ms]$. Due to the large surface to volume ratio, heat dissipation is fast causing the droplet temperature drops to room temperature after leaving the microwave heater region. As a result, the heating induced mixing mechanism is much weakened and thus dominated by molecular diffusion again, which is reflected by the slow increase in the mixing index shown in Figure 4.5.

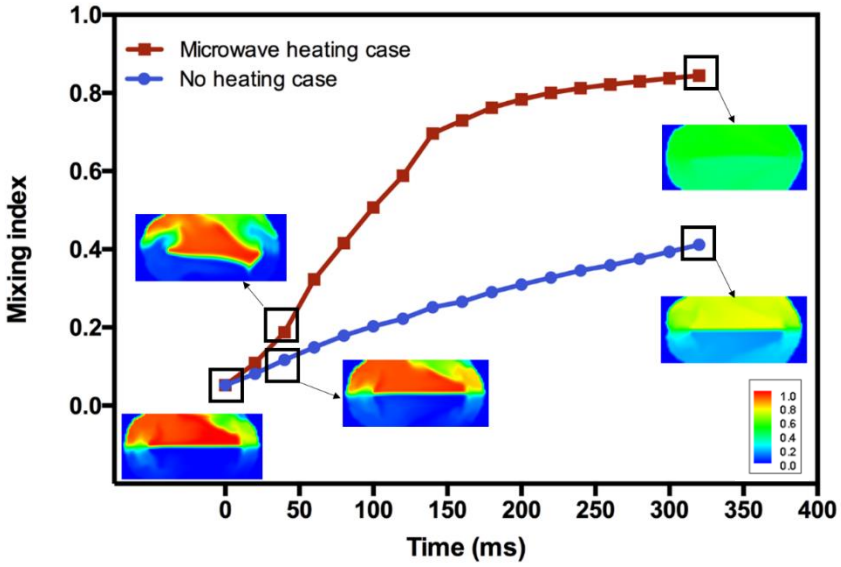

Figure 4.5. A comparison of microwave heating case and no microwave heating case on droplet mixing

4.4.5. Cross-stream velocity with and without heating

The cross-stream flow motion requires the velocity in y-direction inside the droplets (droplet width direction) to realize mixing between the two halves. Figure 4.6 (a) and (b) show the contour of the velocity component in y-direction at a 2D surface without and with microwave heating, respectively. The red and blue colors indicate the upward and downward velocity components in y-direction. It is observed that the y-velocity is small when not being heated with a close to zero value at the horizontal centerline. However, for the droplet with heating, the velocity component

in y-direction becomes much larger, especially near the horizontal centerline indicting lateral flow crossing the centerline, which enhances the mixing between the two halves of the droplet.

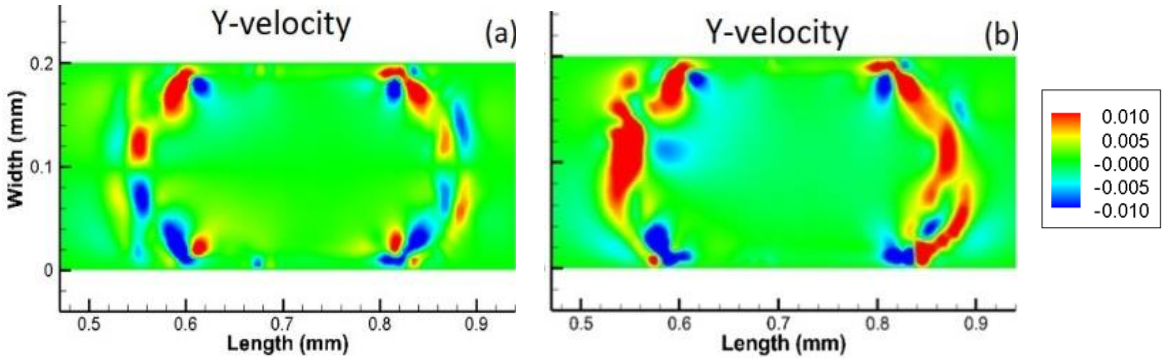

Figure 4.6. Comparison of the contour of the velocity component in y-direction between the droplets without (a) and with microwave heating (b)

4.4.6. Relative effects of the fluid properties on the mixing

Although the microwave heating induced droplet mixing is numerically demonstrated which agrees with the experimental observations [46], the mixing mechanism is not yet fully understood, in particular, the question regarding which temperature-dependent parameter plays a dominant role is not yet answered. The effect of each parameter on mixing is investigated numerically to answer this question, which is very challenging to conduct experimentally due to the difficulty to decouple them. Therefore numerical simulation cases are designed to decouple these parameters by keeping each physical properties constant respectively to eliminate their contribution to microwave induced mixing and then evaluate their effect by observing flow field and concentration field.

Figure 4.7 (a) and (d) show the streamline pattern and the contour of the velocity component in y-direction for the case with constant density. It can be seen that the symmetry is distorted with strong velocity components in y-direction at the head and tail of the droplet which enhances the mixing significantly. This indicates that the temperature dependent density plays insignificant role in microwave heating induced mixing. Similar results are obtained for the case with constant viscosity as shown in Figure 4.7 (b) and (e), which suggests that the temperature-dependent viscosity of the droplet fluid have negligible contributions to microwave heating induced mixing. In contrast, when the interfacial tension is kept constant, the symmetric flow pattern resumes as shown in Figure 4.7 (c) and (f) indicating that the interfacial tension plays the most important role on enhancing mixing.

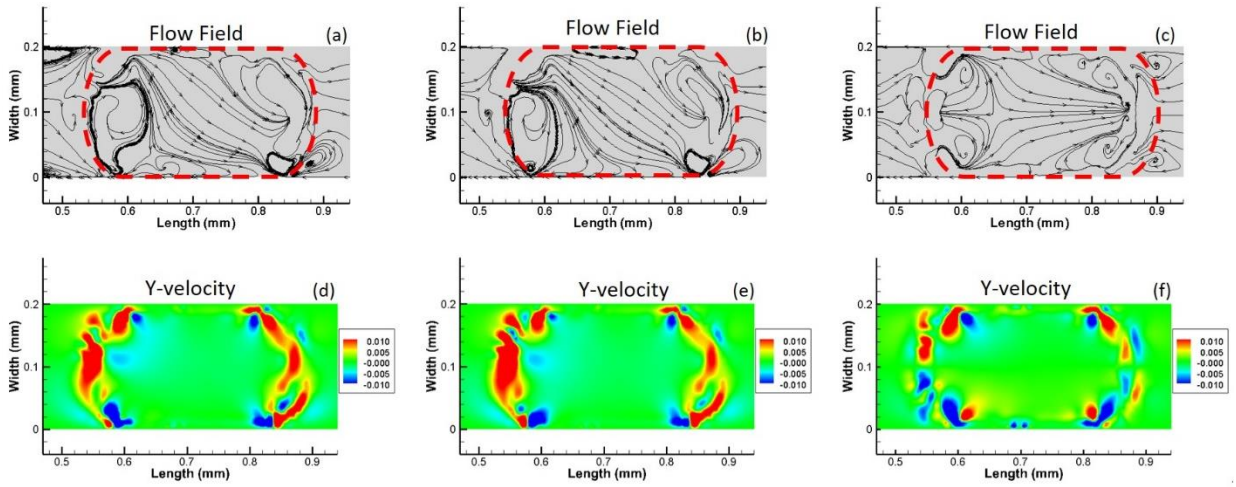

Figure 4.7. Streamline function of droplet for the case with (a) constant density, (b) constant viscosity, (c) constant interfacial tension, and the contour of the velocity in y-direction inside the droplet for the case with (d) constant density (e) constant viscosity, and (f) constant interfacial tension for viscosity constant case

To study the effect of the temperature-dependent diffusion coefficient on mixing, the diffusion coefficient is kept constant for the tracer. The concentration contour in Figure 4.8 (a) shows that although the diffusion coefficient remains constant as the temperature is changing, the mixing

happens between the two halves of the droplet when microwave heating is applied. There is almost no difference between the cases with a constant diffusion coefficient (Figure 4.8 (a)) and a varying diffusion coefficient (Figure 4.4 (d)) indicating that the mixing is weakly influenced by the temperature-dependent diffusion coefficient. Figure 4.8 (b) - (d) further confirm that the dominate role of interfacial tension in the microwave heating induced mixing process. For example, when the density and viscosity are kept constant (Figure 4.8 (b) and (c)), almost homogenous mixing are achieved indicating that mixing is weakly dependent on the density and viscosity. The concentration distribution exhibits great difference for the cases with and without the interfacial tension change as shown in Figure 4.4 (d) and Figure 4.8 (d), respectively. The concentration contour for the case with constant interfacial tension remains stable without any cross-stream mixing shown in Figure 4.8 (d).

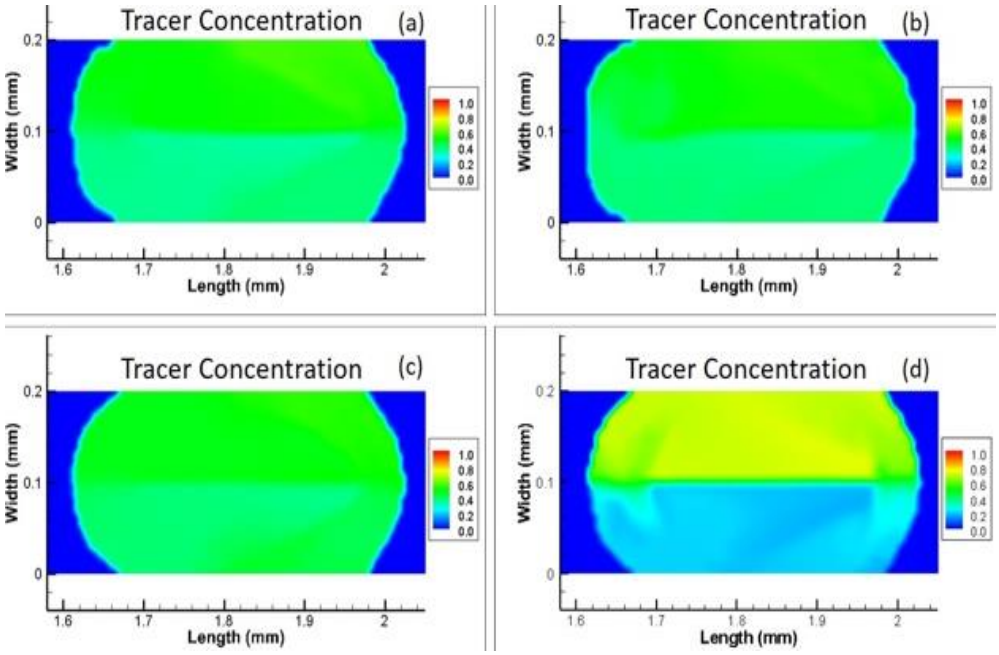

Figure 4.8. Concentration contour of the droplet after microwave heating for 320 [ms] for parametric study (a) constant diffusion coefficient constant, (b) constant density, (c) constant viscosity and (d) constant interfacial tension

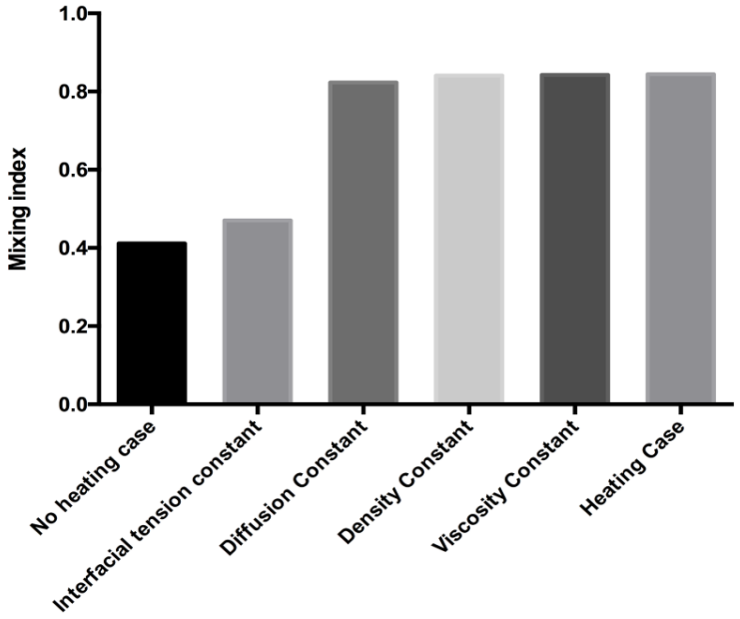

Figure 4.9. A histogram of mixing index for different cases at 320 $[ms]$

Corresponding to the concentration contour in Figure 4.8, Figure 4.9 summaries the mixing index of the studied cases including without heating case, with microwave heating case as well as the cases with one of the physical properties such as density, viscosity, diffusion coefficient or interfacial tension remaining constant. It indicates that a mixing index of 0.4 is reached for no heating case, while the case with microwave heating achieves a mixing index of 0.84. When the diffusion coefficient of the tracer, the density or viscosity of the droplet fluid is kept constant, the mixing index remains almost no change as compared to the one with microwave heating. However, when the interfacial tension is kept constant, the mixing index is around 0.47 indicating that the temperature-dependent interfacial tension plays a key role in microwave heating induced mixing. This result indicates the major role of interfacial tension in the microwave induced droplet mixing which provides stronger evidence to the conclusion made using qualitative analysis in the previous experimental study [46]. The efficient mixing inside droplets requires a stirring mechanism to

disturb the symmetry flow nature between two halves of droplets. In our current design, microwave heating is employed to offer this stirring mechanism by providing nonuniform heating to a droplet. During the heating process, an elongated droplet receives energy from microwave heater which results the temperature difference in the poles and equator of droplets and this temperature difference can produce a secondary flow inside droplet to facility mixing. The nonuniform energy deposition in droplets (Figure 4.3) as long as the moving of droplet results in non-uniform temperature distribution which generates the gradient of interfacial tension at the droplet interface. The gradient of interfacial tension induces Marangoni effect inducing a chaotic flow, which is manifested by the velocity component in the cross-stream direction and thus enhancing the mixing between the two halves of the droplet. Simulation results demonstrate that the origin of this chaotic flow is from the change of interfacial tension rather than other material properties.

4.5. Conclusions

In this study, we numerically studied the thermo-capillary mixing in droplet microfluidics aiming to understand the mixing mechanism induced by microwave heating. In particular, we aimed to evaluate the hypothesis of the mixing mechanism proposed based upon our previous experimental study. By simulating the flow and concentration field inside droplets, we investigated the effects of temperature-dependent parameters including fluid density, viscosity, diffusion coefficient, and interfacial tension on the mixing performance inside droplets. The streamline patterns for the droplet with and without microwave heating indicated that when the interfacial tension is kept constant, the symmetric flow pattern and minimal mixing through molecular diffusion are observed, which confirms the previously proposed hypothesis that the interfacial tension is the dominant factor for enhanced mixing. It therefore provides clear guidance on exploiting

microwave resonator for heating droplets. It also suggests that the use of surfactant which presents strong temperature dependence is helpful for enhanced mixing.

Chapter 5 : Microwave heating induced on-demand droplet generation in microfluidic systems

5.1. Overview

This chapter has been published to Journal of Analytical Chemistry: Cui, Weijia, Gurkan Yesiloz, and Carolyn L. Ren. "Microwave Heating Induced On-Demand Droplet Generation in Microfluidic Systems." Anal. Chem. 2020.

In this study, we report a simple, new method for droplet generation in microfluidic systems using integrated microwave heating. This method enables droplet generation on-demand by using microwave heating to induce Laplace pressure change at the interface of the two fluids. The distance between the interface and junction, and microwave excitation power have been found to influence droplet generation. Although this method is limited in generating droplets with a high rate, the fact that it can be integrated with microwave sensing presents unique advantages for applications that require dynamic tuning of material properties in droplets.

5.2. Introduction

Droplet microfluidics has drawn ever-increase attention from both academia and industry with numerous studies reported on both fundamental research and practical applications over the past two decades and some companies such as Dolomite Bio catching up the developed innovations [25, 186]. Since droplets are isolated from each other and from the channel walls by the carrier fluid, each individual droplet can serve as an encapsulated cargo platform for cells, particles, or biomolecules (DNA, proteins); and can be a microreactor for chemical or biochemical synthesis [37, 187]. Major advantages of using isolated pico- to nanoliter droplets as reaction vesicles instead

of traditional well plates or single-phase microfluidic devices include largely reduced reagent consumption, enhanced mixing, shortened reaction time and unparalleled high throughput [5].

For most applications, droplet generation marks the initial and important step, which is expected to have stable and predictable outcomes [31]. A well-controlled droplet generation process is required for various applications including biochemical screening, click chemistry, and DNA polymerase chain reaction in order to have precise products and results [151, 188, 189].

Although droplets can be generated passively at kHz rates in microchannel networks by varying applied pressures and channel geometries [31], precise control of individual droplets becomes challenging because any design flaws, fabrication defects and pressure fluctuations would affect the designed functionality. It is also difficult to generate droplets on-demand which is important for many applications requiring a higher degree control of droplet number and spacing as well as reaction time [190].

Alternatively, active methods are favorable for on-demand generation of droplets by integrating external forces. For comprehensive understanding of active methods for droplet generation, readers are referred to some excellent reviews [31, 35]. Briefly, some active methods involve the integration of moving parts such as mechanical valves [191, 192] and electrically-actuated membranes [193] while others rely on the applied electrical fields to control droplet volume and generation frequencies [73, 194, 195].

Droplet generation is mainly dominated by the competition between interfacial tension and viscous forces when flow rates are not high (shear force is negligible) and thus varying the interfacial tension becomes one of the effective ways for generating droplet on-demand in addition to varying

flow and geometric conditions. Interfacial tension is influenced by temperature and surfactants that can be added to one or both phases of the fluids [196]. Embedded heaters were straightforward for thermally mediated generation of droplets or bubbles [77, 197]. These resistive heating methods are difficult to achieve localized heating of droplets and have a relatively long response time for switching on/off. Stan et al. reported a method to implement two different temperature zones on a microfluidic flow-focusing generator by using two heat exchangers that are insulated from each other [198]. They achieved independent control of drop size and velocity by varying both temperature and flow rate. The study did not aim at forming droplets through heating rather temperature zones are utilized for manipulation of droplet size.

Cordero et al. later reported the use of a laser beam to generate different optical patterns that were able to localize heating at the desired locations for generating and directing droplets [79]. Park et.al. used laser induced cavitation to improve the high throughput of on-demand droplet generation [78]. These optical methods offer more control over the droplet generation than the traditional thermal methods with the cost of synchronizing the optical system with the fluid system. Microwave heating has also been demonstrated for enhancing droplet mixing [46] and assisting in nanoparticle synthesis [115]. Microwave heating is basically converting electromagnetic energy to thermal energy deposited in droplets of particular dielectric properties efficiently [110]. It can selectively heat droplets leaving the surrounding carrier fluid unheated based on different dielectric properties [45]. Moreover, microwave heating exhibits strong localization and features fast heating and cooling [11, 47], which enables pulse heating, because heating stops once the power is off. This controlled pulse heating provides an opportunity to utilize microwave method as an external source to achieve on demand droplet generation which is demonstrated in this study. The influence

of microwave power on the droplet generation performance is investigated and the generation mechanism is briefly discussed.

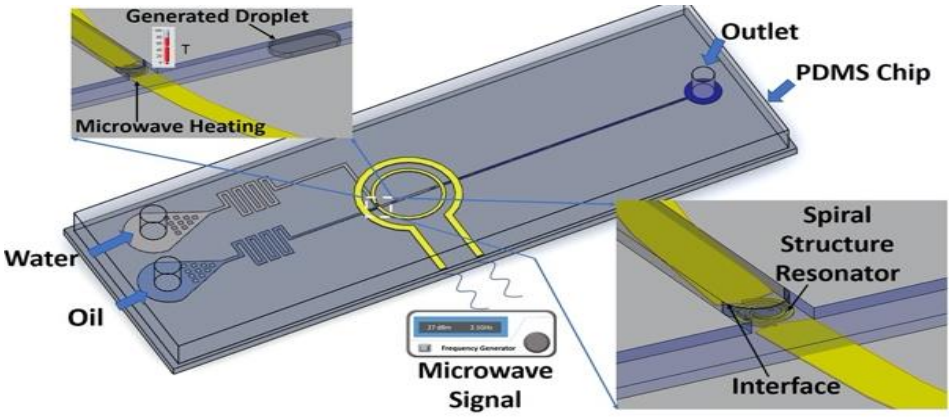

Figure 5.1. Schematic of the microfluidic chip integrated with the microwave heater.

5.3. Experimental

The reported microwave heater is a co-centric ring resonator made of metal traces on a glass slide that is integrated with a Polydimethylsiloxane (PDMS) microfluidic chip as shown in Figure 5.1. The outer ring receives power from a frequency generator (HMC-T2100, Hittite) and the resonating inner ring has a capacitive gap that is aligned with the microfluidic T-junction channel and deposits energy into the liquid at the junction. The fluids including both the carrier phase (fluorinated oil, FC-40 from Sigma-Aldrich) and droplet phases (DI-water) are pumped through the microchannels via a pressure source (Fluigent MFCS-8C) and the droplet generation process is visualized via a CCD camera in a microscope (Eclipse Ti, Nikon, Retiga 2000R, QImaging).

5.3.1. Device design and fabrication

The focus of this study is to demonstrate the feasibility of using microwave heating to generate droplets on-demand, therefore a T-junction generator is chosen because of its simplicity and the

superior control it offers over droplet size. The channel width and height are similar to our previous studies on microwave sensing and heating, which are 210 μm and 40 μm respectively [11].

The microfluidic chip consists of two parts: a glass slide with the microwave components and a PDMS mold. The detailed fabrication procedures can be found from our previous publication [46]. Briefly, the microwave components are fabricated using a combination of photolithography and electroplating while the microchannels are made by using soft-lithography techniques. To ensure the same surface properties for stable droplet formation, a thin PDMS layer is coated on top of the microwave components serving as one of the channel walls when bonded with the PDMS mold via plasma surface treatment.

5.3.2. Droplet Generation mechanism

Although systematic investigation of the mechanism of microwave heating induced on-demand droplet generation is beyond the focus of this study, qualitative discussion is helpful in exploring and designing the system. Most active methods generate droplets by bringing extra energy to disturb the interface. For example, laser mediated droplet generation methods disturb the interface by using the optical cavitation bubble generated with an intense laser pulse focusing on the liquid medium [78, 79]. Droplets can be generated on-demand by controlling the laser beam, e.g. by controlling either the laser beam power or focusing position. On the contrast, the microwave heater presented here localizes heating to the interface region of the two fluids that aligns with the capacitive gap of the resonator. The temperature increase in the interface region reduces the interfacial tension as well as the viscosities of the two fluids allowing the droplet fluid to penetrate into the carrier fluid forming a droplet.

For efficient heating, the resonator should align with the interface of the two fluids. To demonstrate the feasibility of leveraging microwave heating for droplet generation, the generation process should start with a stable interface. When the interface is stable, a pressure balance exists at the interface such that $P_d - P_c = \Delta P$ where P_d [Pa] and P_c [Pa] represent the pressures at the interface from the droplet and carrier fluid side respectively, and $\Delta P = \gamma * (2/H + 2/W)$ is the Laplace pressure where γ [N/m] is the interfacial tension and H [m] and W [m] are the channel height and width respectively. Droplets can be generated by breaking this balance such as increasing the applied pressure drop or reducing the Laplace pressure via microwave heating, which are both influenced by the interface position in relevance to the T-junction. Understanding the required applied pressure drop for generating droplets also provides the guidance in microwave heating mediated droplet generation by predicting the power required.

For simplicity, the pressure applied to the inlet of the carrier fluid is kept constant (i.e. 300mbar) and the pressure applied to the inlet of the droplet fluid is varied to maintain a stable interface at different positions. It is first estimated based on the pressure balance, $P_d - P_c = \gamma * (2/H + 2/W)$, and the hydrodynamic resistance of each channel [199] and then slightly adjusted based on the pressure source and tubing during the experiments. In this study, it is varied from 150 mbar to 155 mbar to maintain the interface position from 150 μm to 1000 μm measured from the top of the horizontal channel as shown in Figure 5.2. The required pressure increase to generate droplets from a stable interface position of 150 μm is around 3 mbar, which increases to 6 mbar when the interface is further away from the T-junction, such as 1000 μm. This information provides guidance in the design and operation of microwave heater for droplet generation.

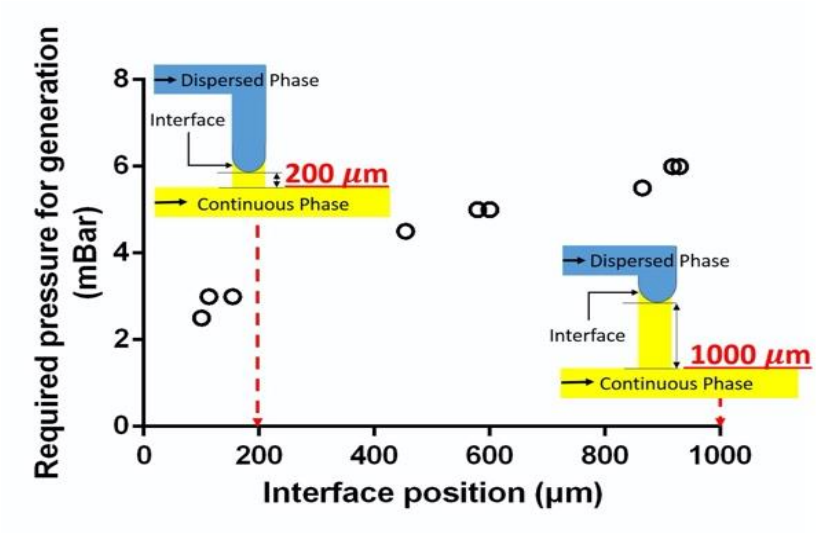

Figure 5.2. Relation between interface position and pressure difference with the microwave heater

In this study, the temperature-dependent interfacial tension was reduced by increasing the temperature of the fluids near the interface using microwave heating while the applied pressures are kept constant. The interfacial tension for the fluid pair (i.e. DI water and FC-40) is 0.052 N/m at room temperature [200]. A Laplace pressure reduction of 4.7 mbar is realized by applying 27 dBm microwave heating as a result of the decreasing of interfacial tension [201]. The change of Laplace pressure is comparable with the required pressure difference when the resonator is positioned close to the junction as shown in Figure 5.2. It suggests that microwave heating has the ability to induce droplet generation by changing the interfacial tension. It should be noted that the fluid viscosity will also decrease with increasing temperature, which would play a role in droplet formation dynamics such as shortening the breakoff time. Quantitative evaluation of the role of viscosity on droplet formation dynamics is beyond the scope of this study.

5.4. Results and Discussion

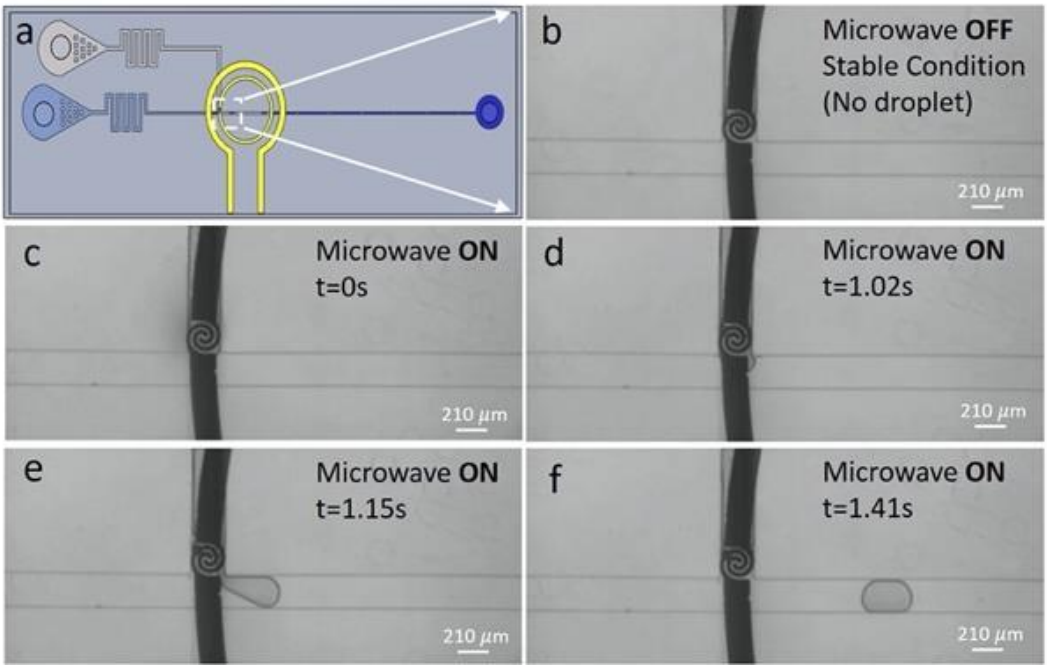

Figure 5.3. Illustration of time-elapsed droplet generation. (a) schematic of the chip with the sensor region corresponding to the rest of the images highlighted, (b) microwave heater is off with a stable interface maintained (hard to see due to the sensor); and (c-f) microwave heater is on with droplets being formed.

Microwave heating mediated on-demand droplet generation is demonstrated using a sequence of images shown in Figure 5.3. Figure 5.3 a shows schematic of the microfluidic chip and the region corresponding to the images. The droplet generation starts with a static interface maintained by the applied pressures (155 mbar and 300 mbar are applied at the inlet of the droplet fluid and carrier fluid respectively), while the microwave heater is turned off (Figure 5.3 b). After the heater is turned on with a power of 27 dBm (Figure 5.3 c), it deposits energy into the fluids near the interface which aligns with the capacitive gap of the resonator (Figure 5.1). The elevated temperature in the interface reduces the interfacial tension and thus the applied pressure difference overcomes the interfacial tension forcing the droplet fluid to penetrate into the oil stream (Figure 5.3 d) and to be dispersed into a droplet (Figure 5.3 e-f). The droplet formation can be stopped almost

instantaneously by turning off the microwave heater because the heat is localized and the fresh room-temperature liquid fills in the heater region lowering down the temperature quickly.

Microwave mediated droplet generation is basically thermal capillary effects; therefore, microwave power should influence the droplet formation. It is expected that droplet generation frequency would decrease with the microwave power decreasing. To verify this concept, the microwave power was varied from 24-27 dBm which would result in temperature increase of around 40-60^{o}C from room temperature [202]. Figure 5.4 depicts the effects of microwave power on droplet generation time. It can be clearly observed that a higher microwave power results in a shorter generation time. This fast change in temperature leads to a fast change in Laplace pressure which facilitates a quick droplet generation process. Therefore, adjusting the power of microwave could be a strategy for controlling droplet generation rate. However, it should be noted that too high temperature could potential overheat the thin PDMS film coated on top of the heater causing it to peel off from the heater and influencing droplet generation.

The microwave mediated droplet generation occurs in the squeezing regime [203] meaning that the interface grows into the oil stream causing obstruction to the upstream oil and then continues to grow till touching the horizontal channel wall and blocking the upstream oil. The build-up pressure in the upstream oil then squeezes and pinches off the droplet. In the squeezing regime, for a given set of fluids pairs, the droplet volume is mainly dominated by the applied pressures and the geometric conditions, which were maintained constant. It is expected that the droplet volume would remain roughly the same while microwave heating mainly influences droplet formation cycle. The volume of the generated droplets was measured and calculated as shown in Figure 5.4 showing that the size of droplets are close for each cases.

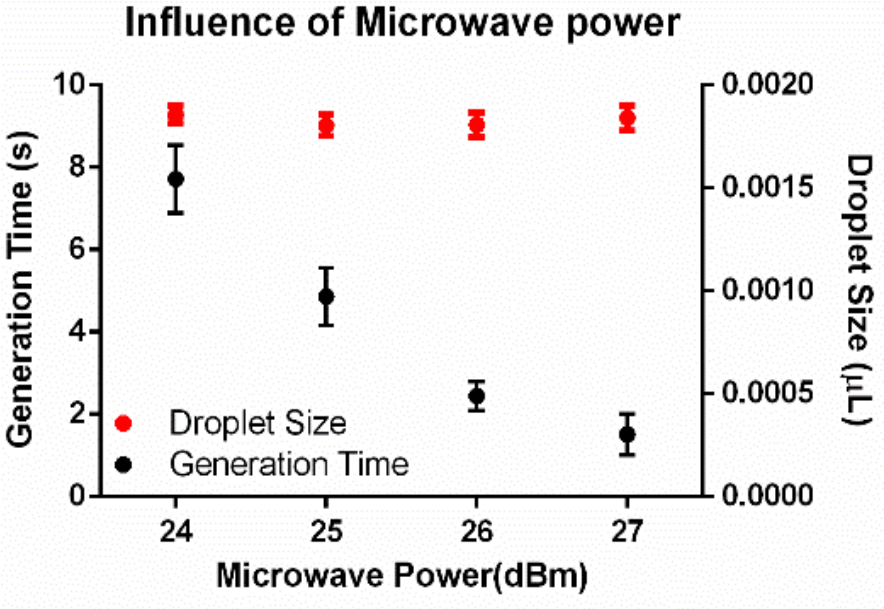

Figure 5.4. Relation between microwave power and droplet generation time and droplet size

The droplet formation cycle is long with the shortest one being around 1 second marking a generation frequency of around 1 Hz or lower. This is low compared with most passive droplet generation methods and some high-throughput active droplet generation methods. However, its advantages of on-demand droplet generation and potential to be integrated with microwave sensing

make it uniquely useful for many applications that require dynamically changing of the materials and well-controlled time for reaction. For example, the required microwave power could be tuned based on the materials that can be sensed.

5.5. Conclusions and future work

In this study, a simple, new method is reported for on-demand droplet generation mediated by microwave heating which generates disturbance to the interface by reducing the interfacial tension. The microwave heater is capable of confining power into a small region realizing localized heating which is advantageous for controlling droplet generation on-demand because the temperature of the fluid can be increased or decreased quickly. The generation cycle can be controlled by the applied microwave power and the droplet volume is mainly dependent on the applied pressures for a given set of geometric conditions and fluid pair. The limited throughput of generation can be further improved by optimizing the microwave resonator design and the droplet generator design, which justify an extensive additional study.

Chapter 6 : Crosstalk Analysis and Optimization in a Compact Microwave-Microfluidic Device for Simultaneous Heating and Sensing

6.1. Overview

This chapter will be submitted: Cui, Weijia, Zahra Abbasi and Carolyn L. Ren. "Crosstalk Analysis and Optimization in a Compact Microwave-Microfluidic Device for Simultaneous Heating and Sensing"

A non-invasive contactless simultaneous heating and sensing in a microfluidic device is enabled using planar Split-Ring Resonators (SRR). Simultaneous heating and sensing offer tremendous potential for tailored reactions, which are in high demand in material synthesis; however, it has always been very challenging. Such a function has been realized previously but was operated in a predefined mode. To fully realize the potential of simultaneous sensing and heating for tailoring the droplet's reaction environment, at least two resonators with one sensing the droplet and the other heating it are needed. The primary concern for two resonators in a single microfluidic chip is the crosstalk between the two resonators. Here, the crosstalk is referred to as the phenomenon that one signal creates the undesired signal in another circuit generating inaccurate results. This study investigates the fundamental challenges of integrating two or more microwave resonators within a typical microfluidic device footprint. In order to prevent crosstalk, numerical simulation is carried out to investigate the limitation of the distance between two adjacent resonators. The ANSYS HFSS is used to perform the electromagnetic analysis based on the finite element method. Experimental studies are also conducted to validate the numerical results using a vector network analyzer (VNA). An optimized distance between two resonators is suggested through this study

and provides design strategies for the future simultaneous microwave-microfluidic sensing and heating experiment.

6.2. Introduction

The Lab-on-Chip (LOC) concept has allowed the miniaturization for the advanced processes to be realized in very small devices. By integrating a series of functions onto one single platform, LOC devices present a number of advantages over their traditional counterparts, such as reduced sample consumption, shortened analysis time, lower cost and higher efficiency [12, 204]. Recently, the development of droplet microfluidic systems has offered a practical solution to improve and study the dynamics of many chemical and biochemical reactions, facilitating the development of LOC [56]. Further reduced sample consumption, increased reaction rate, and isolation of individual droplets by their carrier fluid make droplet microfluidic systems a strong candidates to serve as reactors/detectors, complementing or replacing their conventional counterparts [5]. Integrating droplet microfluidics enabled functions into LOC platforms offers tremendous potential to make typical reactors or detection methods, such as PCR process [37] or heavy metals detection [120], for Point of Use (POU) [205, 206]. However, to realize the potential, some challenges remain related to the applicability of microfluidic systems on a large scale, which lies in both fabrication techniques and the ability to accommodate multiple functional units in limited space without compromising their performance. In addition to droplet manipulations such as droplet generation, splitting and merging, droplet sensing and heating are the key functions to be integrated for chemical and biochemical applications [156].

Sensing in droplet microfluidics devices provides detailed information regarding materials' contents, concentration, size, and temperature, which is essential to fully realize the potential of

droplet microfluidics. Optical methods are commonly used for monitoring and detection in microfluidic systems [207]. In optical sensing, analyzing the light source changes from fluorescent, infrared, or UV provides information about different materials [208]. However, optical methods often require bulk detection systems, tend to exhaust the image analysis processor, and involve fluorescent labeling, limiting their application for POU. Electrical methods are alternative ways used in microfluidics sensing in favor of POU applications [209]. Capacitive sensors, electrochemical sensors, and impedance variation-based detection methods are widely available to extract material information by monitoring and processing the variation in the output electrical signals. Leveraging electrical techniques to detect microfluidic droplets size and flow rate inside the channel, or general control over and handling droplet manipulation, has been widely used in the literature [210, 211]. However, it raises challenges for conventional electrical methods to detect materials that are not electroactive and detect high throughput rates [10].

Planar microwave resonators have recently attracted a lot of attention from academia and industry for sensing applications due to their simple fabrication process, easy integration with CMOS, lab-on-chip compatibility, and flexibility design [212]. In microwave sensing, detection is carried out by utilizing the interaction between the electromagnetic (EM) field around the microwave sensor with the sensing material in the surrounding environment, which empowers them to perform highly accurate non-contact and real-time sensing and detection while materials under the test changes in electrical properties (dielectric permittivity or conductivity). Their exceptional performance in non-contact and distant sensing makes them a strong method for monitoring liquid inside the microfluidic channel since it eliminates the need for chemical modification or physical contact with the sample under the test [10, 213-215]. Researchers have devoted themselves to employing microwave to explore the dielectric properties of materials, especially liquid materials, promoting

using microwave techniques as sensing methods for liquid material detection in microfluidic systems [110]. Additionally, they have been utilized for a wide range of highly sensitive applications, including hazardous gas concentration monitoring[216, 217], biomedical detection[218], and chemical solutions sensing [219-221].

Heating in a microfluidic platform is desired for many applications, such as DNA amplification [147] and materials synthesis [222]. In microfluidics, available popular heating approaches rely on heat conduction using one of the resistant heating, Peltier, and Joule heating methods, where simple elements are used to realize efficient heating [223]. However, these heating techniques suffer from imprecise heating, which is a severe drawback of localized heat production. Optical methods such as laser heating have also been used due to their efficient and precise heat production but relying on expensive equipment and tedious alignment limits their broad applications. As a result, portable, efficient, and low-cost heating methods are desired to be integrated with microfluidic systems for multiple applications.

The application of planar microwave structures in microfluidic systems has been demonstrated for localized heating [11, 185]. In the microwave frequency range, some liquid materials have the ability to convert electromagnetic emerge to heat due to molecular friction. This kind of heating is volumetric and spontaneous in nature, which means that the heating can be self-triggered by materials entering the microwave heater region [45]. Using microwave-based heating structures can directly provide power to the target materials and realize fast heating, significantly reducing reaction time for many applications [127]. These advantages make microwave technology an excellent candidate to be integrated with microfluidic systems for both sensing and heating purposes.

The main element of the proposed microwave system for sensing and heating is a split-ring resonator (SRR). The SRR is able to distinguish materials by their different electrical properties such as permittivity and conductivity. The changes in these properties cause variations in the system's frequency response, which can be used for sensing purposes. Additionally, delivering microwave power to the sensing region of the SRR limits the power to be received only by the droplet passing the resonator, leaving the surrounding media unaffected. Microwave sensing and microwave heating of individual droplets have been demonstrated separately with a single SRR [10, 224]; however, its promise for simultaneous sensing and heating of droplets has not been realized, which requires more than one SRR to be integrated.

Selectively heating individual droplets with a certain content to the desired temperature is very challenging. It needs to acquire the droplet content information by droplet sensing first, which is then used as the feedback for selectively heating this particular droplet. Two resonators are needed to realize this procedure, with one for sensing and the other for heating, and they need to work together and be controlled by a backstage system. Integrating two microwave resonators on a typical microfluidic chip of 1”x3” presents the potential to realize simultaneous microwave sensing and heating and raises a concern of crosstalk between the two resonators. The crosstalk here is referred to the phenomenon that one signal creates the undesired signal in another circuit generating inaccurate results.

This paper proposes a study and detailed analysis of the impact of two SRRs and the crosstalk between them during simultaneous sensing and heat production. The SRRs are a copper trace that offers consistent performance, making the proposed structure highly reliable. Different sets of simulations and experiments have been performed to highlight the effects of varying the design

parameters on the crosstalk and interference level. This brief will be continued in Section 6.3 with a focus on methodology, and the simulations and measurement results for different studies are presented in Section 6.4, followed by a conclusion in Section 6.5.

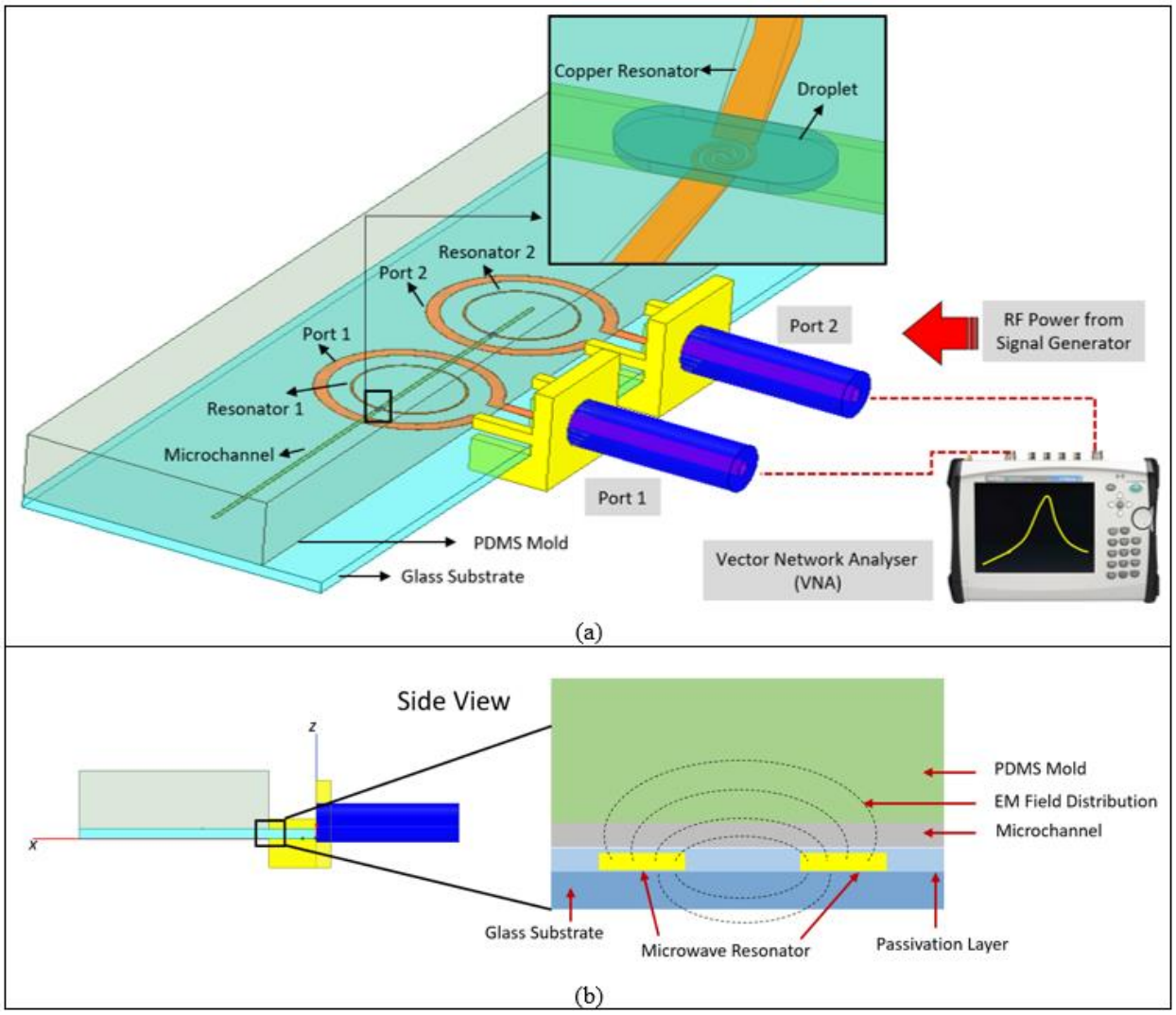

Figure 6.1. (a) Detailed schematic of the proposed microwave-microfluidic device for simultaneous heating and sensing and (b) side view of the microfluidic chip of model.

6.3. Methodology

6.3.1. Effect of Design Parameters on Crosstalk

Figure 6.1(a) shows a schematic of the proposed microwave-microfluidic device, including a sensing resonator (resonator 1), and a heating resonator (resonator 2), fabricated on a glass substrate. The form of the experimental microfluidic system and the shape of droplets are also shown in Figure 6.1(a). The designed microchannel is responsible for carrying the droplets and the details of the microfluidic chip is shown in Figure 6.1(b). The side view of our model exhibited the complex layers of the devices including the glass substrate, two resonators, a passivation layer separating the resonators from the microchannel molded in PDMS and the dashed lines sketching the electrical field line. A signal generator has been used to apply RF power producing heat, and a Vector Network Analyzer (VNA) measures the microwave sensing results. When two resonators are located close to each other, there will be interactions between their EM fields, and as a result of this mutual coupling between the two resonators, crosstalk occurs. This interference could seriously affect the sensing and detection results that influence the control and precision of the whole system since precise sensing is required to create reliable heat on the droplet. In the proposed design, the impact of high-power RF signal exciting the heating resonator on the sensing resonator, which will significantly influence the detection results, is also one of the major concerns. A key factor determining the crosstalk is the physical distance between the two resonators placed on the device, which must be optimized. An optimal distance here indicates that the distance cannot be too small, causing significant crosstalk effects or too large, which is limited by the size of our typical microfluidic device (normally 1”x3”). Additionally, the resonators will not be able to

perform simultaneous sensing and heating when the distance between them is too large due to the time delay for the droplet to travel through both the resonators.

The key objective of this work is to numerically and experimentally investigate the impact of different design factors on the crosstalk between the two-resonators integrated in a microfluidic system. The influence of the distance between the two resonators (refer to as gap distance, d, in Figure 6.2, hereafter), resonator design, and microwave power on crosstalk are investigated. To focus on the crosstalk, the design of the two resonators are considered to be the same. Numerical simulation in this work is served as a main tool to construct the chip model and investigate the crosstalk between the two resonators. ANSYS HFSS is employed to simulate different configurations and conditions with changing parameters. Transmission parameters and the scattering parameters are presented for crosstalk investigation. The justification of the assumptions in this work has been analyzed in detail previously [185]. Therefore, some major assumptions have been made as follows: i) droplets are stationary on the top of resonators, which is considered such that droplet motion does not influence the electrical field; ii) the droplets are studied as directly contacting with the channel wall and the gutter region at the intersection of the cornets, and 3D droplet shapes are considered; and iii) the dielectric constants of the droplet and chip materials in the simulation are considered as constant to neglect their effect on the electrical field.

6.3.2. Designing Microwave Resonator-based Structure

The numerical model is constructed in HFSS with two resonators illustrated in Figure 6.2. A microfluidic system with two identical resonators is designed and simulated, and the dimensions of the design are also included in Figure 6.2. The microwave signal is fed through the outer loop microstrip line, the ports connected to SMA connectors and coaxial cables. The inner loop is the

SRR with a small gap, which is the hotspot of the resonator for sensing application. It is designed in a spiral shape to confine microwave energy and maximize its interaction with the microchannel aligned with the gap area.

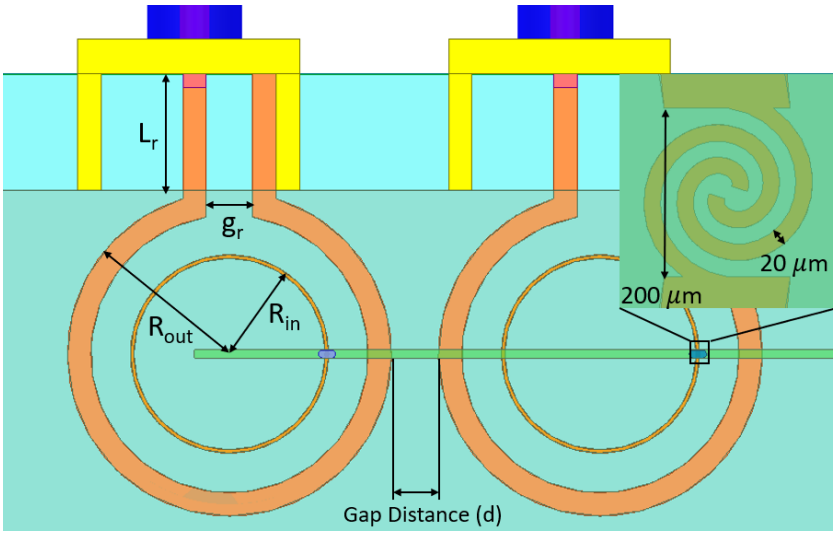

Figure 6.2. The main structure of the proposed design with the dimensions: $L_r = 5mm$, $g_r = 2mm$, $R_{out} = 6.95\ mm$, $R_{in} = 4.25mm$, $d = 2mm$

Another important part of the simulation process and understanding the numerical problems is the boundary conditions setup in HFSS since boundary conditions define the field behavior in the discontinuous boundaries. Applying the boundary conditions in HFSS helps control the characteristics of the planes' faces or interface between objects and reduce the complexity of the model. As a result, specific simulation conditions have been defined and used for reliable and high accuracy simulations, which are listed in Section 3.5. As mentioned before, the purpose of this work is to investigate the crosstalk phenomena in the microfluidic chip with multiple resonators. The gap distance, the radius of the inner and outer loop, and the power of excitation are among the most critical parameters that affect the crosstalk between the two resonators in the system. Figure

6.2 illustrates the geometric parameters including the gap distance (d), the radius of the resonators (R_{in}) and the radius of the ports (R_{out}).

6.3.3. Scattering Parameter and Sensing Analysis

The behavior of the microwave resonator is characterized and evaluated by scattering parameters (S-parameters). In the proposed platform, a two-port network is considered due to the existence of two microwave resonators. S-parameter can help us analyze the power transfer and reflection between each port. The reflection coefficient, S11, is used to determine the material properties change in the resonator region for sensing purposes. It is the ratio of reflected power to incident power. Transmission coefficient, S12, characterizes the ratio of the reflective power in port 1 over the incident power in port 2. In this study, the transmission coefficient is used to evaluate the crosstalk by analyzing the power transferred to port 1 relative to the input power at port 2.

The S12 response of the microwave sensor is dependent on the electrical characteristics of the ambient surrounding it. The main microwave circuit in the proposed design is SRR, and the initial resonant frequency of the resonator is related to its physical length (l) according to the following equation:

$$l = \frac{1}{2\sqrt{\varepsilon_{eff}}}\frac{c}{f_r} \tag{6-1}$$

where c is the speed of light (m/s), f_r is the resonant frequency (Hz), and ε_{eff} is the effective permittivity (F/m) of the resonator medium that is determined by the material surrounding the tag resonator [225]. The variation in ε_{eff} will affect the resonance frequency to shift up/down depending on the sample under test.

Assuming the complex permittivity of the material under test over the tag resonator is a complex value:

$$\varepsilon = \varepsilon_r - j\varepsilon'' \quad (6\text{-}2)$$

where ε_r is the relative permittivity, which is a measure of how much energy from an external electric field is stored in a material. The imaginary part ε" is called the loss factor and is a measure of dissipation or loss of a material in the presence of an external electric field. The presence of the material in the ambient around the resonator will act as the most effecting element to change ε_{eff}, making it suitable for sensing. On the other hand, the variation in ε" will be reflected in amplitude variation and quality factor [215].

6.3.4. Experimental methods

The fabrication of a microfluidic chip is based on soft lithography. The fabrication of microwave resonators relies on electroplating on a copper-coated glass slide (Cu134 from EMF Corporation), and more details can be found elsewhere [46]. The difference between the previously fabricated single resonator and the two resonators lies in the alignment of two resonators in a single glass slide, which requires the entire electroplating process to be more precise and careful. Microfluidic chips with two resonators differing in the gap distance are fabricated to validate the simulation results. After the electroplating procedure mentioned above, plasma treatment is carried out with a glass slide and a polydimethylsiloxane (PDMS) mold. The plasma treatment tightly follows bonding of glass slide and PDMS mold under the microscope, and a marker in the glass slide is used to ensure that both resonators are in the middle of the microchannel in the PDMS mold. The chip image and schematic are shown in Figure 6.3. Vector Network Analyzer (VNA) (MS2028C,

Anritsu) is used here to characterize resonator sensing performance and evaluate crosstalk problem.

6.4. Results and discussion

6.4.1. The effect of gap size on crosstalk

In our work, a typical microfluidic device features a size of 1”x3”, which is a relatively small device limiting the wide deployment of multiple resonators. The first and major parameter to be considered in this work is the gap distance, which directly affects the coupling strength between them, a dominant factor for the determination of crosstalk. The smaller gap distance increases the interference they have on each other in terms of performance. Also, crosstalk becomes a more significant issue for the microfluidic devices due to the small size of the device, which adds a limitation to the location of the transmission lines. Therefore, it is necessary to find an optimized gap distance to prevent crosstalk while designing the microwave-microfluidic device at its minimum size.

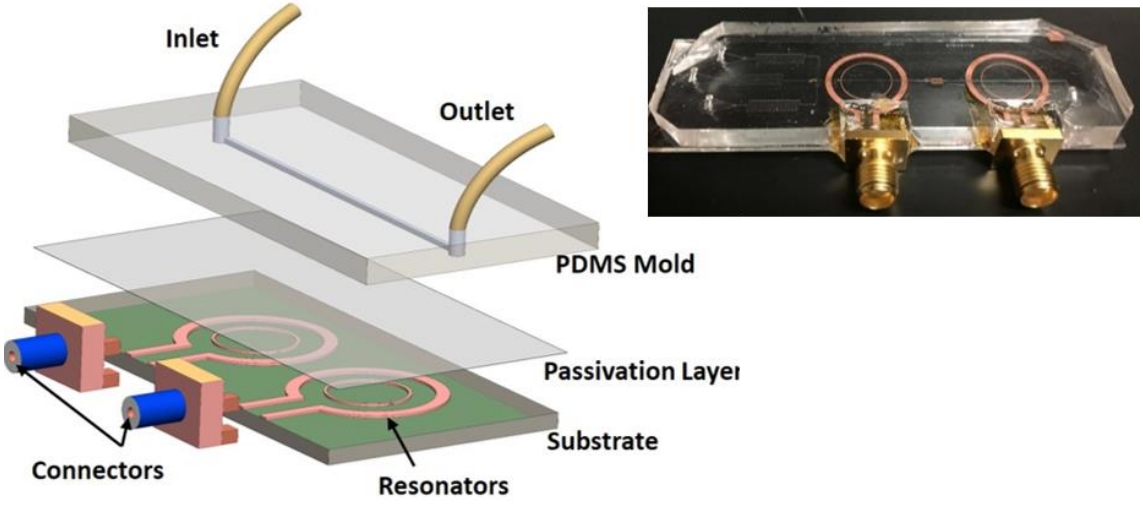

Figure 6.3. The schematic of components and fabricated microfluidic chip for validation.

In the first step of simulations, the variation on the gap distance is studied. The gap distance in the numerical simulation is defined as the minimum distance between two outer loops (d) changing from 2 mm to 12 mm. The choice of 2 mm as the smallest gap distance is due to the fabrication limitations since enough space is required for the two SMA connectors being soldered. Considering the overall channel structure and microchip size and to avoid failure of fabrication process, the upper limit for the gap distance is set as 12 mm. Figure 6.4(a) exhibits the simulation results for S12 parameter versus frequency for different gap distance values. Both the amplitude and resonance frequency variation of the S12 response are affected by d changes as shown in Figure 6.4(a). An overall trend for the frequency variations as d changes is shown in Figure 6.4(b). The results presented in Figure 6.4 also highlight that the S12 response amplitude level increases as the distance between the two ports decreases, which results from stronger coupling and more power transfer from port 1 to port 2. When the S12 goes lower in amplitude in the frequency range, it means less power is coupled between the two resonators, and less crosstalk would be the result. Comparing different S12 responses shown in Figure 6.4(a), less signal tends to be transferred from port 1 to port 2 making the crosstalk effect negligible. In the gap distance variation from 2 mm to 5 mm, the S12 amplitude value at resonance frequency changes 12.2%, and this ratio is 4.3% for 5 mm cases and 10 mm cases. But when distance varies from 10 mm to 12 mm, the S12 valley value at resonance frequency shows a 1.89% difference resulting from weak coupling in 10-12 mm distance range.

Based on the simulation results, microfluidic chips with a different gap distance of 2 mm, 5 mm, and 10 mm are evaluated for crosstalk performance. It is worth mentioning that the 12 mm case is not selected due to its similar performance as 10 mm. The fabricated devices for d=2 mm,5 mm, and 10 mm is presented in Figure 6.4(c) followed by the measurement results in Figure 6.4(d). In

Figure 6.4(d), transmission coefficient S12 shows a similar trend as simulation results. When the gap distance increases, S12 parameter decreases indicating that there is a reduction on crosstalk phenomena. S12 parameter of 10 mm case has the smallest value among three cases showing less coupling effect and presents the best performance to eliminate crosstalk.

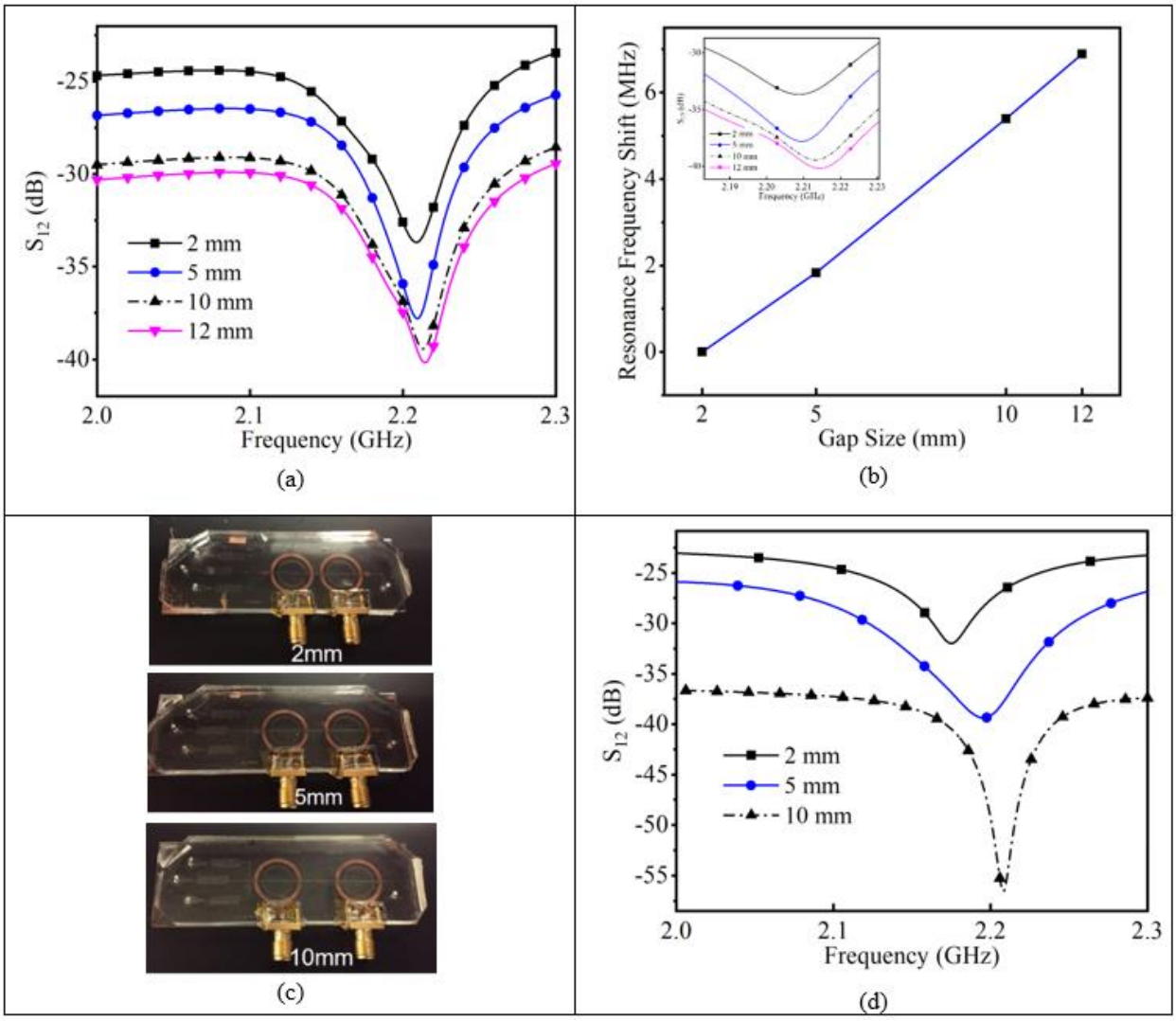

Figure 6.4. (a) Numerical simulation results for S12 while changing minimum gap size between the two resonators: 2 mm, 5 mm, 10 mm, and 12 mm, (b) frequency shift versus gap size as it changes from 2 mm to 12 mm, (c) fabricated device for different gap size values, and (d) Measurement results for the S12 response d=2 mm, 5 mm, and 10 mm

As shown in Figure 6.4(a) and (b), the resonance frequency is also impacted as the gap distance changes. A circuit model of the design is shown in Figure 6.5(a) for further understanding to analyze the resonance frequency variation in the response by changing the gap distance. In Figure 6.5(a), C_μ and L_μ describe the microstrip copper line of port 1 and port 2, which is coupled to the ideal (lossless) resonator with couplings capacitors C_{c1} and C_{c2}. The ideal resonator is modeled with a parallel inductor and capacitor, $C_1 - L_1$ for the resonator coupled to port 1 and $C_2 - L_2$ for the resonator coupled to port 2 [216, 226]. Another considerable effect is created by the presence of $C_{Crosstalk}$ since the closeness between the two ports/resonators results in forming and unwanted capacitor which is a circuit definition for the crosstalk. By increasing the distance, the coupling capacitance in the gap, $C_{Crosstalk}$ becomes a smaller value and as a result of that, the equivalent capacitance of the circuit model (C_{equ}) will be impacted (Figure 6.5(b)). Referring to the relation between the resonance frequency (f_r) and the equivalent capacitance and inductance of the circuit model ($f_r = \frac{1}{2\pi\sqrt{L_{equ}C_{equ}}}$) and considering the fact that C_{equ} and $C_{Crosstalk}$ are directly correlated, the resonance frequency will be impacted by variation of the gap size. A larger gap size results in a smaller value of $C_{Crosstalk}$ and reduces the equivalent capacitance of the whole 2-port circuit and this creates upshift in frequency, which is verified in simulations and measurements.

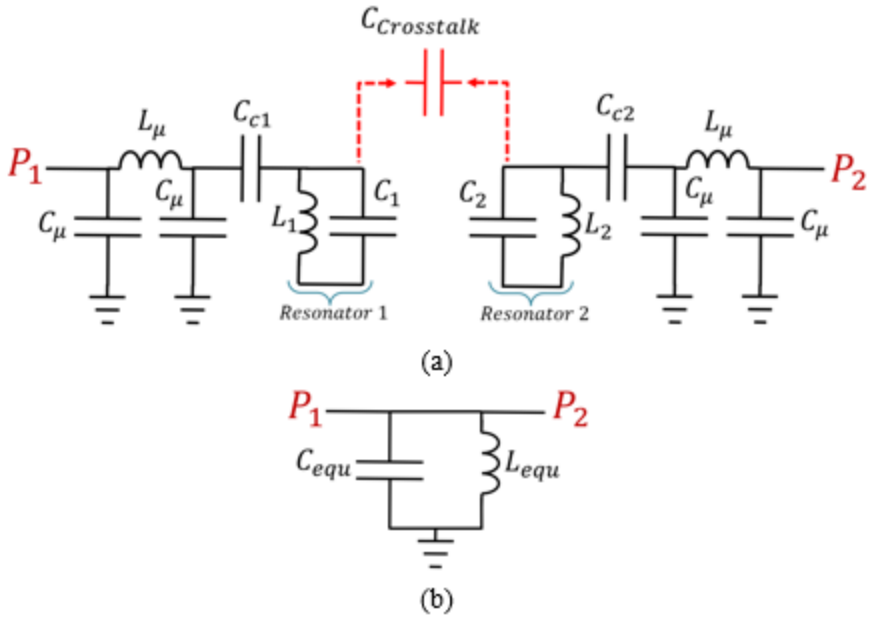

Figure 6.5. (a) Detailed and (b) equivalent Circuit model for the proposed dual-resonator structure with Advanced Design Systems (ADS) simulations

Figure 6.6(a) describes the simulation for S11 while the resonator, coupled with port 2, performs microwave heating. Port 2 is connected to a power input of 26 dBm, a standard power level used in microfluidic heating experiments [46], and port 1 is connected to the VNA to monitor variation around the coupled resonator, which is a microwave sensing device. To evaluate the effect of crosstalk initiated from the strong microwave signal in heating resonator on sensing performance, S11 of a single resonator structure is used as the reference, since there is no effect from a secondary resonator that could cause crosstalk in the response, and other simulations are compared to it. As the gap distance increases and the S11 signal in the dual resonator structure is getting close to that of one resonator case, the result indicates minimum crosstalk. It can be observed that the 2 mm gap distance demonstrates the maximum difference between single and dual resonator cases, and as the gap distance increases, S11 is getting closer to the no crosstalk situation. As shown in Figure

6.6(a), the resonance frequency in the S11 response moves to upper frequencies as the gap distance increases, which is also the result of decreasing $C_{Crosstalk}$ and C_{equ} as a result of it. Figure 6.6(b) shows the S11 measurement results from the fabricated device while the second resonator is used for heat production. It suggests that as the distance increases from 2 mm to 10 mm, the crosstalk is decreasing. The experimental results and the numerical simulation results confirm that a 10 mm interval for two resonators is an optimized distance to minimize crosstalk.

6.4.2. The effect of resonators' radius on crosstalk

Based on the experimental results presented in Figures 6.4 and 6.6, 10 mm is the optimized gap distance which allows the design of the resonators to be tuned to further minimization in the crosstalk. An important parameter worth investigating is the radius of resonators, R_{in}, and the ports, R_{out}. In regular cases, R_{out} is set as 6.95 mm and the R_{in} is 4.25 mm. In order to investigate the influence of different radius on the crosstalk between two resonators, the inner and outer loop radius are considered with the change from 0.25 to 0.5mm in the simulation. Figure 6.7(a) shows the S12 results of the cases with the variations in R_{out} values. The outer loop in the resonator structure is designed to be excited with microwave signal and transfer the signal to the resonator, which is designed as the inner loop, through EM coupling. With different outer loop radius, while keeping the inner loop radius a constant value, it can be observed that the amplitude of the S12 response drops as the outer diameter decreases, which indicates that the decreasing of the outer loop diameter increases the coupling between the excitation ports and the resonator and has a positive effect on reducing crosstalk. In these cases, the resonance frequency stays consistent because changing outer loop radius effect on C_{equ} and L_{equ} is negligible.

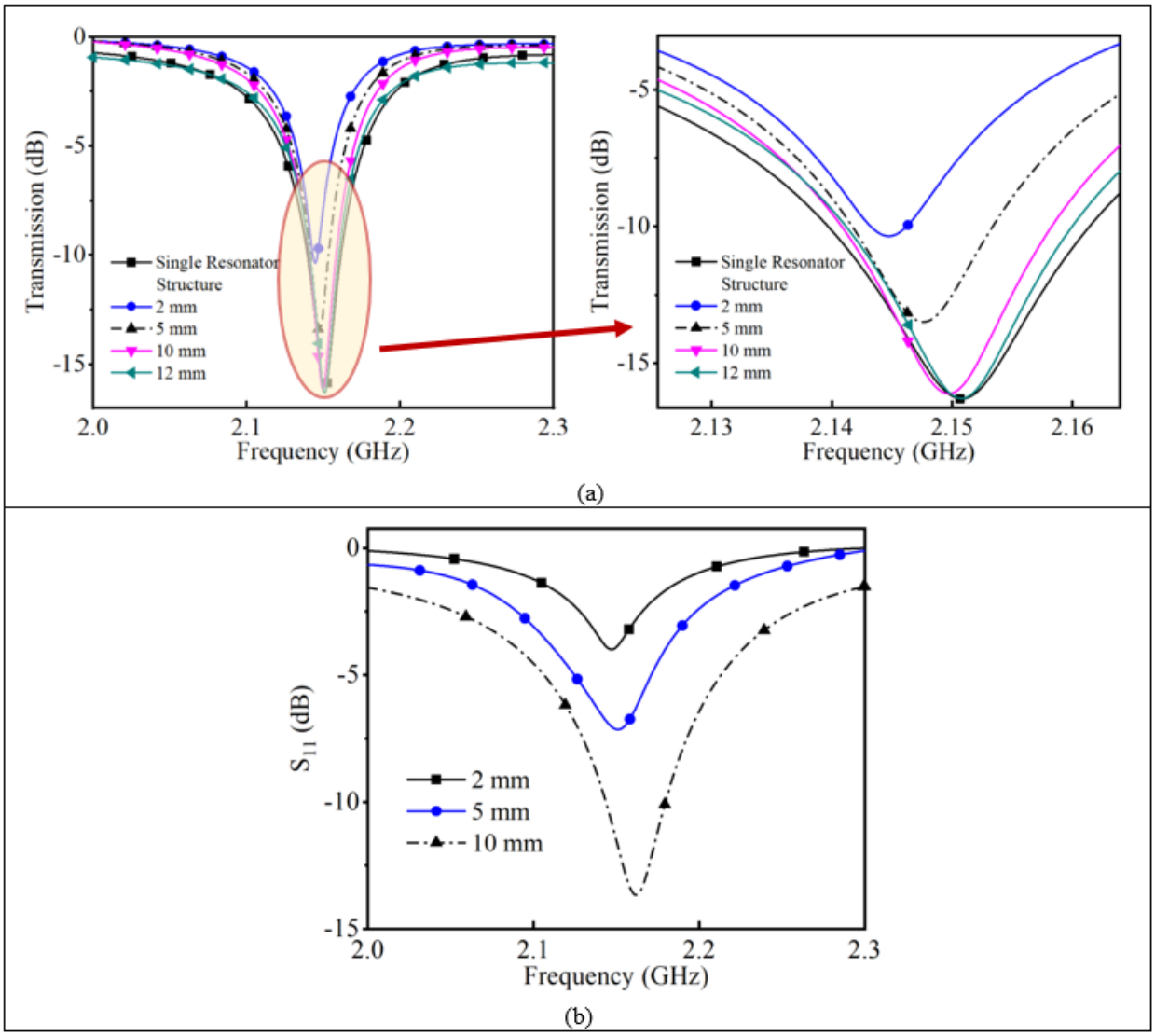

Figure 6.6. S11 (a) Simulation and (b) measurement results for different cases with a changed distance between resonators while using S11 of a single resonator structure as the reference point.

In Figure 6.7(b), S12 parameter of the varying R_{in} is exhibited. When the inner loop radius increases, the amplitude in the S12 has a decreasing trend, implying the reduction of crosstalk and this trend is similar to the outer loop cases. As the increase of the inner loop radius, more power is coupled to the inner loop from the outer loop resulting in a reduction of crosstalk. As the inner

loop radius increases, the resonance frequency of the S12 response reduces since the resonance frequency and the resonator's total length is reversely correlated as mentioned in equation (6-1).

From these two studies investigating the loop design parameters, it can be concluded that optimizing the resonator design by reducing the distance between two resonators (either increasing the radius of the inner loop or decreasing outer loop radius) can help to alleviate crosstalk between two adjacent resonators.

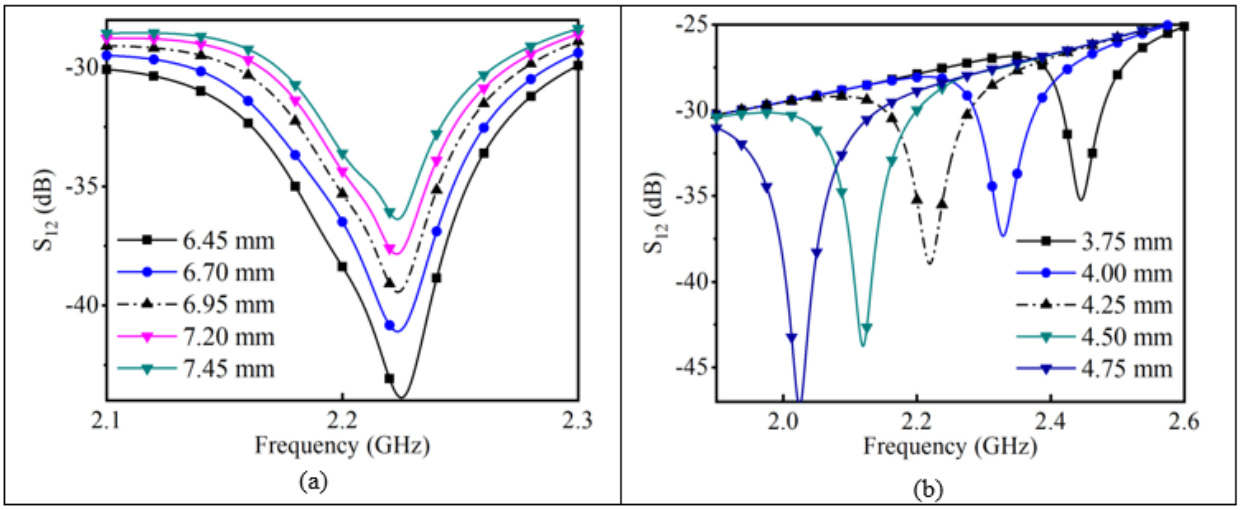

Figure 6.7. Numerical simulation results for different cases with a changed radius for (a) Outer loop (b) Inner loop.

6.4.3. The effect of signal generator power on crosstalk

Any undesired signal that interferes with the target signal can be defined as crosstalk. The signal strength also affects crosstalk, besides manipulating the structure and gap distance of the two elements. The resonator for heating purposes receives signal with high power, and this high-power signal can cause an undesired signal in the resonator for sensing. As a result, it is necessary to

investigate the impact of the power level received in the heating resonator on the sensing resonator coupled to port 1. Changing the input power level connected to port 2 for heating purpose will change the transmitted power from port 1 to port 2, and as a result of it the reflective power characterized by S11 which is an indicator of crosstalk. Therefore, S11 is used to evaluate the effect of microwave power on crosstalk. Figure 6.8 depicts the numerical results of the power effect on crosstalk. The input power is changing from 26 dBm to 20 dBm. The S11 signal with different input power is compared with one resonator case, which is considered no crosstalk. As the input power value decreases, S11 signal gets closer to the no crosstalk case, meaning that the crosstalk is reduced. Therefore, minimized input power is desired to prevent crosstalk if it is high enough to produce the required heating for a specific application.

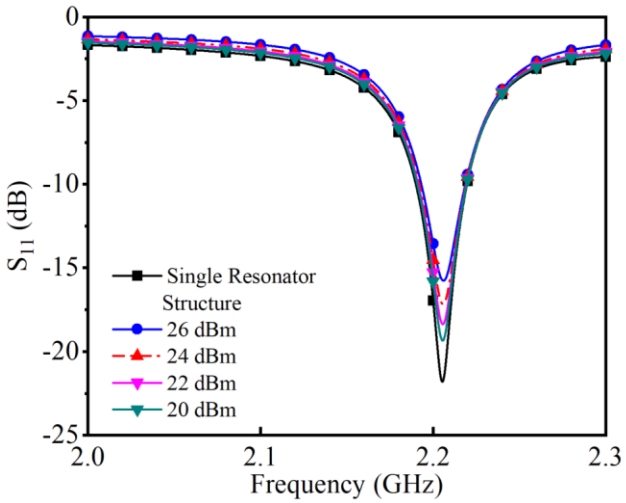

Figure 6.8. Numerical simulation results to investigate the effect of microwave power on crosstalk

6.5. Conclusions

In this study, we numerically and experimentally investigated the crosstalk between two adjacent resonators integrated in a microfluidic chip and the effect of crosstalk on the sensing performance of the design. In particular, we aimed to overcome the crosstalk phenomena by investigating the influence of parameters, including the distance between the two resonators, the radius of the excitation and resonator loops, and the input power. After the calculation of numerical simulation and experimental validation, an optimized distance of 10 mm between the two resonators is confirmed with less crosstalk inference and can be used for the next step experiments. Optimizing design of the resonator design by increasing the inner loop radius or decreasing the outer loop radius can also alleviate the crosstalk between two resonators. Lower input power if applicable is desired to reduce crosstalk. This study gives an understanding about the crosstalk between two resonators in a typical microfluidic chip and offer strategies to minimum the crosstalk influence for double resonators.

Chapter 7 : Lead detection based on nanomaterials modified microwave sensor in microfluidic device

7.1. Overview

This chapter will be submitted as two papers: (1) Cui, Weijia, Zhe Ren, Yongxin Song and Carolyn L. Ren. "Development and potential of heavy metal sensing in microfluidic systems: A Review."; (2) Cui, Weijia, Zhe Ren, Yongxin Song and Carolyn L. Ren. "Lead detection based on nanomaterials modified microwave sensor in microfluidic device"

Lead in drinking water mainly arises from aging pipes and a small amount of lead can cause serious health problems to human. Therefore, constructing early monitor and warning of lead concentration in water is necessary and impactful to prevent any damage caused by lead. Conventional methods suffer from some limitations including high cost and bulk size device which prevent their widely use. In this work, a novel method to detect lead in water is presented based on a microfluidic chip integrated with gold nanoparticles modified sensor. The microwave sensor is designed as a double T structure and aligned with microfluidic channel to detect lead solutions. The results indicate that sensors modified with gold nanoparticles have bigger resonance frequency shifts than bare sensors. Distilled and tap water are both used to dissolve lead and similar results indicate that this method is capable to detect lead in real drinking water system. A portable vector network analyzer is proved to be capable of detecting lead concentration. Using gold nanoparticles modified microwave resonator in a microfluidic chip offers a new pathway to realize real time detection of lead in water.

7.2. Introduction

Lead is an important element which has been widely used in industry areas including construction, batteries, bullets and paint. However, it is hard to avoid lead leaking or exposure to the environment, which can cause serious health problems. Researchers have investigated the toxicity of lead to environment and human body [227]. The pollution of lead has drawn great attention owning to the damage to human body caused by exceed amount lead, including disturbing nervous system and the damage to the brain. The tolerance amount for lead is always small in trace level and many international organizations like World Health Organization (WHO) and countries have set up the safe standard for lead ranging from 5 ppb to 15 ppb [228-231]. One of the major sources of lead is from the lead pipes and aging infrastructure, especially in some old facilities, which has high possibility to leak lead to human's drinking water. An investigation regarding to the amount of lead in Canadian drinking water was carried out by several universities and media institutions. The results showed that most Canadian drinking water has an excessive lead amount [232]. Therefore, it drives us to investigate methods to monitor the level of lead in drinking water system and to control the lead level in the acceptable range.

To detect the level of lead in trace level, conventional methods including atomic absorption spectroscopy (AAS) and mass spectroscopy (MS) have been used in professional laboratories [233]. These methods have great advantages to offer the detection for lead with high sensitivity and selectivity and reaching a good limit of detection (LOD) [234]. However, high cost for bulk devices, tedious sample preparation, and professional personnel are required to carry out the detection for lead based on these methods. And all the processes for conventional methods have to be performed in central laboratories, thus the samples have to experience transportation which

would increase the detection period and the risk of contamination. The shortcoming of these conventional methods limit the large scale use and real time detection for lead detection in the environment and stimulate the advanced methods to realize real-time detection of lead [44, 121, 234].

Microfluidic systems are good solutions to address the disadvantages of conventional methods with bulk devices [44]. Microfluidic systems deal with the fluid in micro and nano scales and enable the physical or chemical process with small amount of samples and short reaction time [12, 138]. The opportunity for using microfluidic systems to detect lead amount lies in the combination of microfluidic systems and lead detection sensors to construct a Point of Care (POC) device [14]. This combination can impact multiplex functions to a small devices and enable small sample volume, short detection time, on-chip sample preparation and detection, which can offer more opportunities to develop real time and in-situ lead detection sensors [44].

Efforts have been made to develop portable heavy metals detection sensors to realize real-time detection based on microfluidics systems. The most representative methods are optical and electrochemical sensing [233]. Optical methods rely on the interaction between target heavy metal ions and designed chemical materials with specific optical properties [235]. The optical signal changes including fluorescent intensity, ramen intensity, UV, and color change are then tracked to detect the existence and the amount of heavy metals [208]. Zhao et al. have presented a method in a microfluidic device for detecting Pb^{2+} using fluorescent sensor Calix-DANS4 which has the selective and sensitive character towards Pb^{2+} detection [236]. The microfluidic chip allows on-chip passive mixing of sample and fluorescent molecular and achieves on-chip fast detection with a LOD of 5 ppb. Faye et al. has synthesized a fluorescent sensor containing three complexing

dansyl fluorophores (Calix-DANS3-OH) to detect Pb^{2+} [237]. An improvement made in this work is to anchor the florescent sensor Calix-DANS3-OH on the microfluidic device. They unutilized covalent bonding by making use of the inert siloxane bonds of PDMS polymer and activating its surface to graft fluorescent sensor to the wall [238]. A fluorescence quenching is then used to observe Pb^{2+} complexation in order to detect Pb^{2+} amount [237]. Optical fluorescence sensing towards Pb^{2+} shows a good selectivity and sensitivity but relies on the special bio-markers as additional chemical modification to bind with Pb^{2+} and requires bulk optical devices like fluorescence spectrometry which could limit the wide use of optical methods. Also in some harsh environments for example the cold areas, it rises the challenge for markers' properties which can be sensitive to temperature. Fan et al. in their work show a simple and portable device to detect Pb^{2+} [239]. The presence of lead can be tracked through observation of the aggregation from the reaction of Pb^{2+} with 11-mercaptoundecanoic acid (MUA)-functionalized gold nanoparticles (MUA-AuNPs). The test is carried out in a PDMS with aggregation generated on the surface of chip and this can be visualized as a solid line. The result can be observed with naked eye or a drop of water as a magnifier which increases the portability for this methods and improvement can be made to enhance the LOD for more sensitive detection. Electrochemical methods for detecting heavy metals deal with the electric signal instead of optical signal. The mechanism is based on the movement of electrons on the electrodes surface [125]. Different electrical signal is detected to distinguish heavy metals ions based on their different redox potential using electrochemical methods. Hong et al. have established a microfluidic sensing platform for cadmium and lead detection [240]. In their work, the microfluidic device is fabricated using 3D printing technique. The electrode is constructed by using screen printed electrodes modified with porous Mn_2O_3 derived from metal organic framework (MOF). MOF based nanomaterials is believed to have high

surface and thus to have high chemical activity, which can greatly increase the sensitivity and selectivity. The LOD for lead can be achieved at 2ug/L by using this electrochemical based sensing systems [241]. Shen et al. exhibit a modifier free and sensitive microfluidic carbon based electrochemical sensing method to detect heavy metal cadmium and lead [242]. They utilized the pristine graphite foil as working electrode to avoid the use of any surface modifier for electrode. They demonstrate a good sensitivity towards heavy metal detection with a LOD less than 2 ppb. Electrochemical methods always need to require a pretreatment or preconcentration process which could increase the complexity of the systems.

Microwave technology can realize detection without any chemical modification and additions and physical contact with samples is not required for microwave sensing which prevent the possibility for cross contamination of the samples [11]. Microwave technology has been used for materials sensing based on the interactions between target materials and generated electromagnetic waves. Microwave sensing can be used to track the difference of materials' electrical properties including permittivity, conductivity, capacitance, resistance, and inductance [134, 139, 243]. Vector network analyzer (VNA) is a common used device to carry out microwave detection process by offering frequency sweep and detecting the magnitude and phase of reflection coefficient (S11) [244]. The planar structured microwave resonator with small size enables the combination with microfluidics to construct a system to realize real-time detection with fast detection rate and low consumption of samples [245]. Boybay et.al have fabricated the microwave resonator using photolithography and electroplating and bound with a Polydimethylsiloxane (PDMS) chip to detect droplet contents using microwave [11]. Droplets with different permittivity and conductivity can be distinguished in a short time. Frau et al. have recently reported a novel approach to detect Zinc in water by using a planar microwave sensor with screen printed based coating [246]. The microwave sensor is

fabricated with gold made eight-pair interdigital electrode by screen printing and coated with β-Bi_2O_3. The utilization of coated β-Bi_2O_3 in their work is aimed to increase the reaction and sensitivity towards zinc detection based on the adsorption and its rapid electron transfer kinetic. They demonstrated that the sensor with 60 μm of β-Bi_2O_3 shows a better sensing performance than bare sensors for zinc detection.

Microwave technology has been proved to be a reliable method to detect materials with different properties. The addition of nanomaterials has been used for many detection applications to improve the sensitivity of tests [44]. In this work, we report a novel method with the ingenious cooperation of nanomaterials, microwave technology and a microfluidic platform, which is capable to detect the amount of lead in water. The addition of nanomaterials on the resonator has been proved to improve the sensitivity for heavy metals detection. The sample is tested in distilled water and tap water to verify the universality of this method. Finally, a portable and low cost Nano-VNA is employed to carry out the sensing experiments to justify that this method can be widely used for real time detection of lead amount in water.

7.3. Experiments

7.3.1. Materials and devices

The detection device is based on a microfluidic chip with fluid inlet, outlet, and microfluidic channel microwave resonator and a VNA. The schematic of the entire devices is shown in Figure 7.1. The microwave resonator is a co-centric ring structure which is fabricated through photolithography and electroplating processing based on purchased 500 Å copper coated glass slide (EMF Corporation). The detailed fabrication process has been described in one of our

previous published paper [11]. In this co-centric structure, the outer loop receives signal from VNA and the inner loop has a capacitive gap which is aligned with microchannel to sense the materials passing through resonator areas. After the fabrication of microwave resonator, 5 µL Au-NPs solution is dropped on the resonator area and let it dry in the fume hood. A passivation layer on top of the resonator can protect the resonator to get contaminated and short circuited. A mixture of Toluene, PDMS, and curing agent with the mass ratio 11:10:1 is prepared and coated onto the resonator. To bond PDMS chip and glass slide with microwave resonator, they are both treated with oxygen plasma at 29.7 W, 500 mTorr for 2 min and the bonding process is operated under microscope. Finally, an SMA connector (Tab Contact, Johnson Components) is soldered with microwave resonator outer loop to connect with VNA. In Figure 7.2, it despites a layer by layer structure of the microfluidic chip with an integrated microwave resonator.

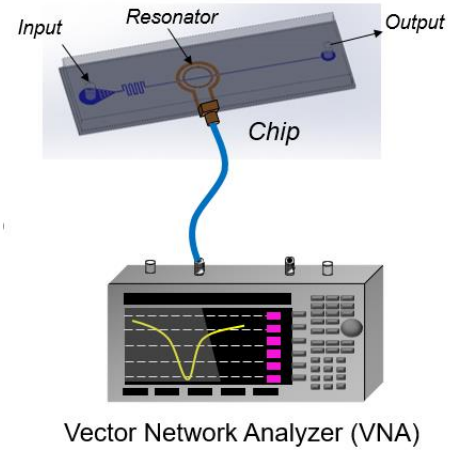

Figure 7.1. The schematic of the detection system including microfluidic chip integrated with microwave sensor and VNA for signal detection connected with coaxial cable

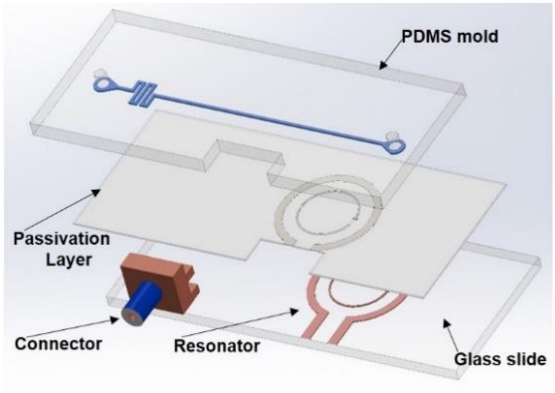

Figure 7.2. A layer by layer structure of microfluidic chip with microwave sensor

7.3.2. Sample preparation

Lead solution in the experiments are prepared based on ICP standard solution (Sigma, 1000 mg/L Pb, 41318-100ML-F). The stock solution is then dissolved in deionized water (Sigma, 8483331000). To prepare different concentration solutions, 10000 ppb and 100 ppb lead solution are firstly prepared as stock solution and then diluted to lower concentration solutions. The following concentration of lead solutions have been prepared including 1 ppb, 5 ppb, 10 ppb, 50 ppb, 100 ppb, 500 ppb, and 1000 ppb. To test the reliability of this method sensing real samples, tap water from Engineering 3 building of University of Waterloo is collected and used to dissolve lead stock solution.

7.3.3. Experiments

In the measurement process, a pressure pump is used to pump the fluid samples to chip inlets and let it pass through resonator areas. Au-NPs modified resonator is firstly compared with regular microwave resonator to test the lead samples dissolved in distilled water using a commercial VNA (Anstrisu MS2028C). To prove the reliability of this method, lead samples then dissolved in

collected tap water and is designed to be detected using the same method. Finally, a portable Nano-VNA is used to carry out the sensing process to replace commercial VNA.

7.4. Results and discussion

Two kinds of microfluidic chips with integrated microwave resonator are prepared for sensing tests. They can be distinguished by the sensor area coating. The first one is bare sensor without any modification in the sensor area as illustrated in Figure 7.3 a. Another chip has the Au-NPs modified sensors which can be seen under microscope which is present in Figure 7.3 b and it demonstrates that Au-NPs is successfully coated onto the resonators area.

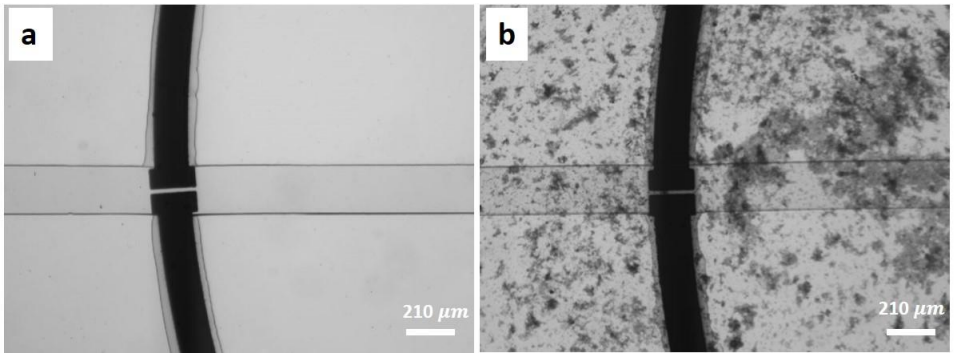

Figure 7.3. Photo of microwave (a) without Au-NPs coating and (b) with Au-NPs coating

The sample containing ICP standard lead dissolved in distilled water is tested for sensing using microfluidic chips with and without Au-NPs modified resonator. In Figure 7.4a and 7.4b, it exhibits the frequency sweep images of two chips for five different concentration of lead solution including 0 ppb, 1ppb, 10 ppb, 100 ppb and 1000 ppb. In microwave sensing, the resonance frequency shift can be used to characterize the dielectric properties of the materials in resonator areas. From the images, frequency sweep lines are different for each concentration of lead solution and a resonance frequency shift can be observed by using Au-NPs coated resonator. Also it exhibits

a clear magnitude difference for different samples. However, for the bare resonator without any surface modification, the frequency sweeps are similar among different concentration samples and resonance frequencies and magnitude of scattering parameters are close to each other, which are hard to be distinguished from the figure. In Figure 7.4c, the resonance frequency shift for two resonators with more concentration cases are summarized and clearly presented. The resonance frequency shift in Y-axis is defined as comparison with pure distilled water case in the Figure 7.4c. The black line in the figure is the frequency shift for Au-coated resonator, which shows a sharper trend than red line of bare sensors case without any modification resonator. For Au-coated resonator, frequency shift changes from 5 MHz to 28 MHz corresponding to the concentration ranges from 1ppb to 1000 ppb. In contrast, the frequency shift for no modification resonator has very small changes about 1-2 MHz for different concentration of lead solutions compared with distilled water. Besides tracking the shift of resonance frequency, one can also use scattering parameters magnitude to determine the lead concentration. In Figure 7.4d, it exhibits the reflection coefficient magnitude change for different concentration lead solution by using Au-NPs modified chip. As the concentration increasing, there is an increase trend for the magnitude of S11 and the magnitude of S11 changes from -16 dB for 1 ppb sample to -10 dB for 1000 ppb sample.

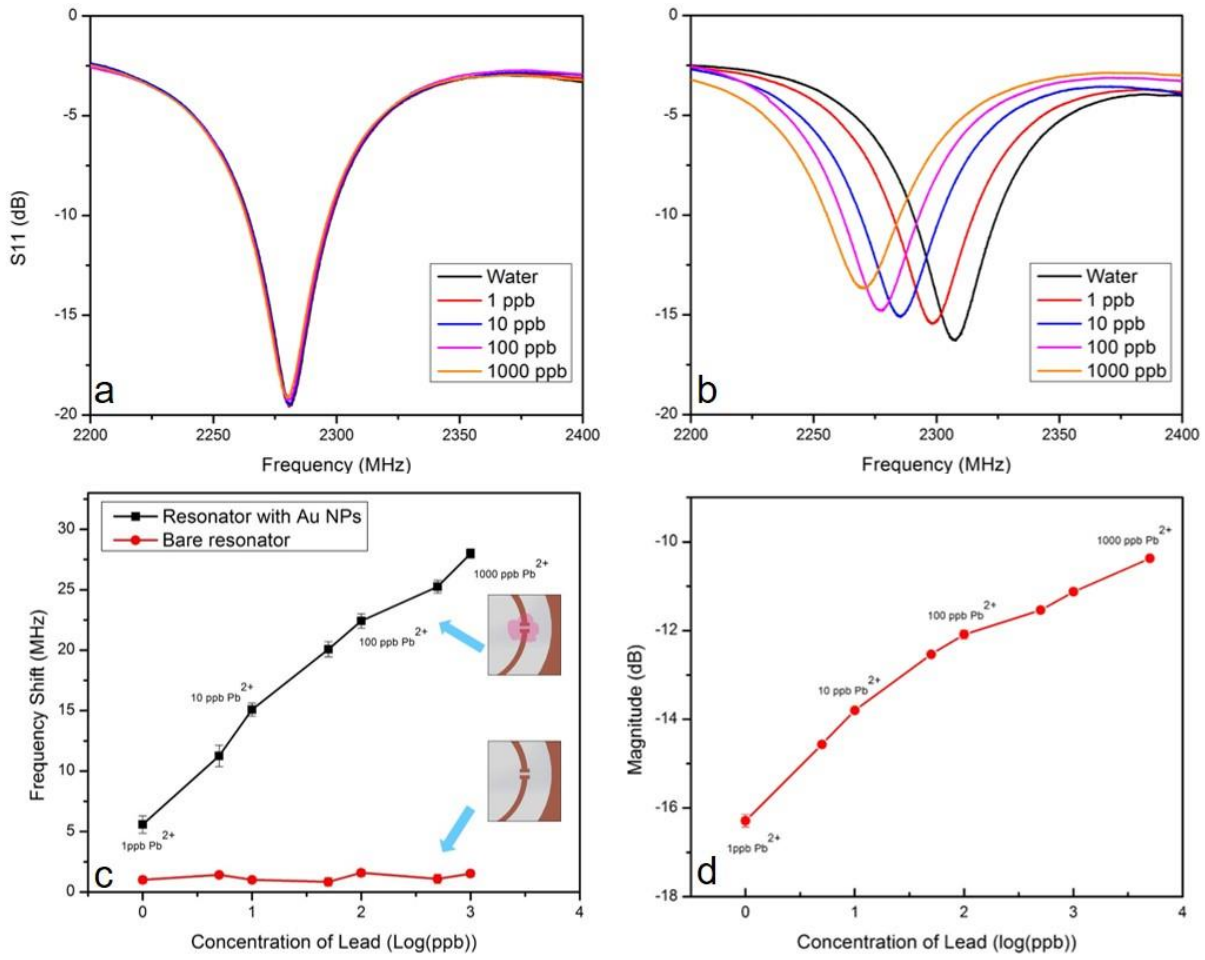

Figure 7.4. Sensing results for lead dissolved in distilled water (a) Frequency sweep for chip without any modification (b) Frequency sweep for chip with Au-NPs coating (c) Summarized frequency shift for two different chips. (d) S11 magnitude change for lead samples with the chip with Au-NPs modification

Dissolving lead samples in distilled water is the ideal case. To demonstrate the ability of this method to detect lead amount in real drinking water, tap water is collected and then used to dissolve lead samples. Tap water is different from distilled water since it has other ions which may influence the sensing results. In Figure 7.5 a and b, they show the frequency sweep for bare sensor and Au-modified sensor. Samples dissolved in tap water shows a similar trend as in distilled water. By comparing Au-NPs coated sensor and bare sensors, it indicates that there is a bigger frequency

shift for different concentration of lead solutions in tap water by using Au-NPs modified sensor. And slightly frequency shift is observed in Figure 7.5a for bare sensor case. In Figure 7.5c, a summarized frequency shift is presented exhibiting the difference between gold modified sensor and bare sensor. The frequency shift plot indicated that for Au-NPs coated sensors, resonance frequency shifts about 25MHz from 1 ppb solution to 1000 ppb solution. However, for the bare sensor, the resonance frequency possesses a tiny change when sample concentration varies. In Figure 7.5d, it shows the magnitude change of scattering parameters. As the increase of lead solution concentration, the magnitude also increases due to the increasing of conductivity. From these experiments, a same trend for these two kinds of resonators is observed for lead in tap water and distilled water showing that this method is capable to detect lead amount in tap water.

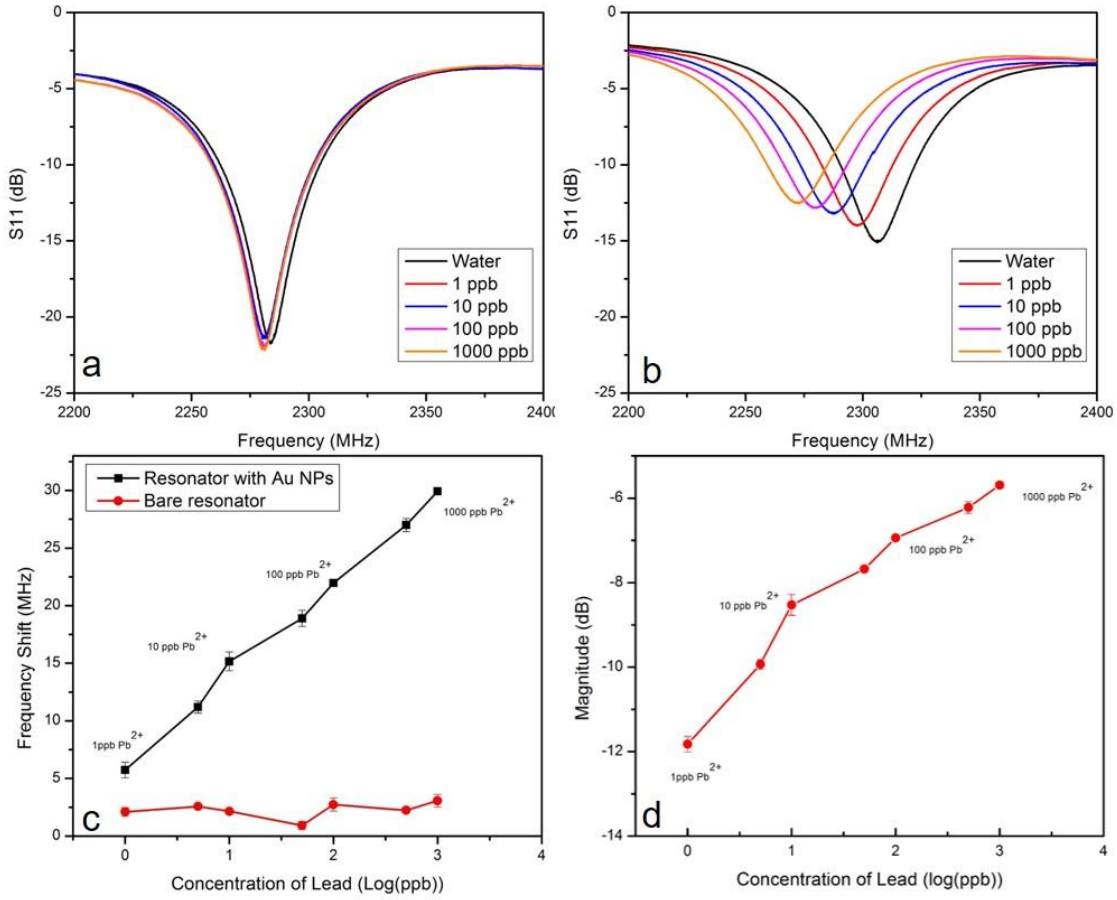

Figure 7.5. Sensing results for lead dissolved in tap water (a) Frequency sweep for chip without any modification (b) Frequency sweep for chip with Au-NPs coating (c) Summarized frequency shift for two different chips. (d) S11 magnitude change for lead samples with the chip with Au-NPs modification

To construct a POC device, detector is another key component besides the microfluidic platform with integrated sensor. In our system, VNA is employed as a detector for analyzing signals. In last two parts experiments, a commercial VNA is employed to provide analysis of microwave signal. These types of VNA can usually give very sensitive analysis with high resolution and wide frequency ranges. However, the shortcoming of this device lies in the high cost which is not affordable for widely use applications. Therefore, here we utilize a low cost and portable Nano-VNA to replace commercial VNA and justify that our method can be used for real-time detection.

The Nano-VNA has a frequency ranging from 50 KHz to 3GHz which is not comparable with commercial VNA. However, since the resonance frequency for our case is around 2.3GHz, it is capability to carry out the microwave sensing for our experiments. In Figure 7.6 a and b, it shows the frequency sweep results for two chips without and with the Au modification. Because the sweep points for NanoVNA has a limitation, in order to maintain high sensitivity, the fweep frequency range of NanoVNA need to be narrow down. This is the reason that Figure 7.6 a and b have a narrower range of frequency sweep than Figure 7.4 a and b.

Similar to the results using commercial VNA, the resonance frequency of lead solution tends to shift by using Au-NPs modified resonator when comparing to that of pure water. For non-coated resonator, it has negligible change in resonance frequency which is different from Au coated one. In Figure 7.6 c and d, it further confirms that the sensing results acquired by NanoVNA have a similar performance as commercial VNA by using same samples and chips. But it is worth taking note of the precision for these two VNA devices is slight different. Comparing the results by using commercial VNA, the utilization of NanoVNA can provide similar results as commercial VNA but there are still spaces for improvement in terms of resolution and accuracy. It can be seen that the frequency sweep in Figure 7.4 a and b have a smoother trend than Figure 7.6 a and b. And for summarized resonance frequency shift, the results acquired from NanoVNA have a bigger error bar than commercial one. Although NanoVNA still has some limitations regarding to the measurement resolution, it is a still promising detection device for heavy metals detection because it is capable to meet the detection standard. And the low cost and portable size of device can make it more appropriate for real-time detection.

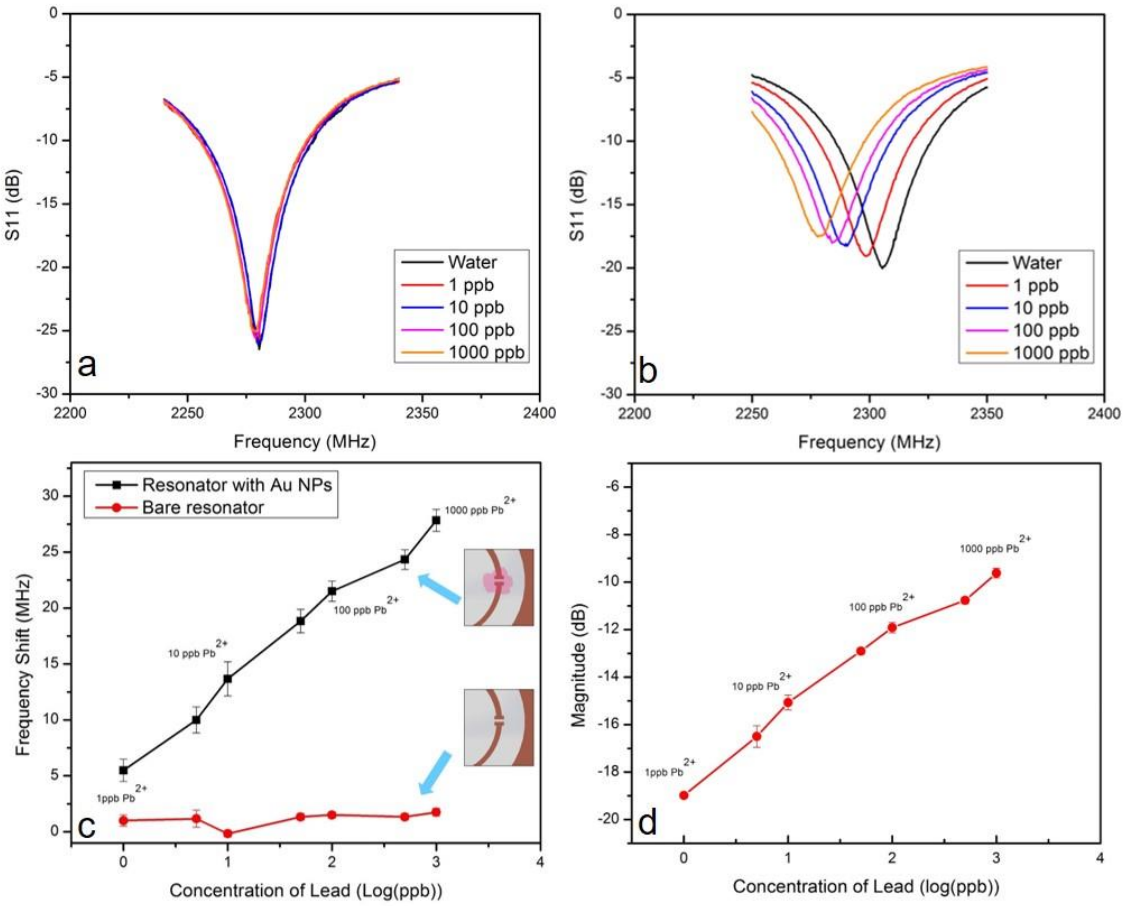

Figure 7.6. Sensing results for lead dissolved in distill water using NanoVNA as a detector(a) Frequency sweep for chip without any modification (b) Frequency sweep for chip with Au-NPs coating (c) Summarized frequency shift for two different chips. (d) S11 magnitude change for lead samples with the chip with Au-NPs modification

7.5. Conclusions

In this work, a new sensing method-microwave sensing is demonstrated for lead detection. The sensing device is based on a microfluidic platform with microwave sensor integrated. The microwave sensor modified with gold nanoparticles shows a bigger frequency shift for different concentration of lead solutions than the sensor without any modification. Tap water is used to mimic the real water sample and tap water obtains similar results as distilled water, validating this

method is eligible to carry out the detection with real samples. Finally, the utilization of a portable NanoVNA is used to perform detections and shows the prospect of this method to be widely used for real time sensing.

Chapter 8 : Conclusions and Recommendations

8.1. Conclusions

The trend for miniaturization have led to a concept LOC which compacts multiple function to a tiny system to operate tasks including reaction, detection and imaging which are normally carried out in bulk laboratory. The utilization of droplet microfluidics in LOC systems offers the opportunities for many fundamental research and practical applications which requires precise measurements and manipulations of samples. Droplet microfluidics features many advantages, which allows great reduction in sample use and reaction time and maintains good control over individual droplets since they are isolated with each other by carrier fluid. Droplet manipulation such as droplet mixing, or generation, is necessary and impactful for many applications. Active methods for droplet manipulation have the promise to offer more control in the manipulation by tuning the external sources and have the potential to realize on demand droplet manipulations. As many applications require precise control over droplets to get accurate results and efficient reaction, it is necessary to have a comprehensive understanding for active methods to better design this process and thus come up with new strategies for active methods to induce droplet manipulations.

Besides precise droplet manipulation, there are other functions in droplet microfluidics systems to meet the requirements for academic and practical research for example heating and sensing. Heating is necessary for tasks in droplet microfluidics which requires energy to facilitate the reactions, while sensing can help to acquire the droplet information including content, temperature, size or concentration for detection and diagnose purposes. Microwave technology can be

integrated with droplet microfluidics for precise and efficient heating and sensing purposes. In order to construct an effective and functional microfluidics systems, mechanism and applications for microwave technology contributing to droplet manipulation, real-time detection and multiple resonators in microfluidic system need to be understood and explored.

The focus of this thesis is to develop microfluidic system with microwave technology for sensing and heating. The main objective was to fundamentally and practically investigate microwave technology for sensing and heating purposes to realize multiple functions in microfluidics systems. Microwave heating has been employed as active methods for microfluidics droplet manipulation including mixing and generation. A fundamental work regarding to crosstalk between two microwave resonators is carried out to find the optimized design for two resonators in a single chip, which can be used for simultaneous microwave sensing and heating. Finally microwave sensing is combined with microfluidic platform to realize an application for real time lead detection. The main conclusions drawn from this work are as follows:

Mechanism of microwave heating induced droplet mixing was studied by numerical method. By simulating the flow and concentration field inside droplets, we investigated the effects of temperature-dependent parameters including fluid density, viscosity, diffusion coefficient, and interfacial tension on the mixing performance inside droplets. Both streamline pattern and concentration field shows the prime role of interfacial tension in this process. For the simulation cases when density, viscosity, diffusion coefficient are kept constant respectively, it is found that the mixing index can reach to around 0.84 within 320 ms with microwave heating and it would be slightly increased to 0.47 when only the interfacial tension was made independent on temperature,

which suggests that the temperature-dependent interfacial tension is the dominant factor for microwave heating induced mixing.

Continuing the mechanism study of microwave heating induced droplet mixing, a simple and novel method is reported for on-demand droplet generation mediated by microwave heating. The microwave heater is capable of confining power into a small region realizing localized heating which is advantageous for controlling droplet generation on-demand because the temperature of the fluid can be increased or decreased quickly. This work demonstrates that microwave heating can induce droplet generation by generates disturbance to the interface by reducing the interfacial tension through temperature change. The oil and water interface should be kept close to the junction for a better generation performance because it requires less pressure to generate droplets. The relationship between microwave power and generation time has been investigated showing that higher microwave power can result a short generation cycle.

Subsequently, to realize multiplex functions for selective heating in microfluidics system, we numerically and experimentally investigated the crosstalk between two adjacent resonators in a microfluidic chips. Work has been done to overcome the crosstalk phenomena by investigating the influence of parameters including two resonators' interval, loop radius, and input power. An optimized design with 10 mm interval between two resonators are confirmed with less crosstalk inference and can be used for next step experiments. Optimizing resonator's design by increasing inner loop radius or decreasing outer loop radius can also alleviate the crosstalk between two resonators. Lower input power if applicable is desired to reduce crosstalk.

Finally, an application based on microfluidics platform with the employment of microwave sensing has been presented. The sensing device is based on a microfluidic platform with

microwave sensor integrated. Gold nanoparticles were used to modify the microwave sensor and it shows a bigger frequency shift for different concentration of lead solutions than the sensor without any modification. Tap water is used to mimic the real water sample and tap water obtains similar results as distilled water, validating this method is eligible to carry out the detection with real samples. The utilization of a portable NanoVNA is used to perform detections and shows the prospect of this method to be widely used for real time sensing. This work develops the potential for microfluidics integrated microwave sensor for in-situ detection of heave metals with addition of nanomaterials.

8.2. Recommendations

This research presents a promising step to improve the understanding of microwave technology used in microfluidic systems. It also explores the applications using microwave technology based on microfluidic platforms. However, there are still spaces for improvement regarding to microfluidic platform integrated with microwave technology.

As the accomplishment of the investigation over crosstalk between double resonators, multiple microwave resonators microfluidic system are expected to be constructed to realize multiplex functions. Different microwave resonators can serve as heater and sensor respectively. Selective heating is one of the applications which can be realized by double resonators system, with one resonator for sensing and another resonator for heating purposes. If two resonators for sensing and heating can be linked together by a backstage system, resonator for sensing can provide fluid information to the resonator for heating. Then, an automatic microwave heating system can be constructed in microfluidic platforms.

There are still many applications related to microwave sensing and heating which can be developed in biochemical areas. The dielectric properties of many biochemical materials or biochemical reaction can be tracked by microwave sensing without any chemical labelling. With the enhancement performance of microwave sensors modified by nanomaterials, microwave sensing can be widely used in biochemical areas for small materials detection and diagnosis.

References

[1] G.M. Whitesides, The origins and the future of microfluidics, Nature, 442 (2006) 368.

[2] H.A. Stone, A.D. Stroock, A. Ajdari, Engineering flows in small devices: microfluidics toward a lab-on-a-chip, Annu. Rev. Fluid Mech., 36 (2004) 381-411.

[3] R. Riahi, A. Tamayol, S.A.M. Shaegh, A.M. Ghaemmaghami, M.R. Dokmeci, A. Khademhosseini, Microfluidics for advanced drug delivery systems, Current Opinion in Chemical Engineering, 7 (2015) 101-112.

[4] L. Dai, X. Zhao, J. Guo, S. Feng, Y. Fu, Y. Kang, J. Guo, Microfluidics-based microwave sensor, Sensors and Actuators A: Physical, 309 (2020) 111910.

[5] S.-Y. Teh, R. Lin, L.-H. Hung, A.P. Lee, Droplet microfluidics, Lab Chip, 8 (2008) 198-220.

[6] P.C. Gach, K. Iwai, P.W. Kim, N.J. Hillson, A.K. Singh, Droplet microfluidics for synthetic biology, Lab Chip, 17 (2017) 3388-3400.

[7] O.J. Dressler, R.M. Maceiczyk, S.-I. Chang, A.J. deMello, Droplet-based microfluidics: enabling impact on drug discovery, Journal of biomolecular screening, 19 (2014) 483-496.

[8] L. Mazutis, J. Gilbert, W.L. Ung, D.A. Weitz, A.D. Griffiths, J.A. Heyman, Single-cell analysis and sorting using droplet-based microfluidics, Nature protocols, 8 (2013) 870-891.

[9] W.-L. Chou, P.-Y. Lee, C.-L. Yang, W.-Y. Huang, Y.-S. Lin, Recent advances in applications of droplet microfluidics, Micromachines, 6 (2015) 1249-1271.

[10] G. Yesiloz, M.S. Boybay, C.L. Ren, Label-free high-throughput detection and content sensing of individual droplets in microfluidic systems, Lab Chip, 15 (2015) 4008-4019.

[11] M.S. Boybay, A. Jiao, T. Glawdel, C.L. Ren, Microwave sensing and heating of individual droplets in microfluidic devices, Lab Chip, 13 (2013) 3840-3846.

[12] P. Abgrall, A. Gue, Lab-on-chip technologies: making a microfluidic network and coupling it into a complete microsystem—a review, Journal of micromechanics and microengineering, 17 (2007) R15.

[13] P.S. Dittrich, A. Manz, Lab-on-a-chip: microfluidics in drug discovery, Nature reviews Drug discovery, 5 (2006) 210-218.

[14] A.K. Yetisen, M.S. Akram, C.R. Lowe, based microfluidic point-of-care diagnostic devices, Lab Chip, 13 (2013) 2210-2251.

[15] P. Gravesen, J. Branebjerg, O.S. Jensen, Microfluidics-a review, Journal of micromechanics and microengineering, 3 (1993) 168.
[16] T.M. Squires, S.R. Quake, Microfluidics: Fluid physics at the nanoliter scale, Reviews of modern physics, 77 (2005) 977.
[17] C. Kleinstreuer, J. Li, J. Koo, Microfluidics of nano-drug delivery, International Journal of Heat and Mass Transfer, 51 (2008) 5590-5597.
[18] T. Sun, H. Morgan, Single-cell microfluidic impedance cytometry: a review, Microfluidics and Nanofluidics, 8 (2010) 423-443.
[19] H. Song, D.L. Chen, R.F. Ismagilov, Reactions in droplets in microfluidic channels, Angew. Chem. Int. Ed., 45 (2006) 7336-7356.
[20] N.-T. Nguyen, S.T. Wereley, S.A.M. Shaegh, Fundamentals and applications of microfluidics, Artech house2019.
[21] S. Haeberle, R. Zengerle, Microfluidic platforms for lab-on-a-chip applications, Lab on a Chip, 7 (2007) 1094-1110.
[22] K.i. Ohno, K. Tachikawa, A. Manz, Microfluidics: applications for analytical purposes in chemistry and biochemistry, Electrophoresis, 29 (2008) 4443-4453.
[23] Y.K. Suh, S. Kang, A review on mixing in microfluidics, Micromachines, 1 (2010) 82-111.
[24] J.M. Ottino, S. Wiggins, Introduction: mixing in microfluidics, Philosophical Transactions: Mathematical, Physical and Engineering Sciences, (2004) 923-935.
[25] R. Seemann, M. Brinkmann, T. Pfohl, S. Herminghaus, Droplet based microfluidics, Rep. Prog. Phys., 75 (2011) 016601.
[26] H. Gu, M.H. Duits, F. Mugele, Droplets formation and merging in two-phase flow microfluidics, International journal of molecular sciences, 12 (2011) 2572-2597.
[27] C.-X. Zhao, A.P. Middelberg, Two-phase microfluidic flows, Chemical Engineering Science, 66 (2011) 1394-1411.
[28] Y. Zhang, P. Ozdemir, Microfluidic DNA amplification—a review, Analytica chimica acta, 638 (2009) 115-125.
[29] H.N. Joensson, H. Andersson Svahn, Droplet microfluidics—A tool for single-cell analysis, Angew. Chem. Int. Ed., 51 (2012) 12176-12192.
[30] X.C. i Solvas, A. DeMello, Droplet microfluidics: recent developments and future applications, Chemical Communications, 47 (2011) 1936-1942.

[31] P. Zhu, L. Wang, Passive and active droplet generation with microfluidics: a review, Lab Chip, 17 (2017) 34-75.
[32] Y.-C. Tan, V. Cristini, A.P. Lee, Monodispersed microfluidic droplet generation by shear focusing microfluidic device, Sensors and Actuators B: Chemical, 114 (2006) 350-356.
[33] C.-Y. Lee, C.-L. Chang, Y.-N. Wang, L.-M. Fu, Microfluidic mixing: a review, International journal of molecular sciences, 12 (2011) 3263-3287.
[34] C.-Y. Lee, W.-T. Wang, C.-C. Liu, L.-M. Fu, Passive mixers in microfluidic systems: A review, Chemical Engineering Journal, 288 (2016) 146-160.
[35] Z.Z. Chong, S.H. Tan, A.M. Gañán-Calvo, S.B. Tor, N.H. Loh, N.-T. Nguyen, Active droplet generation in microfluidics, Lab Chip, 16 (2016) 35-58.
[36] H.-D. Xi, H. Zheng, W. Guo, A.M. Gañán-Calvo, Y. Ai, C.-W. Tsao, J. Zhou, W. Li, Y. Huang, N.-T. Nguyen, Active droplet sorting in microfluidics: a review, Lab Chip, 17 (2017) 751-771.
[37] A.L. Markey, S. Mohr, P.J. Day, High-throughput droplet PCR, Methods, 50 (2010) 277-281.
[38] F. Schuler, M. Trotter, M. Geltman, F. Schwemmer, S. Wadle, E. Domínguez-Garrido, M. López, C. Cervera-Acedo, P. Santibáñez, F. von Stetten, Digital droplet PCR on disk, Lab Chip, 16 (2016) 208-216.
[39] Y.-F. Yap, S.-H. Tan, N.-T. Nguyen, S.S. Murshed, T.-N. Wong, L. Yobas, Thermally mediated control of liquid microdroplets at a bifurcation, Journal of Physics D: Applied Physics, 42 (2009) 065503.
[40] C.H. Ahn, J.-W. Choi, G. Beaucage, J.H. Nevin, J.-B. Lee, A. Puntambekar, J.Y. Lee, Disposable smart lab on a chip for point-of-care clinical diagnostics, Proceedings of the IEEE, 92 (2004) 154-173.
[41] C. Elbuken, T. Glawdel, D. Chan, C.L. Ren, Detection of microdroplet size and speed using capacitive sensors, Sensors and Actuators A: Physical, 171 (2011) 55-62.
[42] D. Wong, G. Yesiloz, M.S. Boybay, C.L. Ren, Microwave temperature measurement in microfluidic devices, Lab Chip, 16 (2016) 2192-2197.
[43] O. Krivosudský, D. Havelka, D.E. Chafai, M. Cifra, Microfluidic on-chip microwave sensing of the self-assembly state of tubulin, Sensors and Actuators B: Chemical, (2020) 129068.
[44] M. Li, H. Gou, I. Al-Ogaidi, N. Wu, Nanostructured sensors for detection of heavy metals: a review, ACS Publications, 2013.

[45] D. Issadore, K.J. Humphry, K.A. Brown, L. Sandberg, D.A. Weitz, R.M. Westervelt, Microwave dielectric heating of drops in microfluidic devices, Lab Chip, 9 (2009) 1701-1706.
[46] G. Yesiloz, M.S. Boybay, C.L. Ren, Effective thermo-capillary mixing in droplet microfluidics integrated with a microwave heater, Anal. Chem., 89 (2017) 1978-1984.
[47] T. Chen, S. Li, H. Sun, Metamaterials application in sensing, Sensors, 12 (2012) 2742-2765.
[48] D.J. Rowe, S. Al-Malki, A.A. Abduljabar, A. Porch, D.A. Barrow, C.J. Allender, Improved split-ring resonator for microfluidic sensing, IEEE Transactions on Microwave Theory and Techniques, 62 (2014) 689-699.
[49] D.C. Duffy, J.C. McDonald, O.J. Schueller, G.M. Whitesides, Rapid prototyping of microfluidic systems in poly (dimethylsiloxane), Analytical chemistry, 70 (1998) 4974-4984.
[50] K.E. Herold, A. Rasooly, Lab on a Chip Technology: Fabrication and microfluidics, horizon scientific press2009.
[51] B. Zheng, L.S. Roach, R.F. Ismagilov, Screening of protein crystallization conditions on a microfluidic chip using nanoliter-size droplets, Journal of the American chemical society, 125 (2003) 11170-11171.
[52] H. Song, J.D. Tice, R.F. Ismagilov, A microfluidic system for controlling reaction networks in time, Angewandte Chemie, 115 (2003) 792-796.
[53] A. Huerre, M.-C. Jullien, O. Theodoly, M.-P. Valignat, Absolute 3D reconstruction of thin films topography in microfluidic channels by interference reflection microscopy, Lab Chip, 16 (2016) 911-916.
[54] D. Malsch, M. Kielpinski, R. Merthan, J. Albert, G. Mayer, J. Köhler, H. Süße, M. Stahl, T. Henkel, μPIV-analysis of Taylor flow in micro channels, Chemical Engineering Journal, 135 (2008) S166-S172.
[55] Z. Li, P. Wang, L. Tong, L. Zhang, Gold nanorod-facilitated localized heating of droplets in microfluidic chips, Optics express, 21 (2013) 1281-1286.
[56] M.T. Guo, A. Rotem, J.A. Heyman, D.A. Weitz, Droplet microfluidics for high-throughput biological assays, Lab Chip, 12 (2012) 2146-2155.
[57] N.R. Beer, E.K. Wheeler, L. Lee-Houghton, N. Watkins, S. Nasarabadi, N. Hebert, P. Leung, D.W. Arnold, C.G. Bailey, B.W. Colston, On-chip single-copy real-time reverse-transcription PCR in isolated picoliter droplets, Anal. Chem., 80 (2008) 1854-1858.

[58] B.K. Yen, Microfluidic reactors for the synthesis of nanocrystals, Massachusetts Institute of Technology, 2007.
[59] C.N. Baroud, H. Willaime, Multiphase flows in microfluidics, Comptes Rendus Physique, 5 (2004) 547-555.
[60] P. Guillot, A. Colin, A.S. Utada, A. Ajdari, Stability of a jet in confined pressure-driven biphasic flows at low Reynolds numbers, Physical review letters, 99 (2007) 104502.
[61] S.K. Cho, H. Moon, C.-J. Kim, Creating, transporting, cutting, and merging liquid droplets by electrowetting-based actuation for digital microfluidic circuits, Journal of microelectromechanical systems, 12 (2003) 70-80.
[62] M. Pollack, A. Shenderov, R. Fair, Electrowetting-based actuation of droplets for integrated microfluidics, Lab on a Chip, 2 (2002) 96-101.
[63] G.M. Walker, D.J. Beebe, A passive pumping method for microfluidic devices, Lab on a Chip, 2 (2002) 131-134.
[64] r.-h.i. co., Information on Contact Angle.
[65] X. Chen, T. Glawdel, N. Cui, C.L. Ren, Model of droplet generation in flow focusing generators operating in the squeezing regime, Microfluidics and Nanofluidics, 18 (2015) 1341-1353.
[66] P. Garstecki, M.J. Fuerstman, H.A. Stone, G.M. Whitesides, Formation of droplets and bubbles in a microfluidic T-junction—scaling and mechanism of break-up, Lab on a Chip, 6 (2006) 437-446.
[67] J.-C. Baret, Surfactants in droplet-based microfluidics, Lab on a Chip, 12 (2012) 422-433.
[68] Q. Xu, M. Nakajima, The generation of highly monodisperse droplets through the breakup of hydrodynamically focused microthread in a microfluidic device, Applied Physics Letters, 85 (2004) 3726-3728.
[69] A. Magasinski, P. Dixon, B. Hertzberg, A. Kvit, J. Ayala, G. Yushin, High-performance lithium-ion anodes using a hierarchical bottom-up approach, Nature Materials 9(2010) 353-358.
[70] Y. Hong, F. Wang, Flow rate effect on droplet control in a co-flowing microfluidic device, Microfluidics and Nanofluidics, 3 (2007) 341-346.
[71] R. Xiong, M. Bai, J.N. Chung, Formation of bubbles in a simple co-flowing micro-channel, Journal of Micromechanics and Microengineering, 17 (2007) 1002.

[72] Y. Li, M. Jain, Y. Ma, K. Nandakumar, Control of the breakup process of viscous droplets by an external electric field inside a microfluidic device, Soft Matter, 11 (2015) 3884-3899.
[73] D.R. Link, E. Grasland-Mongrain, A. Duri, F. Sarrazin, Z. Cheng, G. Cristobal, M. Marquez, D.A. Weitz, Electric control of droplets in microfluidic devices, Angew. Chem. Int. Ed., 45 (2006) 2556-2560.
[74] S.H. Tan, N.-T. Nguyen, Generation and manipulation of monodispersed ferrofluid emulsions: The effect of a uniform magnetic field in flow-focusing and T-junction configurations, Phys. Rev. E, 84 (2011) 036317.
[75] C.-P. Lee, T.-S. Lan, M.-F. Lai, Fabrication of two-dimensional ferrofluid microdroplet lattices in a microfluidic channel, Journal of Applied Physics, 115 (2014) 17B527.
[76] S.H. Tan, B. Semin, J.-C. Baret, Microfluidic flow-focusing in ac electric fields, Lab Chip, 14 (2014) 1099-1106.
[77] N.-T. Nguyen, T.-H. Ting, Y.-F. Yap, T.-N. Wong, J.C.-K. Chai, W.-L. Ong, J. Zhou, S.-H. Tan, L. Yobas, Thermally mediated droplet formation in microchannels, Appl. Phys. Lett., 91 (2007) 084102.
[78] S.-Y. Park, T.-H. Wu, Y. Chen, M.A. Teitell, P.-Y. Chiou, High-speed droplet generation on demand driven by pulse laser-induced cavitation, Lab Chip, 11 (2011) 1010-1012.
[79] M.L. Cordero, D.R. Burnham, C.N. Baroud, D. McGloin, Thermocapillary manipulation of droplets using holographic beam shaping: Microfluidic pin ball, Appl. Phys. Lett., 93 (2008) 034107.
[80] M. Washizu, Electrostatic actuation of liquid droplets for micro-reactor applications, IEEE transactions on industry applications, 34 (1998) 732-737.
[81] A. Nightingale, S. Krishnadasan, D. Berhanu, X. Niu, C. Drury, R. McIntyre, E. Valsami-Jones, A stable droplet reactor for high temperature nanocrystal synthesis, Lab on a Chip, 11 (2011) 1221-1227.
[82] A. Ozcelik, D. Ahmed, Y. Xie, N. Nama, Z. Qu, A.A. Nawaz, T.J. Huang, An acoustofluidic micromixer via bubble inception and cavitation from microchannel sidewalls, Analytical chemistry, 86 (2014) 5083-5088.
[83] M. Muradoglu, H.A. Stone, Mixing in a drop moving through a serpentine channel: A computational study, Physics of Fluids, 17 (2005) 073305.

[84] A. Chandorkar, S. Palit, Simulation of droplet dynamics and mixing in microfluidic devices using a VOF-based method, Sensors & Transducers, 7 (2009) 136.
[85] F. Sarrazin, L. Prat, N. Di Miceli, G. Cristobal, D. Link, D. Weitz, Mixing characterization inside microdroplets engineered on a microcoalescer, Chemical Engineering Science, 62 (2007) 1042-1048.
[86] A.D. Stroock, S.K. Dertinger, A. Ajdari, I. Mezić, H.A. Stone, G.M. Whitesides, Chaotic mixer for microchannels, Science, 295 (2002) 647-651.
[87] H.S. Heo, Y.K. Suh, Enhancement of stirring in a straight channel at low Reynolds-numbers with various block-arrangement, Journal of mechanical science and technology, 19 (2005) 199-208.
[88] J. Wang, J. Wang, L. Feng, T. Lin, Fluid mixing in droplet-based microfluidics with a serpentine microchannel, RSC advances, 5 (2015) 104138-104144.
[89] I. Glasgow, N. Aubry, Enhancement of microfluidic mixing using time pulsing, Lab on a Chip, 3 (2003) 114-120.
[90] D. Ahmed, X. Mao, B.K. Juluri, T.J. Huang, A fast microfluidic mixer based on acoustically driven sidewall-trapped microbubbles, Microfluidics and nanofluidics, 7 (2009) 727.
[91] P. Paik, V.K. Pamula, R.B. Fair, Rapid droplet mixers for digital microfluidic systems, Lab on a Chip, 3 (2003) 253-259.
[92] B.J. Hindson, K.D. Ness, D.A. Masquelier, P. Belgrader, N.J. Heredia, A.J. Makarewicz, I.J. Bright, M.Y. Lucero, A.L. Hiddessen, T.C. Legler, High-throughput droplet digital PCR system for absolute quantitation of DNA copy number, Anal. Chem., 83 (2011) 8604-8610.
[93] H. Huang, Y. Yu, Y. Hu, X. He, O.B. Usta, M.L. Yarmush, Generation and manipulation of hydrogel microcapsules by droplet-based microfluidics for mammalian cell culture, Lab Chip, 17 (2017) 1913-1932.
[94] L. Yu, M.C. Chen, K.C. Cheung, Droplet-based microfluidic system for multicellular tumor spheroid formation and anticancer drug testing, Lab Chip, 10 (2010) 2424-2432.
[95] W. Zhang, H. Zhang, S.E. Williams, A. Zhou, Microfabricated three-electrode on-chip PDMS device with a vibration motor for stripping voltammetric detection of heavy metal ions, Talanta, 132 (2015) 321-326.
[96] B. Schlicht, M. Zagnoni, Droplet-interface-bilayer assays in microfluidic passive networks, Scientific reports, 5 (2015) 9951.

[97] V. Srinivasan, V.K. Pamula, R.B. Fair, Droplet-based microfluidic lab-on-a-chip for glucose detection, Analytica Chimica Acta, 507 (2004) 145-150.
[98] L.M. Fidalgo, G. Whyte, B.T. Ruotolo, J.L. Benesch, F. Stengel, C. Abell, C.V. Robinson, W.T. Huck, Coupling microdroplet microreactors with mass spectrometry: reading the contents of single droplets online, Angew. Chem. Int. Ed., 121 (2009) 3719-3722.
[99] U.E.A. Fittschen, S. Hauschild, M. Amberger, G. Lammel, C. Streli, S. Förster, P. Wobrauschek, C. Jokubonis, G. Pepponi, G. Falkenberg, A new technique for the deposition of standard solutions in total reflection X-ray fluorescence spectrometry (TXRF) using pico-droplets generated by inkjet printers and its applicability for aerosol analysis with SR-TXRF, Spectrochimica Acta Part B: Atomic Spectroscopy, 61 (2006) 1098-1104.
[100] S.E. Barnes, Z.T. Cygan, J.K. Yates, K.L. Beers, E.J. Amis, Raman spectroscopic monitoring of droplet polymerization in a microfluidic device, Analyst, 131 (2006) 1027-1033.
[101] J. Kim, M. Khan, S.-Y. Park, Glucose sensor using liquid-crystal droplets made by microfluidics, ACS applied materials & interfaces, 5 (2013) 13135-13139.
[102] L. Shi, K. Li, L.-L. Li, S.-Y. Chen, M.-Y. Li, Q. Zhou, N. Wang, X.-Q. Yu, Novel easily available purine-based AIEgens with colour tunability and applications in lipid droplet imaging, Chemical science, 9 (2018) 8969-8974.
[103] G. Su, P.W. Longest, R.M. Pidaparti, A novel micropump droplet generator for aerosol drug delivery: design simulations, Biomicrofluidics, 4 (2010) 044108.
[104] S.L. Sjostrom, H.N. Joensson, H.A. Svahn, Multiplex analysis of enzyme kinetics and inhibition by droplet microfluidics using picoinjectors, Lab Chip, 13 (2013) 1754-1761.
[105] C.N. Baroud, J.-P. Delville, F. Gallaire, R. Wunenburger, Thermocapillary valve for droplet production and sorting, Physical Review E, 75 (2007) 046302.
[106] H.F. Arata, F. Gillot, T. Nojima, T. Fujii, H. Fujita, Millisecond denaturation dynamics of fluorescent proteins revealed by femtoliter container on micro-thermodevice, Lab on a Chip, 8 (2008) 1436-1440.
[107] D. Erickson, D. Sinton, D. Li, Joule heating and heat transfer in poly (dimethylsiloxane) microfluidic systems, Lab on a Chip, 3 (2003) 141-149.
[108] J. Khandurina, T.E. McKnight, S.C. Jacobson, L.C. Waters, R.S. Foote, J.M. Ramsey, Integrated system for rapid PCR-based DNA analysis in microfluidic devices, Analytical Chemistry, 72 (2000) 2995-3000.

[109] R.M. Guijt, A. Dodge, G.W. van Dedem, N.F. de Rooij, E. Verpoorte, Chemical and physical processes for integrated temperature control in microfluidic devices, Lab on a Chip, 3 (2003) 1-4.
[110] A.A. Abduljabar, Compact microwave microfluidic sensors and applicator, Cardiff University, 2016.
[111] D. Mark, S. Haeberle, G. Roth, F. Von Stetten, R. Zengerle, Microfluidic lab-on-a-chip platforms: requirements, characteristics and applications, Microfluidics based microsystems, Springer2010, pp. 305-376.
[112] A. Yussuf, I. Sbarski, J. Hayes, M. Solomon, N. Tran, Microwave welding of polymeric-microfluidic devices, Journal of Micromechanics and Microengineering, 15 (2005) 1692.
[113] J.J. Shah, S.G. Sundaresan, J. Geist, D.R. Reyes, J.C. Booth, M.V. Rao, M. Gaitan, Microwave dielectric heating of fluids in an integrated microfluidic device, Journal of Micromechanics and Microengineering, 17 (2007) 2224.
[114] K.J. Shaw, P.T. Docker, J.V. Yelland, C.E. Dyer, J. Greenman, G.M. Greenway, S.J. Haswell, Rapid PCR amplification using a microfluidic device with integrated microwave heating and air impingement cooling, Lab Chip, 10 (2010) 1725-1728.
[115] D. Koziej, C. Floryan, R.A. Sperling, A.J. Ehrlicher, D. Issadore, R. Westervelt, D.A. Weitz, Microwave dielectric heating of non-aqueous droplets in a microfluidic device for nanoparticle synthesis, Nanoscale, 5 (2013) 5468-5475.
[116] B. Kuswandi, J. Huskens, W. Verboom, Optical sensing systems for microfluidic devices: a review, Analytica chimica acta, 601 (2007) 141-155.
[117] N. Alizadeh, A. Salimi, Polymer dots as a novel probe for fluorescence sensing of dopamine and imaging in single living cell using droplet microfluidic platform, Analytica chimica acta, 1091 (2019) 40-49.
[118] T.D. Rane, H.C. Zec, C. Puleo, A.P. Lee, T.-H. Wang, Droplet microfluidics for amplification-free genetic detection of single cells, Lab Chip, 12 (2012) 3341-3347.
[119] M. Srisa-Art, E.C. Dyson, A.J. deMello, J.B. Edel, Monitoring of real-time streptavidin−biotin binding kinetics using droplet microfluidics, Anal. Chem., 80 (2008) 7063-7067.
[120] G. Wang, C. Lim, L. Chen, H. Chon, J. Choo, J. Hong, A.J. DeMello, Surface-enhanced Raman scattering in nanoliter droplets: towards high-sensitivity detection of mercury (II) ions, Analytical and bioanalytical chemistry, 394 (2009) 1827-1832.

[121] B. Bansod, T. Kumar, R. Thakur, S. Rana, I. Singh, A review on various electrochemical techniques for heavy metal ions detection with different sensing platforms, Biosensors and Bioelectronics, 94 (2017) 443-455.
[122] M. Medina-Sánchez, M. Cadevall, J. Ros, A. Merkoçi, Eco-friendly electrochemical lab-on-paper for heavy metal detection, Analytical and bioanalytical chemistry, 407 (2015) 8445-8449.
[123] A. Waheed, M. Mansha, N. Ullah, Nanomaterials-based electrochemical detection of heavy metals in water: current status, challenges and future direction, TrAC Trends in Analytical Chemistry, 105 (2018) 37-51.
[124] G. Zhao, H. Wang, G. Liu, Recent advances in chemically modified electrodes, microfabricated devices and injection systems for the electrochemical detection of heavy metals: A review, Int. J. Electrochem. Sci, 12 (2017) 8622-8641.
[125] V. Subramanian, S. Lee, S. Jena, S.K. Jana, D. Ray, S.J. Kim, P. Thalappil, Enhancing the sensitivity of point-of-use electrochemical microfluidic sensors by ion concentration polarisation–A case study on arsenic, Sensors and Actuators B: Chemical, 304 (2020) 127340.
[126] S.G. Yoon, S.T. Chang, Microfluidic capacitive sensors with ionic liquid electrodes and CNT/PDMS nanocomposites for simultaneous sensing of pressure and temperature, Journal of Materials Chemistry C, 5 (2017) 1910-1919.
[127] H.M. Hamzah, Microwave microfluidic resonant sensors and applicators, Cardiff University, 2017.
[128] G.P. Srivastava, V.L. Gupta, Microwave devices and circuit design, PHI Learning Pvt. Ltd.2006.
[129] I.J. Bahl, P. Bhartia, Microwave solid state circuit design, John Wiley & Sons2003.
[130] H.-J. Lee, J.-H. Lee, H.-I. Jung, A symmetric metamaterial element-based RF biosensor for rapid and label-free detection, Applied Physics Letters, 99 (2011) 163703.
[131] R. Joffe, E. Kamenetskii, R. Shavit, Novel microwave near-field sensors for material characterization, biology, and nanotechnology, Journal of Applied Physics, 113 (2013) 063912.
[132] Y. Seo, M.U. Memon, S. Lim, Microfluidic eighth-mode substrate-integrated-waveguide antenna for compact ethanol chemical sensor application, IEEE Transactions on Antennas and Propagation, 64 (2016) 3218-3222.
[133] C.-F. Liu, M.-H. Wang, L.-S. Jang, Microfluidics-based hairpin resonator biosensor for biological cell detection, Sensors and Actuators B: Chemical, 263 (2018) 129-136.

[134] A.A. Abduljabar, D.J. Rowe, A. Porch, D.A. Barrow, Novel microwave microfluidic sensor using a microstrip split-ring resonator, IEEE Transactions on Microwave Theory and Techniques, 62 (2014) 679-688.
[135] A.A. Abduljabar, A. Porch, D.A. Barrow, Real-time measurements of size, speed, and dielectric property of liquid segments using a microwave microfluidic sensor, Microwave Symposium (IMS), 2014 IEEE MTT-S International, IEEE, 2014, pp. 1-4.
[136] L.Y. Zhang, C.B.M. du Puch, C. Dalmay, A. Lacroix, A. Landoulsi, J. Leroy, C. Mélin, F. Lalloué, S. Battu, C. Lautrette, Discrimination of colorectal cancer cell lines using microwave biosensors, Sensors and Actuators A: Physical, 216 (2014) 405-416.
[137] H. Torun, F. Cagri Top, G. Dundar, A. Yalcinkaya, An antenna-coupled split-ring resonator for biosensing, Journal of Applied Physics, 116 (2014) 124701.
[138] G. Sriram, M.P. Bhat, P. Patil, U.T. Uthappa, H.-Y. Jung, T. Altalhi, T. Kumeria, T.M. Aminabhavi, R.K. Pai, M.D. Kurkuri, based microfluidic analytical devices for colorimetric detection of toxic ions: A review, TrAC Trends in Analytical Chemistry, 93 (2017) 212-227.
[139] H.-J. Lee, H.-S. Lee, K.-H. Yoo, J.-G. Yook, DNA sensing using split-ring resonator alone at microwave regime, Journal of Applied Physics, 108 (2010) 014908.
[140] H.-J. Lee, J.-G. Yook, Biosensing using split-ring resonators at microwave regime, Applied Physics Letters, 92 (2008) 254103.
[141] H. Zhou, C. Yang, D. Hu, S. Dou, X. Hui, F. Zhang, C. Chen, M. Chen, Y. Yang, X. Mu, Integrating a microwave resonator and a microchannel with an immunochromatographic strip for stable and quantitative biodetection, ACS applied materials & interfaces, 11 (2019) 14630-14639.
[142] Y. Xia, G.M. Whitesides, Soft lithography, Annual review of materials science, 28 (1998) 153-184.
[143] M. Baltussen, J. Kuipers, N. Deen, A critical comparison of surface tension models for the volume of fluid method, Chemical Engineering Science, 109 (2014) 65-74.
[144] C.W. Hirt, B.D. Nichols, Volume of fluid (VOF) method for the dynamics of free boundaries, Journal of computational physics, 39 (1981) 201-225.
[145] E. Roohi, A.P. Zahiri, M. Passandideh-Fard, Numerical simulation of cavitation around a two-dimensional hydrofoil using VOF method and LES turbulence model, Applied Mathematical Modelling, 37 (2013) 6469-6488.

[146] M. Weiss, J.P. Frohnmayer, L.T. Benk, B. Haller, J.-W. Janiesch, T. Heitkamp, M. Börsch, R.B. Lira, R. Dimova, R. Lipowsky, Sequential bottom-up assembly of mechanically stabilized synthetic cells by microfluidics, Nature materials, 17 (2018) 89.
[147] F. Wang, M.A. Burns, Performance of nanoliter-sized droplet-based microfluidic PCR, Biomedical microdevices, 11 (2009) 1071.
[148] S.-I. Yeh, H.-J. Sheen, J.-T. Yang, Chemical reaction and mixing inside a coalesced droplet after a head-on collision, Microfluidics and Nanofluidics, 18 (2015) 1355-1363.
[149] C.-X. Zhao, L. He, S.Z. Qiao, A.P. Middelberg, Nanoparticle synthesis in microreactors, Chemical Engineering Science, 66 (2011) 1463-1479.
[150] K. Ward, Z.H. Fan, Mixing in microfluidic devices and enhancement methods, Journal of Micromechanics and Microengineering, 25 (2015) 094001.
[151] M. Courtney, X. Chen, S. Chan, T. Mohamed, P.P. Rao, C.L. Ren, Droplet microfluidic system with on-demand trapping and releasing of droplet for drug screening applications, Analytical chemistry, 89 (2016) 910-915.
[152] S. Duraiswamy, S.A. Khan, Droplet-Based Microfluidic Synthesis of Anisotropic Metal Nanocrystals, Small, 5 (2009) 2828-2834.
[153] N.-T. Nguyen, Z. Wu, Micromixers—a review, Journal of micromechanics and microengineering, 15 (2004) R1.
[154] Z. Stone, H. Stone, Imaging and quantifying mixing in a model droplet micromixer, Physics of Fluids, 17 (2005) 063103.
[155] K.-Y. Tung, C.-C. Li, J.-T. Yang, Mixing and hydrodynamic analysis of a droplet in a planar serpentine micromixer, Microfluidics and Nanofluidics, 7 (2009) 545.
[156] X. Chen, C.L. Ren, A microfluidic chip integrated with droplet generation, pairing, trapping, merging, mixing and releasing, RSC advances, 7 (2017) 16738-16750.
[157] I.-F. Cheng, S.-C. Chiang, C.-C. Chung, T.-M. Yeh, H.-C. Chang, Ripple structure-generated hybrid electrokinetics for on-chip mixing and separating of functionalized beads, Biomicrofluidics, 8 (2014) 061102.
[158] M.L. Sin, Y. Shimabukuro, P.K. Wong, Hybrid electrokinetics for separation, mixing, and concentration of colloidal particles, Nanotechnology, 20 (2009) 165701.

[159] E.N. Wang, M.A. Bucaro, J.A. Taylor, P. Kolodner, J. Aizenberg, T. Krupenkin, Droplet mixing using electrically tunable superhydrophobic nanostructured surfaces, Microfluidics and nanofluidics, 7 (2009) 137-140.
[160] F. Mugele, J.-C. Baret, D. Steinhauser, Microfluidic mixing through electrowetting-induced droplet oscillations, Applied Physics Letters, 88 (2006) 204106.
[161] S.H. Lee, D. van Noort, J.Y. Lee, B.-T. Zhang, T.H. Park, Effective mixing in a microfluidic chip using magnetic particles, Lab on a Chip, 9 (2009) 479-482.
[162] L.-H. Lu, K.S. Ryu, C. Liu, A magnetic microstirrer and array for microfluidic mixing, Journal of microelectromechanical systems, 11 (2002) 462-469.
[163] C.Y. Wen, C.P. Yeh, C.H. Tsai, L.M. Fu, Rapid magnetic microfluidic mixer utilizing AC electromagnetic field, Electrophoresis, 30 (2009) 4179-4186.
[164] Y. Liao, J. Song, E. Li, Y. Luo, Y. Shen, D. Chen, Y. Cheng, Z. Xu, K. Sugioka, K. Midorikawa, Rapid prototyping of three-dimensional microfluidic mixers in glass by femtosecond laser direct writing, Lab on a Chip, 12 (2012) 746-749.
[165] W. Hu, A.T. Ohta, Aqueous droplet manipulation by optically induced Marangoni circulation, Microfluidics and nanofluidics, 11 (2011) 307-316.
[166] D. Ahmed, X. Mao, J. Shi, B.K. Juluri, T.J. Huang, A millisecond micromixer via single-bubble-based acoustic streaming, Lab on a Chip, 9 (2009) 2738-2741.
[167] K. Sritharan, C. Strobl, M. Schneider, A. Wixforth, Z.v. Guttenberg, Acoustic mixing at low Reynold's numbers, Applied Physics Letters, 88 (2006) 054102.
[168] G.G. Yaralioglu, I.O. Wygant, T.C. Marentis, B.T. Khuri-Yakub, Ultrasonic mixing in microfluidic channels using integrated transducers, Analytical chemistry, 76 (2004) 3694-3698.
[169] H. Van Phan, M.B. Coşkun, M. Şeşen, G. Pandraud, A. Neild, T. Alan, Vibrating membrane with discontinuities for rapid and efficient microfluidic mixing, Lab on a Chip, 15 (2015) 4206-4216.
[170] B. Xu, T.N. Wong, N.-T. Nguyen, Z. Che, J.C.K. Chai, Thermal mixing of two miscible fluids in a T-shaped microchannel, Biomicrofluidics, 4 (2010) 044102.
[171] M.L. Cordero, H.O. Rolfsnes, D.R. Burnham, P.A. Campbell, D. McGloin, C.N. Baroud, Mixing via thermocapillary generation of flow patterns inside a microfluidic drop, New Journal of Physics, 11 (2009) 075033.

[172] R.H. Liu, J. Yang, R. Lenigk, J. Bonanno, P. Grodzinski, Self-contained, fully integrated biochip for sample preparation, polymerase chain reaction amplification, and DNA microarray detection, Anal. Chem., 76 (2004) 1824-1831.
[173] A.J. De Mello, M. Habgood, N.L. Lancaster, T. Welton, R.C. Wootton, Precise temperature control in microfluidic devices using Joule heating of ionic liquids, Lab Chip, 4 (2004) 417-419.
[174] G. Maltezos, M. Johnston, A. Scherer, Thermal management in microfluidics using micro-Peltier junctions, Appl. Phys. Lett., 87 (2005) 154105.
[175] C.N. Baroud, M.R. de Saint Vincent, J.-P. Delville, An optical toolbox for total control of droplet microfluidics, Lab Chip, 7 (2007) 1029-1033.
[176] W. Jeon, C.B. Shin, Design and simulation of passive mixing in microfluidic systems with geometric variations, Chemical engineering journal, 152 (2009) 575-582.
[177] Y. Fu, L. Bai, S. Zhao, K. Bi, Y. Jin, Y. Cheng, Droplet in droplet: LBM simulation of modulated liquid mixing, Chemical Engineering Science, 155 (2016) 428-437.
[178] Y. Fu, L. Bai, S. Zhao, X. Zhang, Y. Jin, Y. Cheng, Simulation of reactive mixing behaviors inside micro-droplets by a lattice Boltzmann method, Chemical Engineering Science, 181 (2018) 79-89.
[179] M. van Sint Annaland, N. Deen, J. Kuipers, Numerical simulation of gas bubbles behaviour using a three-dimensional volume of fluid method, Chemical Engineering Science, 60 (2005) 2999-3011.
[180] X. Sun, M. Sakai, Numerical simulation of two-phase flows in complex geometries by using the volume-of-fluid/immersed-boundary method, Chemical Engineering Science, 139 (2016) 221-240.
[181] G.C.L.R. Weijia Cui, Appendix A: Supplementary material of Numerical analysis on droplet mixing induced by microwave heating: Decoupling of influencing physical properties, Chemical Engineering Science, (2020).
[182] J. Braga, J.M. Desterro, M. Carmo-Fonseca, Intracellular macromolecular mobility measured by fluorescence recovery after photobleaching with confocal laser scanning microscopes, Molecular biology of the cell, 15 (2004) 4749-4760.
[183] F. Sarrazin, T. Bonometti, L. Prat, C. Gourdon, J. Magnaudet, Hydrodynamic structures of droplets engineered in rectangular micro-channels, Microfluidics and Nanofluidics, 5 (2008) 131-137.

[184] F. Jousse, G. Lian, R. Janes, J. Melrose, Compact model for multi-phase liquid–liquid flows in micro-fluidic devices, Lab Chip, 5 (2005) 646-656.
[185] W. Cui, G. Yesiloz, C.L. Ren, Numerical Analysis on Droplet Mixing Induced by Microwave Heating: Decoupling of Influencing Physical Properties, Chemical Engineering Science, (2020) 115791.
[186] C.W. Shields IV, C.D. Reyes, G.P. López, Microfluidic cell sorting: a review of the advances in the separation of cells from debulking to rare cell isolation, Lab Chip, 15 (2015) 1230-1249.
[187] C.-H. Yang, K.-S. Huang, Y.-S. Lin, K. Lu, C.-C. Tzeng, E.-C. Wang, C.-H. Lin, W.-Y. Hsu, J.-Y. Chang, Microfluidic assisted synthesis of multi-functional polycaprolactone microcapsules: incorporation of CdTe quantum dots, Fe 3 O 4 superparamagnetic nanoparticles and tamoxifen anticancer drugs, Lab on a Chip, 9 (2009) 961-965.
[188] T. Rossow, J.A. Heyman, A.J. Ehrlicher, A. Langhoff, D.A. Weitz, R. Haag, S. Seiffert, Controlled synthesis of cell-laden microgels by radical-free gelation in droplet microfluidics, J. Am. Chem. Soc., 134 (2012) 4983-4989.
[189] R. Shemer, J. Magenheim, Y. Dor, Digital Droplet PCR for Monitoring Tissue-Specific Cell Death Using DNA Methylation Patterns of Circulating Cell-Free DNA, Curr. Protoc. Mol. Biol., 127 (2019) e90.
[190] T.S. Kaminski, O. Scheler, P. Garstecki, Droplet microfluidics for microbiology: techniques, applications and challenges, Lab Chip, 16 (2016) 2168-2187.
[191] K. Churski, P. Korczyk, P. Garstecki, High-throughput automated droplet microfluidic system for screening of reaction conditions, Lab Chip, 10 (2010) 816-818.
[192] C.-T. Chen, G.-B. Lee, Formation of microdroplets in liquids utilizing active pneumatic choppers on a microfluidic chip, J. Microelectromech. Syst., 15 (2006) 1492-1498.
[193] A. Bransky, N. Korin, M. Khoury, S. Levenberg, A microfluidic droplet generator based on a piezoelectric actuator, Lab Chip, 9 (2009) 516-520.
[194] M. He, J.S. Kuo, D.T. Chiu, Electro-generation of single femtoliter-and picoliter-volume aqueous droplets in microfluidic systems, Appl. Phys. Lett., 87 (2005) 031916.
[195] F. Malloggi, H. Gu, A. Banpurkar, S. Vanapalli, F. Mugele, Electrowetting--A versatile tool for controlling microdrop generation, Eur. Phys. J. E, 26 (2008) 91-96.
[196] C.N. Baroud, F. Gallaire, R. Dangla, Dynamics of microfluidic droplets, Lab Chip, 10 (2010) 2032-2045.

[197] M. Prakash, N. Gershenfeld, Microfluidic bubble logic, Science, 315 (2007) 832-835.
[198] C.A. Stan, S.K. Tang, G.M. Whitesides, Independent control of drop size and velocity in microfluidic flow-focusing generators using variable temperature and flow rate, Anal. Chem., 81 (2009) 2399-2402.
[199] T. Glawdel, C. Elbuken, C.L. Ren, Droplet formation in microfluidic T-junction generators operating in the transitional regime. I. Experimental observations, Phys. Rev. E, 85 (2012) 016322.
[200] B.M. Brewer, M. Shi, J.F. Edd, D.J. Webb, D. Li, A microfluidic cell co-culture platform with a liquid fluorocarbon separator, Biomed. Microdevices, 16 (2014) 311-323.
[201] E. Yakhshi-Tafti, R. Kumar, H.J. Cho, Measurement of surface interfacial tension as a function of temperature using pendant drop images, Int. J. Optomechatronics, 5 (2011) 393-403.
[202] G. Yesiloz, M.S. Boybay, C.L. Ren, SI of Effective thermo-capillary mixing in droplet microfluidics integrated with a microwave heater, Anal. Chem., 89 (2017).
[203] G.F. Christopher, S.L. Anna, Microfluidic methods for generating continuous droplet streams, J. Phys. D: Appl. Phys, 40 (2007) R319.
[204] A.W. Chow, Lab-on-Chip: Opportunities for chemical engineering, American Institute of Chemical Engineers. AIChE Journal, 48 (2002) 1590.
[205] R. Soares, D. Ramadas, V. Chu, M. Aires-Barros, J. Conde, A. Viana, A. Cascalheira, An ultrarapid and regenerable microfluidic immunoassay coupled with integrated photosensors for point-of-use detection of ochratoxin A, Sensors and Actuators B: Chemical, 235 (2016) 554-562.
[206] C.D. Chin, V. Linder, S.K. Sia, Commercialization of microfluidic point-of-care diagnostic devices, Lab Chip, 12 (2012) 2118-2134.
[207] H. Li, D. Men, Y. Sun, T. Zhang, L. Hang, D. Liu, C. Li, W. Cai, Y. Li, Optical sensing properties of Au nanoparticle/hydrogel composite microbeads using droplet microfluidics, Nanotechnology, 28 (2017) 405502.
[208] N. Ullah, M. Mansha, I. Khan, A. Qurashi, Nanomaterial-based optical chemical sensors for the detection of heavy metals in water: Recent advances and challenges, TrAC Trends in Analytical Chemistry, 100 (2018) 155-166.
[209] B. Hadwen, G. Broder, D. Morganti, A. Jacobs, C. Brown, J. Hector, Y. Kubota, H. Morgan, Programmable large area digital microfluidic array with integrated droplet sensing for bioassays, Lab on a Chip, 12 (2012) 3305-3313.

[210] X. Niu, M. Zhang, S. Peng, W. Wen, P. Sheng, Real-time detection, control, and sorting of microfluidic droplets, Biomicrofluidics, 1 (2007) 044101.
[211] N. Srivastava, M.A. Burns, Electronic drop sensing in microfluidic devices: automated operation of a nanoliter viscometer, Lab on a Chip, 6 (2006) 744-751.
[212] M. Abdolrazzaghi, M. Daneshmand, A.K. Iyer, Strongly enhanced sensitivity in planar microwave sensors based on metamaterial coupling, IEEE Transactions on Microwave Theory and Techniques, 66 (2018) 1843-1855.
[213] P. Vélez, L. Su, K. Grenier, J. Mata-Contreras, D. Dubuc, F. Martín, Microwave microfluidic sensor based on a microstrip splitter/combiner configuration and split ring resonators (SRRs) for dielectric characterization of liquids, IEEE Sens. J., 17 (2017) 6589-6598.
[214] P. Vélez, J. Muñoz-Enano, K. Grenier, J. Mata-Contreras, D. Dubuc, F. Martín, Split ring resonator-based microwave fluidic sensors for electrolyte concentration measurements, IEEE Sens. J., 19 (2018) 2562-2569.
[215] Z. Abbasi, M. Baghelani, M. Nosrati, A. Sanati-Nezhad, M. Daneshmand, Real-time non-contact integrated chipless RF sensor for disposable microfluidic applications, IEEE Journal of Electromagnetics, RF and Microwaves in Medicine and Biology, (2019).
[216] Z. Abbasi, P. Shariaty, M. Nosrati, Z. Hashisho, M. Daneshmand, Dual-band microwave circuits for selective binary gas sensing system, IEEE Transactions on Microwave Theory and Techniques, 67 (2019) 4206-4219.
[217] Z. Abbasi, M.H. Zarifi, P. Shariati, Z. Hashisho, M. Daneshmand, Flexible coupled microwave ring resonators for contactless microbead assisted volatile organic compound detection, 2017 IEEE MTT-S International Microwave Symposium (IMS), IEEE, 2017, pp. 1228-1231.
[218] M. Baghelani, Z. Abbasi, M. Daneshmand, P.E. Light, Non-invasive continuous-time glucose monitoring system using a chipless printable sensor based on split ring microwave resonators, Scientific Reports, 10 (2020) 1-15.
[219] V. Turgul, I. Kale, Permittivity extraction of glucose solutions through artificial neural networks and non-invasive microwave glucose sensing, Sensors and Actuators A: Physical, 277 (2018) 65-72.
[220] H. Hamzah, J. Lees, A. Porch, Split ring resonator with optimised sensitivity for microfluidic sensing, Sensors and Actuators A: Physical, 276 (2018) 1-10.

[221] J. Muñoz-Enano, P. Vélez, M. Gil, F. Martín, Planar Microwave Resonant Sensors: A Review and Recent Developments, Applied Sciences, 10 (2020) 2615.
[222] S.S. Murshed, C.N. De Castro, Nanofluids: synthesis, properties, and applications, Nova Science Publishers, Incorporated2014.
[223] V. Miralles, A. Huerre, F. Malloggi, M.-C. Jullien, A review of heating and temperature control in microfluidic systems: techniques and applications, Diagnostics, 3 (2013) 33-67.
[224] W. Cui, G. Yesiloz, C.L. Ren, Microwave Heating Induced On-Demand Droplet Generation in Microfluidic Systems, Anal. Chem., (2020).
[225] H.-J. Lee, K.-A. Hyun, H.-I. Jung, A high-Q resonator using biocompatible materials at microwave frequencies, Appl. Phys. Lett., 104 (2014) 023509.
[226] M. Nosrati, M. Daneshmand, Substrate integrated waveguide L-shaped iris for realization of transmission zero and evanescent-mode pole, IEEE Transactions on Microwave Theory and Techniques, 65 (2017) 2310-2320.
[227] W.H. Organization, Lead in drinking-water: background document for development of WHO guidelines for drinking-water quality, World Health Organization, 2003.
[228] F. Edition, Guidelines for drinking-water quality, WHO chronicle, 38 (2011) 104-108.
[229] H. Canada, Guidelines for Canadian drinking water quality—Summary table, Water and Air Quality Bureau, Healthy Environments and Consumer Safety Branch, Health Canada, Ottawa, (2017).
[230] USEPA, Announcement of Completion of EPA's Review of Existing Drinking Water Standards and Request for Public Comment and/or Information on Related Issue, Fed. Reg., 75 (2010) 15500.
[231] C. Directive, On the quality of water intended for human consumption, Official Journal of the European Communities, 330 (1998) 32-54.
[232] D.K. Robert Cribb, Charles Buckley, Ben Cohen and Julie Mutis, Is there lead in your tap water? Canada-wide investigation exposes dangerous levels of toxic metal, THE STAR, 2019.
[233] P. Kumar, K.-H. Kim, V. Bansal, T. Lazarides, N. Kumar, Progress in the sensing techniques for heavy metal ions using nanomaterials, Journal of industrial and engineering chemistry, 54 (2017) 30-43.
[234] G. Aragay, J. Pons, A. Merkoçi, Recent trends in macro-, micro-, and nanomaterial-based tools and strategies for heavy-metal detection, Chemical reviews, 111 (2011) 3433-3458.

[235] A.N. Uglov, A. Bessmertnykh-Lemeune, R. Guilard, A.D. Averin, I.P. Beletskaya, Optical methods for the detection of heavy metal ions, Russian Chemical Reviews, 83 (2014) 196.
[236] L. Zhao, T. Wu, J.-P. Lefèvre, I. Leray, J.A. Delaire, Fluorimetric lead detection in a microfluidic device, Lab on a Chip, 9 (2009) 2818-2823.
[237] D. Faye, J.-P. Lefevre, J.A. Delaire, I. Leray, A selective lead sensor based on a fluorescent molecular probe grafted on a PDMS microfluidic chip, Journal of Photochemistry and Photobiology A: Chemistry, 234 (2012) 115-122.
[238] M.-E. Vlachopoulou, P. Petrou, S. Kakabakos, A. Tserepi, K. Beltsios, E. Gogolides, Effect of surface nanostructuring of PDMS on wetting properties, hydrophobic recovery and protein adsorption, Microelectronic Engineering, 86 (2009) 1321-1324.
[239] C. Fan, S. He, G. Liu, L. Wang, S. Song, A Portable and Power-Free Microfluidic Device for Rapid and Sensitive Lead (Pb2+) Detection, Sensors, 12 (2012) 9467-9475.
[240] Y. Hong, M. Wu, G. Chen, Z. Dai, Y. Zhang, G. Chen, X. Dong, 3D printed microfluidic device with microporous Mn2O3-modified screen printed electrode for real-time determination of heavy metal ions, ACS applied materials & interfaces, 8 (2016) 32940-32947.
[241] J. Chang, G. Zhou, E.R. Christensen, R. Heideman, J. Chen, Graphene-based sensors for detection of heavy metals in water: a review, Analytical and bioanalytical chemistry, 406 (2014) 3957-3975.
[242] L.-L. Shen, G.-R. Zhang, W. Li, M. Biesalski, B.J. Etzold, Modifier-free microfluidic electrochemical sensor for heavy-metal detection, ACS omega, 2 (2017) 4593-4603.
[243] M. Schueler, C. Mandel, M. Puentes, R. Jakoby, Metamaterial inspired microwave sensors, IEEE Microwave Magazine, 13 (2012) 57-68.
[244] Z. Abedeen, P. Agarwal, Microwave sensing technique based label-free and real-time planar glucose analyzer fabricated on FR4, Sensors and Actuators A: Physical, 279 (2018) 132-139.
[245] T. Chretiennot, D. Dubuc, K. Grenier, A microwave and microfluidic planar resonator for efficient and accurate complex permittivity characterization of aqueous solutions, IEEE Transactions on Microwave Theory and Techniques, 61 (2012) 972-978.
[246] I. Frau, S. Wylie, P. Byrne, J. Cullen, O. Korostynska, A. Mason, Detection of Zn in water using novel functionalised planar microwave sensors, Materials Science and Engineering: B, 247 (2019) 114382.